

ABSTRACT

Gain control in *Drosophila* Olfactory Receptor Neurons

Srinivas Gorur-Shandilya

2017

Insects find food and mates by navigating odor plumes that can be highly intermittent, with intensities and durations that vary rapidly over orders of magnitude. Much is known about olfactory responses to simple pulses and steps of odor, but it remains unclear how Olfactory Receptor Neurons (ORNs) detect the intensity and timing of natural signals, where the absence of a characteristic scale in the stimulus makes detection a formidable task.

Here we propose a method by which odorant signals with naturalistic and Gaussian statistics can be generated in a reproducible manner, and show how the instantaneous flux of odorant molecules can be measured. By eliciting ORN responses to these stimuli, we show *in vivo* that *Drosophila* ORNs contribute to naturalistic sensing by using receptor adaptation and saturation to change their gain in response to stimulus mean and variance. Mean-dependent gain control followed the Weber-Fechner relation and occurred primarily at odor transduction, while variance-dependent gain control occurred both at transduction and at spiking. Odorant transduction and spiking generation possessed complementary kinetic properties, that together preserved the timing of odor encounters in ORN spiking despite the fact that adaptation slowed transduction.

Gain Control in *Drosophila* Olfactory Receptor Neurons



A DISSERTATION

PRESENTED TO THE FACULTY OF THE GRADUATE SCHOOL

OF

YALE UNIVERSITY

IN CANDIDACY FOR THE DEGREE OF

DOCTOR OF PHILOSOPHY

by

Srinivas Gorur-Shandilya

Dissertation Director: Thierry Emonet

Chair of advisory committee: Damon A. Clark

December 2017

Srinivas Gorur-Shandilya: *Gain Control in Drosophila Olfactory Receptor Neurons*, © May 2017

This work is free information: you can redistribute it and/or modify it under the terms of the GNU General Public License as published by the Free Software Foundation, either version 3 of the License, or (at your option) any later version.

This work is distributed in the hope that it will be useful, but without any warranty, without even the implied warranty of merchantability or fitness for a particular purpose. See the GNU General Public License for more details, available here: <https://www.gnu.org/licenses/gpl-3.0>.

CONTENTS

Acknowledgements	xiii
Disclosures	xiv
Publications during thesis work	xv
I INTRODUCTION 1	
1 INTRODUCTION 2	
1.1 The olfactory world of insects 2	
1.1.1 Features of olfactory stimuli 2	
1.1.2 Olfactory behavior 6	
1.2 Anatomy of the olfactory system 8	
1.2.1 Comparison with other olfactory systems 10	
1.3 ORN responses, adaptation, and gain control 11	
1.3.1 Baseline activity 12	
1.3.2 ORN response phenomenology 12	
1.3.3 Adaptation and gain control 14	
1.3.4 The effect of adaptation on response kinetics 15	
1.4 Studying ORN response and adaptation 17	
II METHODS 20	
2 MEASURING AND CONTROLLING ODORANT STIMULI 21	
2.1 Introduction 21	
2.1.1 Delivering odorants: olfactometer design 22	
2.1.2 Delivering odorants: stimulus waveforms 26	
2.1.3 Measuring odorants 27	
2.2 Results 30	
2.2.1 Modeling the diversity of stimulus kinetics 30	

2.2.2	A simple procedure to calibrate the PID to any odorant	36
2.2.3	How to deliver pulses of odorant with different intensities	40
2.2.4	How to deliver fluctuating odorant signals	43
2.2.5	How to deliver Gaussian odorant signals with different means and variances	45
2.3	Discussion	48
2.3.1	Flux or concentration detectors?	49
2.3.2	Delivering and measuring mixtures of odorants	49
3	BLACK BOX ANALYSIS OF ORN RESPONSES	51
3.1	Linear kernel extraction	51
3.1.1	Spike triggered average and linear filters	51
3.1.2	Regularization	53
3.2	LN Modeling and gain estimation	55
III	EXPERIMENTS	60
4	OLFACTOORY RECEPTOR NEURONS USE GAIN CONTROL AND COMPLEMENTARY KINETICS TO ENCODE INTERMITTENT ODORANT STIMULI	61
4.1	Introduction	61
4.2	Results	64
4.2.1	ORN responses to broadly distributed naturalistic stimuli.	64
4.2.2	ORNs adapt to stimulus background by decreasing gain according to the Weber-Fechner Law	73
4.2.3	Fast variance-dependent gain control in ORNs	78
4.2.4	Mean and variance gain control occur at different stages of odor encoding, and are mechanistically distinct	81

4.2.5	Modularity of gain control at transduction and spiking	84
4.2.6	Despite slowdown in transduction, ORN firing rate preserves timing of odor encounters	89
4.2.7	An adaptive two-state receptor-complex model reproduces Weber-Fechner scaling, slow down of LFP kinetics, and responses to intermittent and Gaussian stimuli.	92
4.3	Discussion	96
4.3.1	The Weber-Fechner Law in olfaction	98
4.3.2	Variance gain control in olfaction	99
4.3.3	Models and mechanisms of ORN response and gain control	100
4.3.4	Dynamic gain control could aid in naturalistic odor detection	102
4.3.5	Invariant firing rate kinetics could improve odor-guided flight behavior	103
4.4	Methods	105
4.4.1	Electrophysiology	105
4.4.2	Fly stocks and genetic strategies	106
4.4.3	Stimulus measurement	106
4.4.4	Odor stimulus generation	107
4.4.5	Numerical Methods	109
4.4.6	Modeling	112
5	THE TETHERED FLY ASSAY	117
5.1	Goals	117
5.2	Results	118
5.2.1	Flight responses to pulses of different odorants	118

5.2.2	Flight responses to pulses with different amplitudes	120
5.2.3	Flight responses to pulses of different durations	123
5.2.4	Trial-to-trial variations in behavioral response	124
5.2.5	A better olfactometer	126
5.2.6	A tale of diminishing responses	129
5.3	Discussion	130
IV CONCLUSION		133
6 CONCLUSION		134
BIBLIOGRAPHY		136

LIST OF FIGURES

Figure 2.1	The olfactometer zoo	23
Figure 2.2	Relying on liquid phase concentrations can bias estimates of neuron response	28
Figure 2.3	Schematic of a typical odorant delivery system	31
Figure 2.4	A model that reproduces the diversity of odorant pulse kinetics	35
Figure 2.5	How to calibrate PIDs to any odorant	38
Figure 2.6	How to reproducibly deliver pulses of odorant with different intensities	41
Figure 2.7	How to deliver fluctuating odorant signals	44
Figure 2.8	Gaussian odorant signals with controlled means and variances	47
Figure 3.1	Extracting linear filters from input and output time series data	52
Figure 3.2	Extracting linear filters from correlated stimuli	55
Figure 3.3	Gain defined using a LN model	59
Figure 4.1	Adaptation and saturation modulate ORN responses to broadly distributed naturalistic stimuli	65
Figure 4.2	Statistics of the ethyl acetate stimulus with naturalistic temporal structure	66
Figure 4.3	Deviations from linearity persist even when filters extracted from Gaussian stimuli are used to project naturalistic stimulus	68

Figure 4.4	Adaptation and saturation modulate ORN responses to broadly distributed naturalistic stimuli	70
Figure 4.5	An NL model cannot reproduce context-dependence of LFP responses to similar-sized whiffs	72
Figure 4.6	ORNs decrease gain with stimulus mean, consistent with the Weber-Fechner Law	74
Figure 4.7	Weber-Fechner Law broadly observed across odor-receptor combinations	76
Figure 4.8	Ability of NL models to reproduce observed change in input-output curves	77
Figure 4.9	ORNs decrease gain with stimulus variance	79
Figure 4.10	Variance gain control in Gaussian stimuli	80
Figure 4.11	Mean gain control occurs primarily at transduction, and variance gain control occurs both at transduction and at the firing machinery	82
Figure 4.12	Mean and variance gain control at transduction and spiking	83
Figure 4.13	Intracellular Calcium increases with odor concentration	85
Figure 4.14	Intracellular Calcium does not change with stimulus variance	86
Figure 4.15	Modularity of gain control revealed by optogenetic stimulation	88
Figure 4.16	Adaptation to the mean slows down LFP, but not firing rate	90
Figure 4.17	Variance gain control does not change response kinetics	91

Figure 4.18	Steady state activity of the two-state receptor model as a function of the stimulus background	
		94
Figure 4.19	A modified two state receptor model reproduces Weber's Law and adaptive slowdown in LFP responses	95
Figure 4.20	Front-end adaptation followed by a LN model reproduces firing rate responses to Gaussian and naturalistic stimuli	97
Figure 5.1	Schematic of the tethered flight assay	119
Figure 5.2	Flight responses to different odorants	121
Figure 5.3	Flight responses to ethyl acetate pulses of different concentrations	122
Figure 5.4	Flight responses to ethyl acetate pulses with different durations	124
Figure 5.5	Trial-to-trial variability in flight responses	125
Figure 5.6	A better olfactometer	128
Figure 5.7	Flight responses to ethyl acetate pulses delivered by olfactometer design #2	130
Figure 5.8	Flight responses to ethyl acetate pulses delivered by olfactometer design #3	131

LIST OF TABLES

Table 2.1 PID calibration techniques used in the literature. [36](#)

ACRONYMS

ab₃A antennal basiconic 3 A

ab₂A antennal basiconic 2 A

cAMP cyclic adenosine monophosphate

DA Dynamical Adaptation

FCD Fold Change Detection

FT-IR Fourier-Transform Infrared Spectroscopy

GC-MS Gas Chromatography - Mass Spectroscopy

HH Hodgkin Huxley

IR Infra red

KS Kolmogorov-Smirnov

LFP Local Field Potential

LED Light Emitting Diode

LN Linear-Nonlinear

MFC Mass Flow Controller

NLN Nonlinear-Linear-Nonlinear

NL Nonlinear-Linear

ORN Olfactory Receptor Neuron

OR Olfactory Receptor

Orco Olfactory coreceptor

PID Photo Ionization Detector

PN Projection Neuron

TFA Tethered Fly Assay

TTX Tetrodotoxin

UV Ultra Violet

WBA Wing Beat Amplitude

WBF Wing Beat Frequency

ACKNOWLEDGMENTS

- My advisor, Prof. Thierry Emonet, for the mentoring.
- Prof. Damon A. Clark, for introducing me to the problem of gain control, and for close support during my thesis work.
- My thesis committee, Profs. Damon A. Clark (chair), Charles Greer and John R. Carlson for their guidance and support during the twists and turns.
- The Yale INP department, especially Carol Russo, for making academic life at Yale a pleasure.
- My colleagues in the Emonet lab, past and present, especially Mahmut Demir, Carlotta Martelli, Yann Dufour, Nicholas Frankel, Amitabha Nandi, Xiongfei Fu, Setsu Kato, and Junjiajia Long, for pushing, pulling, and walking with.
- My colleagues in the Carlson lab, especially Zhe He, Neeraj Soni, Jennifer Sun, Tong-Wey Koh and Karen Menuz, for selfless help and opening their lab to me.
- My partner, Vanessa, for welcome distraction.

DISCLOSURES

- This dissertation was written in partial fulfillment of the requirements for a Doctor of Philosophy degree.
- All of Chapter 4 has been closely reproduced from a manuscript (Gorur-Shandilya S*, Demir M*, Long J, Clark DA[†], Emonet T[†], eLife 2017 ¹).
- All the electrophysiology in Chapter 4 was performed by Mahmut Demir. Some data in Chapter 2 was originally collected by Carlotta Martelli, and was originally published in [113].
- The work shown in Chapter 2 is being prepared as a manuscript for publication (Gorur-Shandilya S, Demir M, Emonet T, in preparation).
- The model shown in §4.2.7 was developed by Junjiajia Long and Thierry Emonet.
- The model shown in §2.2.1 was developed by Thierry Emonet.

¹ *, † (equal contribution)

PUBLICATIONS DURING THESIS WORK

1. Gorur-Shandilya S & Timme M. (2011) *Inferring network topology from complex dynamics*. New Journal of Physics. Available at <http://iopscience.iop.org/1367-2630/13/1/013004>
2. Koh TW, He Z, Gorur-Shandilya S, Menuz K, Larter N, Stewart S & Carlson JR. (2014) *The Drosophila IR20a Clade of Ionotropic Receptors Are Candidate Taste and Pheromone Receptors*. Neuron. Available at <https://www.sciencedirect.com/science/article/pii/S0896627314006230>
3. Raccuglia D, McCurdy LY, Demir M, Gorur-Shandilya S, Kunst M, Emonet T & Nitabach M. (2016) *Presynaptic GABA receptors mediate temporal contrast enhancement in Drosophila olfactory sensory neurons and modulate odor-driven behavioral kinetics*. eNeuro. Available at <http://eneuro.org/content/3/4/ENEURO.0080-16.2016>
4. Gorur-Shandilya S*, Demir M*, Long J, Clark DA[†], Emonet T[†]. (2017) eLife 2017 *Olfactory receptor neurons use gain control and complementary kinetics to encode intermittent odorant stimuli*. Available at <https://elifesciences.org/articles/27670>²).

² *, † (equal contribution)

Part I

INTRODUCTION

INTRODUCTION

1.1 THE OLFACTORY WORLD OF INSECTS

Olfaction — the sense of smell — is a key sensory modality in animals. Airborne chemicals can be transported through the air over long distances, and their detection allows insects to navigate plumes of odors to their source, helping them find food and mates [61, 119, 142]. For example, mosquitoes use their sense of smell to detect a variety of volatile molecules produced by humans and animals, especially carbon dioxide, to find hosts to feed on [134, 171, 175]. Male moths use specialized, exquisitely sensitive neurons on their antenna to detect trace amounts of pheromone released by female moths up to 200 m away and reach them in a few minutes [178]. Insects – either as pests or pollinators of crops – play a large role in human welfare and olfaction plays a key role in their behavior.

The study of insect olfaction spans a number of broad questions across many disciplines. What are the possible chemical signals that can be detected in the environment that insects inhabit? What are the molecules and cells that insects use to sense these signals? What are the challenges in signal detection and how do insects overcome them?

1.1.1 *Features of olfactory stimuli*

An odor stimulus consists of one or more volatilized chemicals (odorants) that are typically of low molecular weight (< 300 Da [143]) trans-

ported from a source through the air to the olfactory organ on an animal. Since odor stimuli, unlike light or sound stimuli, necessitate physical movement of molecules, the dominant feature of an odor stimulus is the identity of the molecules being transported. The number of possible odors is very large, because there exists a large number of odorants that can be volatilized and that can, individually, act as ligands for the olfactory system; and because these odorants can be mixed together combinatorially to create an even greater number of odors that may be perceived differently and convey a different message. However, the fact that all these molecules have to be transported by the air and are detected by insects means that many olfactory stimuli share commonalities regardless of their chemical compositions. A useful approach to describe the diversity of olfactory stimuli is therefore to consider the physical interactions that produce, transport and modify olfactory stimuli.

1.1.1.1 *The physics of the odor environment*

All olfactory stimuli begin by odorant molecules evaporating from some source, like a pollinating flower, or an insect releasing a pheromone. The volatilized molecules that constitute the odor move with the air that surrounds them, and the temporal evolution and statistics of odor signals depends therefore on the movement of the air that they are carried by. Two non-dimensional numbers, the Péclet number and the Reynolds number, are useful descriptors of moving airstreams that can predict the statistics of the odor signals within them.

The Péclet number is defined as the ratio of the advective and diffusive transport rates of a species in a flow. These two rates are determined by the ambient motion of the air and molecular diffusion that occurs by Brownian motion. For most insects that navigate airborne odor stimuli, these two processes occur at very different scales: diffu-

sion is slow and local, and advection is fast and extensive. Thus, the Péclet number is typically large and odorant motion is dominated by advection [142]. This means that the motion of the air cannot be neglected when considering odor signals, and that in many cases, fluctuations in odor signals are correlated with fluctuations in instantaneous flows, a fact that has important consequences for insects whose primary organ of olfaction is co-located with their primary organ of mechanosensation in their antennae. The domination of advection also influences how odor stimuli are delivered to insects in the lab: most odor delivery systems use moving airstreams to deliver odors. Some of these techniques are discussed in Chapter 2.

The Reynolds number is the ratio of the inertial forces to viscous forces within a fluid. It can be used to predict the transition from laminar to turbulent flow, and since the temporal statistics of odor signals are expected to be very different in the two cases, the Reynolds number is an important determinant of the olfactory environment. Insects navigating to an odor source in large Reynolds number environments will experience intermittent, filamentous odor stimuli, as is the case for insects on the wing [30]. Insects navigating low Reynolds environments will experience odor signals that can be closer to smooth gradients [142], which can occur during periods of still air. The temporal statistics of odors in many environments may therefore be very skewed [30]. While a large number of studies have used simple odor stimuli to characterize the behavioral and sensory responses as a function of the identity and intensity of odor stimuli [19, 20, 74], fewer studies have studied how intermittent odor stimuli are encoded by sensory neurons [113, 125], and how they modulate olfactory behavior. In §4.2.1, I present reproducible intermittent stimuli created to mimic the statistics of odors in the conditions described above.

1.1.1.2 Odor plumes

Odor plumes are columns of air that contain a higher concentration of odors created by evaporation of odors from small sources. Due to the large Péclet numbers of flows in ecologically relevant contexts, the chemical nature of the odor does not dominate the statistics of plumes, and plume structure can be considered to be largely independent of its components [119]. Insects can find the source of odor plumes, such as a flowering plant, by navigating up odor plumes, often by flight. Odor plumes are “patchy” or intermittent at short temporal scales and large spatial scales (< 1 s and > 1 mm), and are composed of narrow “whiffs” of odor interspersed with periods of low odor called blanks [142]. These whiffs tend to occur in bursts called “clumps”, and the time between subsequent whiffs, and between subsequent blanks is distributed according to a power law [30].

At a given location, odor plumes are intermittent, and characterized by the absence of a continuous signal at a given intensity. The intermittency of odor plumes is a direct consequence of the motion of the air carrying the odor. Turbulence can cause filaments in odor plumes to become thinner, increase intermittency, and decrease the effective intensity of odor signals in filaments [142]. The Kolmogov length is a measure of the size of the smallest turbulent motions in a flow, and is a function of the wind speed and height above ground, and is typically 1 cm [119].

The location of the odor source can also determine intermittency and temporal structure of an odor plume. *Agave palmeri*, the largest agave species in the United States, produces flowers on stalks that can be as high as 5 m tall, and thus experience large wind speeds; while flowers of the jimsonweed plant, *Datura wrightii*, are close to the ground and experience lower wind velocities [142]. The Reynolds and Péclet numbers are thus very different for odor plumes from these

two flowers, posing different challenges to the insects that find them using olfaction. In addition, wind speed, an important determinant of the temporal structure of odor plumes, can vary significantly over time. Most importantly, the daily rhythm of the sun can change wind speed and atmospheric turbulence dramatically from day to night, offering windows of opportunity to insects like hawkmoths that use periods of low turbulence following sunset to find flowers [142].

1.1.2 *Olfactory behavior*

Olfactory behaviors benefit insects when they lead to a source of food or mates. However, search strategies vary across insects, based on the size of the insect, the quality, reliability and volume of the olfactory signal, the environment they search in, and the range of sensors available to them.

An optimal strategy for small insects (whose body size is smaller than the length scale of the plume) has been suggested to be to fly crosswind; and for large insects to fly up and downwind; till contact is made with an odor plumes [28]. Pheromones produced by female moths are an unambiguous and loud signal for male moths, given the specificity of the pheromone to moths and the sensitivity of antennae of male moths to that pheromone [90]. Mosquitoes that sense carbon dioxide to find hosts must do so despite ambient carbon dioxide in the atmosphere, and carbon dioxide released from non-host sources [171]. Search strategies in these two cases are likely different.

Because odor stimuli are carried by the air, and because Péclet numbers are typically large, odorant stimuli may be correlated with changes in airspeed. In fact, in insects, the antennae are both olfactory and mechanosensory organs, and are actively positioned during flight [112]. Flight is advantageous in navigating olfactory landscapes,

as it allows insects to sample odor plumes in the air, far from surfaces, and flight is fast [172], allowing for rapid movement towards the source of odor [49]. However, flight brings its own challenges: while walking, it is easy to determine airspeed and walk upwind, as relative motion of air is likely due to wind. Walking up airstreams to sources of odor can therefore be realized using just mechanosensation. However, upwind flight is more complicated, as wind speed and direction have to be deconvolved from the self motion of the insect. Typically, insects use multi-sensory fusion to solve this problem, pooling information from visual cues and other mechanosensory organs [49, 57, 66].

Heading upwind is not sufficient to reliably find sources of odor, since plumes typically become narrower closer to the source [119, 121]. This means that the same error in positioning is more likely to move an insect outside the plume closer to the source than farther away from it. Casting, an iterative zigzag flight pattern that progressively widens crosswind at the expense of upwind progress, is a behavior used by many insects to navigate to odor sources, as it enhances the likelihood of directly making contact with the plume as the cast widens [21]. It can also act to maintain the position of the insect relatively constant crosswind till the plume shifts back to the insects position [41].

The set of sensors available to an insect allows it to use a variety of strategies to find sources of odor. Insects have a pair of antennae, and can measure the difference in odor concentrations across left and right antennae [62]. Insects can use osmotropotaxis, a behavior where insects turn towards the side that has higher concentration, during walking [15] and flight [48]. Olfactory behavior is likely high multimodal, integrating information from olfactory, visual and mechanosensory systems. Odor localization by *Drosophila* has been

shown the require visual feedback [59], and the behavioral response of flies is a linear superposition of both visual and olfactory inputs [58].

The primary challenge in studying olfactory behavior is measuring the behavior of the insect together with the stimulus that it detects. One technique is to let insects fly freely in wind tunnels, where well-controlled flows constrain odors to a known volume of the wind tunnel, and the position of the insect can be used to estimate the stimulus it encounters. Such an approach, combined with 3-D tracking of the insect, has been used with moths [144, 176] and *Drosophila* [59]. An alternative approach is to tether the insect, either to a rotatable or fixed pin, and present controlled odor stimuli to the insect. Such an approach has identified behavioral responses to a variety of monomolecular and complex odors, either combined with visual stimuli [34, 35, 48, 58, 101], or in darkness [13]. Chapter 5 describes attempts at using a tethered fly assay to determine how olfactory stimuli modulate flight behavior.

1.2 ANATOMY OF THE OLFACTORY SYSTEM

The fruit fly, *Drosophila melanogaster*, has been the system of choice for many studies on insect olfaction. The focus on *Drosophila* stems from several reasons: (i) it is easy to grow and maintain in laboratories, with a short generation time; (ii) its genome has been sequenced, and a large variety of genetic tools are available for *Drosophila*; (iii) its olfactory system is similar to other insects, and even to vertebrates in rough organization, though numerically simpler. The olfactory anatomy of *Drosophila* also loosely resembles the circuitry of visual processing [181]. While the olfactory anatomy of *Drosophila* is

described in the following section, many features are common to the olfactory system of other insects.

The primary olfactory organs in *Drosophila* are the antennae and the maxillary palps. The antennae are not just olfactory organs but are also organs of audition and mechanosensation. The olfactory functions of the antenna are localized to its third segment, which are covered in fine sensory hairs called sensilla. Sensilla are also present on the maxillary palp. Based on their morphology, sensilla can be divided into three types: basiconic (10 functional types), coeloconic (4 types) and trichoid (4 types) [154]. Based on identified ligands, basiconic sensilla largely respond to volatile food odors; coeloconic sensilla largely respond to amines, humidity and a few food odors; and trichoid sensilla respond to volatile compounds and pheromones from other flies, like cis-vaccenyl acetate [37]. The antenna has all three types of sensilla, that exhibit some degree of grouping on the surface [155], while the maxillary palp only has basiconic sensilla. The structural and functional organization of sensilla into these groups is similar in other insects [18].

Each sensillum contains the dendrites of 2 (sometimes up to 4) different primary sensory neurons, called Olfactory Receptor Neurons (ORNs). In *Drosophila*, there are ~1320 ORNs in each antenna [71]. The sensillum also contains a lymph that the dendrites of ORNs are surrounded by, and contains pores, grooves or other opening based on the type of sensilla through which odor molecules enter the sensillum, diffuse through the lymph, and reach the neuron [154, 155]. ORNs appear to be generic, with little functional specialization between ORNs [181]. What gives a ORN a particular response profile, and connectivity appears to be the specialized receptor that it expresses [74].

Receptors in ORNs can belong to one of three families: the *olfactory receptors* (ORs), of which there are around 60 types; the *gustatory receptors* (GRs), and the *ionotropic receptors* (IRs). ORNs in basiconic sensilla mostly express one OR, together with the olfactory co-receptor Orco that together make a ligand-gated ion channel [102, 180]. Some ORNs in basiconic sensilla express the GRs GR21a and GR63a, that are unusual among GRs in their expression on the antenna, and mediate responses to carbon dioxide. Most coeloconic sensilla express IRs.

While ORNs that express the same OR can be housed in sensilla that may be distributed across the antenna, their output is pooled in a remarkable structure that organizes the axon terminals of ORNs by the receptor they express called the glomerulus [78]. All ORNs that express the same OR project to one out of ~60 glomeruli in the antennal lobe, where they make synaptic contact with second order neurons called Projection Neurons (PNs). Typically, a single glomerulus pools ORs of a single type, though there are exceptions in some specialized glomeruli. For example, in male moths, ORs that detect different components of a pheromone are pooled together in a single glomerulus [75].

1.2.1 Comparison with other olfactory systems

The olfactory system of *Drosophila* exhibits many similarities with that of other insects, and even with the mammalian olfactory system. Both the mammalian and the insect olfactory system use several primary olfactory organs: mammals' primary olfactory organ is the olfactory epithelium in the nose, but also include the vomeronasal organ, the Gureneberg ganglion, and the septal organ of Masera [167]. The insect olfactory system is distributed across the antennae and the maxillary palp. The overall cellular structure of the olfactory system is

also similar, where primary sensory neurons (ORNs) express olfactory receptors, and ORNs that express the same OR project to the same glomerulus.

Insect olfactory systems differ from mammalian olfactory systems in many ways. Primarily, they are much smaller, and numerical less complex. While *Drosophila* have only ~60 olfactory receptors [71, 177], and mosquitoes ~80, humans have around ~350, and mice over 1000. The gross anatomy of the olfactory system is very different between insects and mammals, that has important consequences on their function. In insects, ORNs are housed in sensilla on external organs, where they can directly sample volatile ligands the air without any intermediate step. In mammals, respiration and the housing of the ORNs within the nose means that mammals sniff in order to smell. While this has the advantage of giving a degree of control over the flow of olfactory stimuli over ORNs, it also means that mammalian ORNs are locked to the kinetics of respiration. Recent studies have begun to uncover the consequences of this coupling [139, 158, 161].

1.3 ORN RESPONSES, ADAPTATION, AND GAIN CONTROL

The response of ORNs to odorants occurs in two stages. First, odor binding induces transduction, which leads to an inward current from the sensillum lymph to the dendrite of ORNs. This transduction current can be detected by changes in the Local Field Potential (LFP) in extracellular single-sensillum recordings. Transduction leads to action potential generation, and spikes generated at ORNs propagate down the axon to glomeruli, where they activate downstream neurons.

1.3.1 *Baseline activity*

All ORNs fire spontaneously, even in the absence of any ligand. Mutating a ORN's odorant receptor changes the baseline firing rate [127], suggesting that baseline spiking of ORNs may be a consequence of receptors being active even when there is no ligand. Different ORNs have different characteristic spontaneous firing rates; for example, the ab₃B ORN has a relatively high spontaneous firing rate (~10 Hz), while the ab₂B ORN has a very low one (< 2 Hz). The diversity in spontaneous activity may reflect a diversity in the equilibrium constants between different receptors in these neurons [182]. This is supported by the fact that expressing novel receptors in ORNs changes not only their response profile but also their spontaneous activity levels [72, 74]. No clear explanation for the baseline activity of ORNs currently exists, though several possibilities have been proposed. The partially active state of receptors with no ligand might make them more sensitive to small stimuli, or the small but non zero activity of the neuron might keep the ORN's membrane potential close to its spike threshold, making it easier and faster to respond to signals [182]. On the other hand, it might not be possible to evolve odorant receptor systems that are entirely inactive when unbound, and spontaneous activity of receptors and ORNs might be an unavoidable price to pay.

1.3.2 *ORN response phenomenology*

Despite being housed in sensilla that are exposed externally, ORNs are difficult to record from as they are small, and protected by a thick and hard-to-breach cuticle [177]. One of the first attempts to record from ORNs directly using patch clamp electrophysiology reported a low yield, and involved a preparation that dissected the antennae,

that made it hard to know the identity of the neuron being recorded from [47]. An improvement of the technique involved slicing the antenna into thin sections, and recording from flies where ORNs of interest were genetically labelled, allowing identification and targeting of individual ORNs of known type [26]. However, this approach involved introducing odorant stimuli in liquid phase, which is not natural, and reported oscillatory responses to pulses of odorant, which have not been observed using other techniques.

The most common technique to record from ORNs is to use single sensillum extracellular recordings [19, 20, 125]. In this technique, a recording electrode is introduced into the sensillum of an immobilized *Drosophila*. This technique can record spikes from both ORNs in the sensillum, and can also record the LFP, which has been used a measure of the transduction current in the sensillum. All the results presented in Chapter 4 use this technique.

The large diversity in ORs leads to diverse response of ORNs to odor stimuli. Most ORNs respond to multiple ligands, and many ligands activate multiple ORNs [74, 100]. Increasing the concentration of the applied ligand has two effects. First, ORN response amplitudes increases sigmoidally with the log of the concentration [19, 20, 113]. Second, more ORNs expressing different ORs start responding to the ligand, as ORNs are more broadly tuned to large stimuli, presumably due to the increasing effects of non-specific activation of ORs by ligands [182].

1.3.2.1 Odorant transduction

Odorant transduction can be fast, with initiation within milliseconds of odor reaching the antenna [170]. Transduction currents integrate temporally over brief stimuli, with more prolonged stimuli leading to larger responses [26]. Long pulses of odorant induce a rapid in-

crease in transduction responses, followed by decay to some steady state value. These responses have been observed both using the LFP as a proxy for transduction [19, 20, 125], and by direct patch clamp measurements [26]. ORNs which express two different receptors, one native and one mis-expressed, and which are activated by two ligands that activate the two receptors independently show cross-adaptation between receptors, suggesting that adaptation state affects the entire neuron [125].

1.3.2.2 Spiking

Odor transduction leads to spike generation in the ORN. Spikes are elicited preferentially by the rate of change of transduction, rather than simply by the magnitude of transduction [125, 181]. This means that the firing rate to a pulse of odor peaks when transduction rises rapidly, and is suppressed below baseline when transduction currents fall back to baseline. The transformation of transduction currents to firing rates is therefore partially derivative taking [125], which means that ORN spike rates encode both the magnitude of the stimulus and its derivative [96].

1.3.3 Adaptation and gain control

Adaptation is a process by which the encoding of odorants in ORN responses is modified, usually in response to a change in local stimulus statistics. These modifications are *adaptive* in the sense that they may encode the stimulus more efficiently, or make use of the response range more effectively.

The term “adaptation” has been used to refer to a wide variety of phenomenon in ORN response kinetics:

- A. the decrease in response following an initial transient on a step change in stimulus [25, 26, 125].
- B. the decrease in responses to brief test pulses following previous, identical, pulses [26]
- C. the decrease in response to brief test pulses following longer conditioning pulses [20, 125]
- D. the decrease in response to brief test pulses presented on a background, *vs.* those presented without a background [25, 26, 113]

This wide range of phenomenon reflects the variety of different experimental assays designed to probe adaptation, and it is not clear if these disparate phenomenon are different manifestations of the same underlying mechanisms. In this dissertation, I use a Linear-Nonlinear (LN) model to quantify and describe ORN responses to odorant stimuli. Using this phenomenological model lets me describe adaptation as any change in the parameters of the best-fit LN model, similar to the approach used by earlier work that studied the response and adaptation of visual cells [6]. Since the LN model consists of two modules, a linear filter and a static output nonlinearity, adaptation can change either the kinetic properties of the response, or it can change the output nonlinearity. Changes in the slope of the output nonlinearity are defined to be changes in the gain of the system. Thus, gain control is a consequence of adaptation.

1.3.4 *The effect of adaptation on response kinetics*

Adaptation can also change the kinetic parameters of the best-fit LN model. Many sensory systems adapt in a manner that changes both the gain and the kinetics of the response. Specifically, decreases in gain typically speed up the kinetics of the system. Such a gain-speed

tradeoff is seen in photoreceptors (see [36] for a summary), and is a consequence of simple rules that govern responses of cells [153], as shown in the following. Consider the activity of a simple sensory cell that updates its response based on some stimulus $S(t)$ and its own response $r(t)$:

$$\tau \frac{dr}{dt} + r = Fr + S \quad (1.1)$$

where τ is the time constant of its response and F is a parameter that defines how the response depends on its current value. When $F = 0$, the cell behaves like a low-pass filter acting on the stimulus, and does not adapt in any way. When $F > 1$, the system is unstable, and the response diverges due to runaway feedback. When $F < 1$, the system is stable, and eq. 1.1 can be rewritten to be

$$\frac{\tau}{1 - F} \frac{dr}{dt} + r = \frac{S}{1 - F}$$

This reformulation allows us to identify terms that correspond to the steady state gain ($1/(1 - F)$) and the effective timescale $\tau/(1 - F)$, making it clear that increases in gain necessarily lead to decreases in effective timescale, thus recapitulating the gain-speed tradeoff. Such a tradeoff is seen in many models of sensory cells [36, 125, 152].

However, the effect of adaptation on ORN transduction kinetics cannot be reproduced by this formulation. In ORNs, transduction kinetics slows down with adaptation, a result observed both with extracellular LFP recordings [125] and with patch clamp recordings [26]. This suggests that the adaptation mechanisms in ORNs cannot be reduced to a simple linear formulation as in eq. 1.1, which may be related to the fact that ORNs are unusual among sensory neurons in that they are activated by chemical ligands, implying strong front-end nonlinearities arising the receptor binding and activation. Intrigu-

ingly, the kinetics of firing rate responses display some invariance to the stimulus amplitude and background [113], a result that is seemingly in contradiction to the earlier results arguing that adaptation slows down transduction responses. ORN responses whose kinetics are invariant to stimulus amplitude or background could preserve the timing of odor encounters in neural encoding, a feature that may be critical to some search strategies and may aid in navigating odor plumes (as discussed in §1.1).

1.4 A MULTIDISCIPLINARY APPROACH TO STUDY ORN RESPONSE AND ADAPTATION

Arising from the literature surveyed above, I identify the following areas of interest:

- A. **ORN ADAPTATION.** Given the wide range of statistics of odor signals that insects might encounter (as discussed in §1.1), how do ORNs change their encoding rule with the stimulus background? What features of odor stimuli induce adaptation? How quickly can ORNs adapt? How similar is adaptation in ORNs to adaptation in other sensory cells?
- B. **TIMING OF ODOR ENCOUNTERS.** The time of odor encounters may be useful for olfactory search strategies. However, several studies have suggested that adaptation at transduction slows response kinetics. Intriguingly, the kinetics of firing rate responses display some invariance to the stimulus amplitude and background. Can ORNs preserve the timing of odor encounters in their response? How can this information be preserved despite transduction kinetics that depend on adaptation state?

To address these questions, it is first necessary to assemble a number of techniques, practical, conceptual and numerical: electrophysiological tools to record from *Drosophila* ORNs, genetic tools to express proteins in cells of interest, apparatus to control and measure odorant signals precisely, and linear-nonlinear modeling to quantitatively describe the features of ORN response. These techniques borrow extensively from various fields: neuroscience, engineering, applied mathematics and genetics. While many of these techniques and tools have been long established, some of them are novel, and combining them as I have in this dissertation permits me to ask and answer novel questions about odor encoding in *Drosophila*.

In Part II, I describe the methodology and tools that lets me answer these questions experimentally. The rich diversity of odor stimuli that insects likely encounter in their natural environment (§1.1) is in sharp contrast to the simple stimuli often used in experiments. While there exist several legitimate reasons to use simple stimuli, practical difficulties in measuring and controlling odor stimuli have long hindered researchers from using more complex stimuli, like those that exist in the turbulent environments of insects. Chapter 2 details techniques to deliver odorant stimuli to animals in olfactory systems, with a novel technique to measure the absolute flux of odorant that is being delivered. The novel methods described in this chapter let me deliver pulses of various amplitudes, fluctuating stimuli, and Gaussian stimuli with controlled means and variances. In Chapter 3, I present numerical methods to analyze time series data of inputs and outputs from a system, e.g., the dual time series of odorant stimulus presented to a ORN and its firing rate responses. I describe how Linear-Nonlinear (LN) modeling lets me quantitatively describe the response and adaptation properties of systems solely from time se-

ries data, without necessitating a detailed knowledge of the inner mechanisms of that system.

In Part III, I describe experimental results from *Drosophila* ORNs and behavior. In Chapter 4, I will describe experiments studying how *Drosophila* ORNs respond and adapt to naturalistic and Gaussian stimuli with controlled means and variances. I will show that *Drosophila* ORNs can vary their gain on rapid timescales in response to naturalistic stimuli, and that they decrease their gain with the mean stimulus (following the Weber-Fechner law) and with the variance of the stimulus. I will also show how adaptation in these ORNs changes the kinetics of transduction, but that complementary mechanisms preserve the timing of odor encounters in the firing rate of these ORNs. This result resolves apparent contradictions between recently published studies from our lab [113] and elsewhere [26, 125]. In Chapter 5, I describe the development of an assay to probe how various features of olfactory stimuli modulate the flight behavior of tethered *Drosophila*. Pitfalls encountered while using this assay are described, together with potential workarounds, as a reference for future researchers considering this assay for their experiments.

Finally, in Part IV, I bring together the results described earlier to examine the impact of this dissertation on future research on these topics. My goal here is to present these results in a framework that will be useful for the study of other systems, sensory and otherwise.

Part II

METHODS

MEASURING AND CONTROLLING ODORANT STIMULI

2.1 INTRODUCTION

The study of sensory neurons, especially primary sensory cells, requires the ability to precisely control and measure the stimulus applied. In the study of vision and audition, the ease of generation and measurement of light and sound stimuli have led to a detailed understanding of how primary visual and auditory neurons encode visual and auditory stimuli. Olfactory stimuli are harder to deliver than sound or light, and even harder to measure. This is because olfactory stimuli consist not of energy but of small, volatile molecules of bewildering variety that have to be mechanically transported from the source, typically through the air, to the Olfactory Receptor Neuron ([ORN](#)). Furthermore, odorant molecules interact extensively with their environment, including during transport from the odorant source to the sensory neuron. These interactions, that depend on odorant identity, have been shown to result in a diversity of temporal structures of identically delivered stimuli, that can affect the response kinetics of receptor neurons [[113](#)].

In this work, we put forward methods to deliver and measure odorant stimuli that can be used by researchers studying olfaction. These methods do not require any bespoke hardware; instead, they rely on two off-the-shelf components (a fast Photo Ionization Detector ([PID](#)) and a Mass Flow Controller ([MFC](#))) to construct flexible odorant deliv-

ery systems that can deliver i) reproducible pulses of odorant at various intensities (§2.2.3) ii) fluctuating Gaussian stimuli with controlled means and variances (§2.2.5). We also introduce a simple procedure to calibrate the PID to any detectable odorant without using any additional equipment (§2.2.2). The focus of this work is on experimental applications where changes in airspeed do not significantly affect the response properties of ORNs, for example, in *Drosophila* ORNs [187], and to deliver monomolecular odorant stimuli.

2.1.1 Delivering odorants: olfactometer design

There exists a variety of methods of delivering odorants. Figure 2.1 shows a sample of the zoo of olfactometers (devices for delivering odorants) that have been developed to deliver odorants in experimental preparations. While the full assortment of olfactometers is too rich to comprehensively survey here, all olfactometers can be classified into a few basic types based on:

- A. **VALVE POSITION.** A valve is typically used to turn airstreams on or off. Is this valve upstream or downstream of the odorant?
- B. **AIRSPED CHANGE.** Does delivering the odorant lead to a change (typically an increase) in the airspeed at the outlet?
- C. **ODORANT PHASE.** Odorants can be in liquid phase, pure or diluted, or can be contained on a solid substrate like a filter paper.

These design decisions come with intrinsic tradeoffs. Positioning the valve upstream of the valve means that no odorant is directly in contact with the valve, and that in principle, the valve is not contaminated by the odorant¹ (Fig. 2.1a). This has led previous work to

¹ However, odorants can diffuse when there is no flow, contaminating valves upstream of odorants

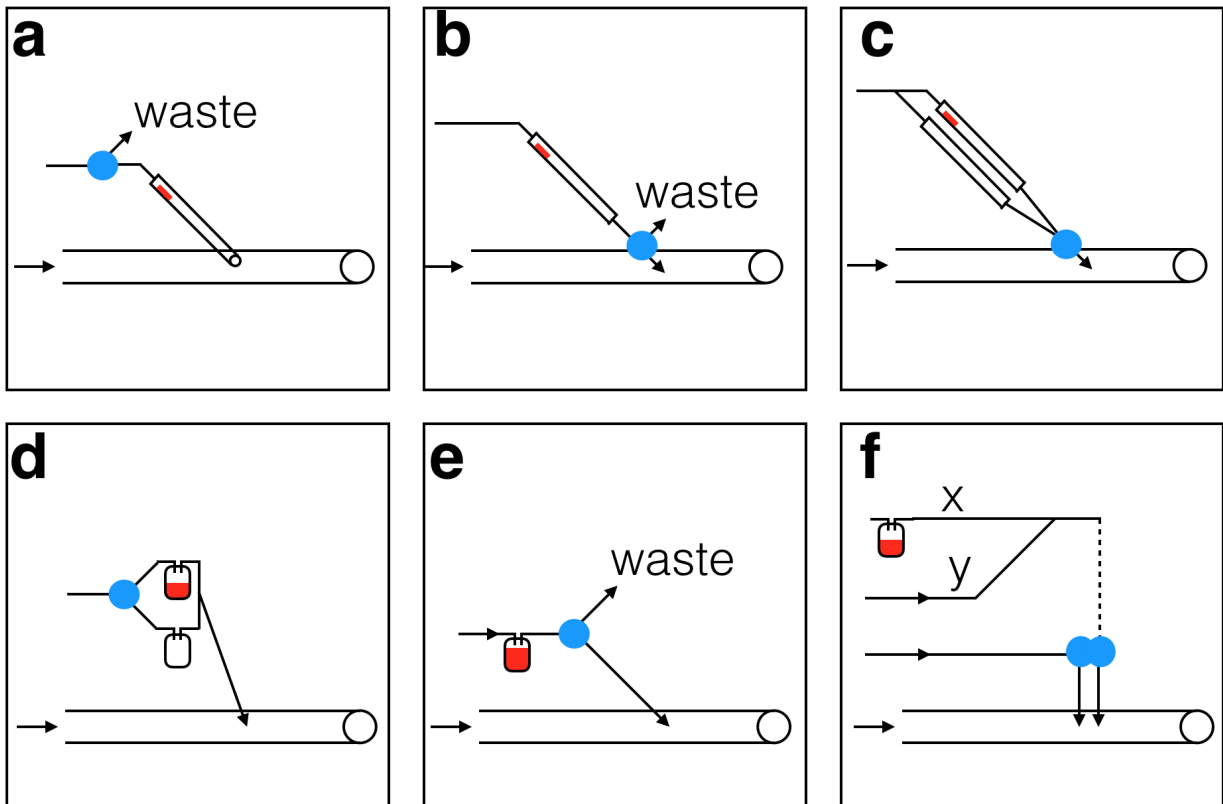


Figure 2.1: *Different olfactometer designs used in the literature.* (a) The “cartridge” system, as used in [73, 76, 103, 116]. Odorant is in liquid phase, on a filter paper disk, within a Pasteur pipette. The valve is upstream of the odorant. A valve upstream of the odorant forces. (b) A design similar to (a), but with the valve downstream of the odorant, as in [55, 149–151]. (c) A design similar to (a), but with two pipettes to minimise airflow changes on valve switch, as in [170]. (d) In this design, odorant is stored in a scintillation vial, allowing greater volumes of odorant. An upstream valve delivers either odorized air or clean air to the preparation, as in [68, 96, 131]. (e) In this variant, the odorant containing vial is filled almost to the top with odorant, minimizing the headspace, making it replenish quickly, as in [125]. (f) In this design, an odorized airstream x is mixed with a clean airstream y and passed through a capillary (dotted line). A dual valve switches simultaneously between two airstreams and waste, keeping airspeeds invariant with valve state, as in [70, 139, 158]. In all panels, the valve is shown in blue, the odorant in red, Pasteur pipettes as narrow rectangles, scintillation vials as rounded rectangles, the main air delivery tube as a hollow tube, and other tubes as lines.

use a single valve with many different odorants, lowering cost and speeding up the process of delivering several different odorants [20, 73]. In this configuration, air flows over and depletes the odorant *only* when the stimulus is being delivered. This has the advantage of conserving odorant, as all odorant that enters gas phase is delivered to the preparation, a feature that could be useful when small quantities of odorant are used, for example, when the odorant is expensive or hard to produce, like a pheromone. Positioning the valve upstream of the odorant also necessarily introduces transients in the signal, as the odorant-vapor system is never at steady state. On the other hand, positioning the valve downstream of the odorant (2.1b, c) means that the odorant flows through the valve, necessitating using a different valve for every odorant to avoid cross-contamination. The costs of choosing to place valves downstream of odorants, both of material and time, can be significant if hundreds of odorant-receptor combinations are to be tested, as in [73, 74, 100, 114]. Since the valve is downstream of the odorant, air always flows over the odorant, and the valve diverts this odorized airstream either to waste (normally), or to the preparation. While this design consumes more odorant, the liquid odorant in its chamber can reach steady state with the vapor in the chamber, and the state of the valve downstream of the odorant does not disturb this equilibrium, which could lead to more reproducible stimuli.

The topology of the olfactometer also determines whether diverting the odorized airstream into the main airstream necessarily leads to changes in the airspeed of the main flow. Unless explicitly compensated for, introducing a new channel into the main airstream will increase the airspeed at the outlet, which may be undesirable for some organisms or experiments. A simple way to compensate for this increase in the airstream is to use another valve to switch between an additional clean airstream and the odorized stream, as in Fig. 2.1d.

Special valves with two inputs and outputs are typically used, as pairing two valves is often impractical due to variations in the resistances from valve to valve, that make symmetric switches hard to achieve (Fig. 2.1f).

Odorants are typically diluted in mineral oil or paraffin oil, since odorants evaporating from paraffin oil are believed to exhibit a linear relationship between their liquid and gas phase concentrations [17]. Traditionally, serial dilutions of odorants have been prepared in paraffin oil, and small quantities of these mixtures have been applied to filter paper disks in glass Pasteur pipettes [37]. “Cartridges” so prepared contain odorant in the gas phase that evaporates from the filter paper disk, and are typically used in conjunction with a valve before the cartridge, that pushes the odorized air towards the preparation [20, 73]. An alternative is to use a vial containing a larger quantity of the diluted odorant liquid, either with a very small headspace (Fig. 2.1e), as in [125], to ensure that the headspace gas phase concentration is dominated by the bulk of the liquid odorant, or with a larger headspace, as in [96], to create a large volume of odorized air that can be pushed towards the preparation (Fig. 2.1d).

Diluting odorants in liquid phase using mineral or paraffin oil leads to intrinsic non-reproducibility, since every passage of air over the mixture depletes the liquid phase concentration of the odorant and the diluent at different rates. In the extreme case, mineral oil and paraffin oil are practically nonvolatile and every passage of air over the oil-odorant mixture depletes the odorant but not the diluent. Since the gas phase concentration of odorant in the headspace depends on the liquid phase concentration of odorant in a region close to the boundary layer, the gas phase concentration of the odorant continuously decreases with time. One way to ameliorate this depletion is to use a very large volume of odorant mixture, and to stir

the mixture continuously [113]. Stirring expands the effective boundary layer of the mixture, and enables the gas phase concentration of the headspace to track the liquid phase concentration more closely. However, stirring odorants may be impractical in some applications, especially in the cramped and electrically sensitive environment of an electrophysiology rig, and doesn't ultimately solve the problem of odorant depletion.

2.1.2 *Delivering odorants: stimulus waveforms*

Odorant stimuli can be defined by their chemical identity, amplitude and temporal structure. The choice of odorant, and their concentration define the first two features. Pulses of odorant have been used as a common stimulus waveform [37, 102], as they are easily generated by briefly turning on a valve that directs odorized air to the preparation. These simple stimuli reveal whether the neuron of interest responds to the odorant tested or not, and can also reveal the kinetics of response [20, 74].

More complicated stimuli are difficult to generate due to two reasons: (i) the non-uniform rates of evaporation of volatile odorants makes delivering long stimuli challenging and (ii) a valve has only two positions, on or off, limiting the temporal structure of the odorant stimulus. Various studies have worked around these limitations to deliver more complex odorant stimuli. Using large volumes of liquid odorant and stirring to fight depletion, some studies have used a valve to randomly turn on and off an odorant airstream, generating a random binary signal that has been used to characterize the response properties of ORNs [55, 113, 125, 150]. While stimuli generated this way are typically bimodal, corresponding to on and off states of the valves, unimodal stimulus distributions can be achieved

with combinations of valve switching time and some odorants with slower intrinsic kinetics [113]. Other studies have used custom-made olfactometers using computer controlled MFCs to generate triangular, staircase and Gaussian stimulus waveforms [95, 96]. However, there exists no easily-reproducible method to realize complex odorant waveforms using easy-to-acquire hardware.

2.1.3 Measuring odorants

Light can be measured by cameras and sound by microphones, and the sensitivity and range of these electronic sensors can exceed that of the human eye or ear. However, no equivalent electronic “nose” has been developed. Therefore, measuring odorants is not standard practice in olfactory research. One of the earliest attempts to measure odorant stimuli used gas-chromatography on the headspace [83]. Though cumbersome, slow and expensive, gas-chromatographic techniques are still useful, especially in studies of the chemical ecology of olfactory animals, and coupled with presentations of many odorants eluted from a single, natural odor source [51].

Another approach is to use a visible tracer and measure the stimulus optically. While this is an indirect measure, and is not informative of the absolute amount of odorant, it can reveal the spatial and temporal pattern of odorant stimuli, and has been used in applications where the precise timing of odorant stimuli is key [170]. Another optical method is to use Fourier-Transform Infrared Spectroscopy (FT-IR). This method has been used to measure the gas-phase concentration of known odorants from their absorption using the Beer-Lambert law [108, 152].

An increasingly common measurement technique is to use a PID to measure odorant stimuli in the gas phase. First used in olfac-

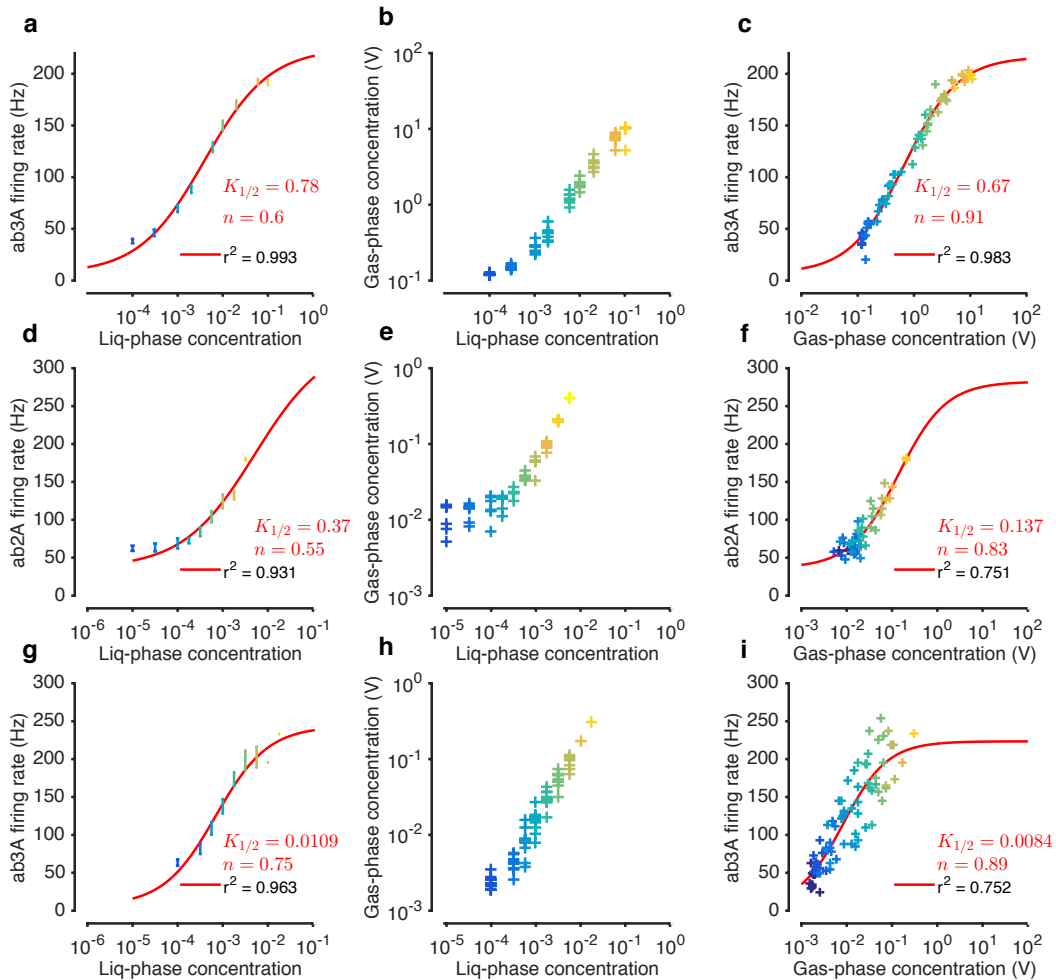


Figure 2.2: Relying on liquid phase concentrations can bias estimates of neuron response. (a) Dose-response curve of ab3A responding to pulses of ethyl acetate stimulus, plotted as a function of the concentration in liquid phase. Red line is best fit Hill function, and text shows the parameters of the best fit. (b) Gas phase concentration *vs.* liquid phase concentration, showing variability and non-linearity in mapping between liquid-phase and gas-phase concentration. (c) Dose-response curve of ab3A plotted *vs.* gas phase concentration. Red curve is the best fit Hill function. (d-f) Similar plots for ab2A responses to pulses of methyl butyrate. (g-i) Similar plots for ab3A responses to pulses of 1-octen-3-ol. Note that the best-fit parameters are different in the first and third columns. In all plots, values of $K_{1/2}$ are reported in V.

tory research to measure the pheromone intensity delivered to moths, they have been used in a variety of roles, including for concentration control in an olfactometer [86]. The PID works by sucking odorized air into a small chamber, where a Ultra Violet (UV) light ionizes molecules in the sample. These ions set up a current between two charged plates, which is converted into a voltage and reported by the instrument. We use a PID in this study to measure odorant stimuli, as it is a fast, approximately linear, and general-purpose instrument that is easy to use.

While it is commonplace in olfactory studies to not measure the stimulus, and to compare responses to liquid-phase dilutions of the odorant [19, 74, 103, 183], measuring the stimulus presented to ORNs is key to quantitatively describing their response, and relying on liquid phase concentrations can bias characterizations of their response phenomenology. For example, consider a typical dose-response experiment where ethyl acetate stimuli of varying concentration are presented to a ab₃A ORN. Peak ORN responses exhibit a sigmoidal relationship with the log of the liquid phase dilution (Fig. 2.2a). However, simultaneous measurement of the stimulus using a PID (Fig. 2.2b) reveals that (i) the stimulus is variable from trial to trial and (ii) the gas phase concentration is not linear with the liquid phase concentration, as assumed in Fig. 2.2a. Plotting the peak ORN response *vs.* the measured gas phase concentration reveals the true dose-response curve (Fig. 2.2c). Fitting Hill functions to the curves in Fig. 2.2a and fig. 2.2c yield different parameters, suggesting that relying on liquid phase dilutions as a proxy for gas phase concentration can bias estimates of ORN response, even in this simple case where odorant and ORN kinetics are neglected.

2.2 RESULTS

2.2.1 Modeling the diversity of stimulus kinetics

A common method of delivering odorants is to prepare “cartridges” from Pasteur pipettes containing $50 \mu\text{L}$ of odorant diluted in Paraffin Oil on a small filter paper disk, and to force a small volume of air through the cartridge. Odorants delivered this way exhibit a broad range of stimulus kinetics (Fig. 2.2.1), that depend on the chemical identity of the odorant [113]. Since the conditions of the delivery are identical across odorants, we reasoned that the origin of the diversity of stimulus kinetics is variation in the interactions of the odorant with the surfaces of the delivery system, and simple physical properties of the odorants like their vapor pressure. We therefore set out to develop a simple model of odorant evaporation from the filter paper, interaction with the surfaces of the delivery system, and transport by the air flowing through the delivery system.

Consider a typical delivery system, where a main airstream blows clean air onto the preparation/PID, while a smaller airstream introduces odorized air into the main airstream when a valve is activated. Such a device corresponds to the design shown in Fig. 2.1a and is shown schematized in Fig. 2.3. Clean air flows through main delivery tube at a flow rate Q_2 . A small filter paper disk containing odorant diluted in Paraffin Oil is located in tube 1 (the Pasteur pipette), at a length L_1 from the main air tube. For simplicity, we assume that the internal radius of both tubes is the same, R . When the valve is activated, air flows through tube 1 with rate $Q_1 < Q_2$. The junction between the two tubes is at a distance L_2 from the outlet of the tube, where the preparation/PID is located.

We define the following terms:

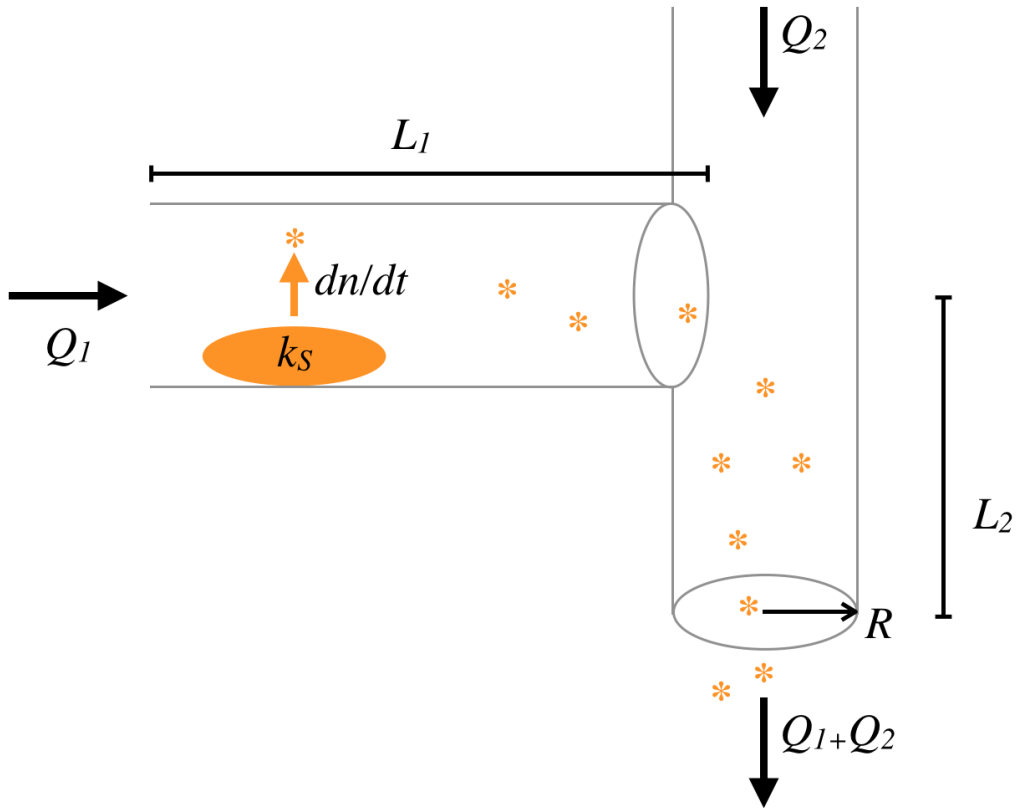


Figure 2.3: Schematic of a typical odorant delivery system. Clean air flows through main delivery tube at a flow rate Q_2 . A small filter paper disk containing odorant diluted in Paraffin Oil is located in tube 1, at a length L_1 from the main air tube. For simplicity, we assume that the internal radius of both tubes is the same, R . When the valve is activated, air flows through tube 1 with rate $Q_1 < Q_2$. The junction between the two tubes is at a distance L_2 from the outlet of the tube, where the preparation/PID is located.

- \tilde{c}_1 and \tilde{c}_2 are the concentrations of odorant in gas phase in tube 1 (the Pasteur pipette) and tube 2 (the main delivery tube)
- $w\theta_1$ and $w\theta_2$ are the surface concentrations of odorants bound to tubes 1 and 2; w is a material constant describing the density of binding sites on the glass, and θ_1 and θ_2 are the surface coverages for tubes 1 and 2 ($\theta_{1,2} \in [0, 1]$).
- \tilde{n} and \tilde{n}_p are the amount in moles of odorant and paraffin oil in liquid phase.
- $q(t)Q_1$ and Q_2 are the flow rates in the pipette and the delivery tube, where $q(t) = 1$ when the valve is on, and is 0 otherwise.
- A_1, A_2, V_1 and V_2 are the surface areas and volumes of the pipette (1) and delivery tube (2).
- A_S is the surface area of the filter paper, assumed to determine the surface area of the odorant

At the boundary between the liquid on the paper filter and the air, the gas phase concentration is at steady state with the liquid phase and $\tilde{c}_1|_{surface} = c_S \gamma(x)x$, where the molar ratio in liquid phase is $x = \tilde{n}/(\tilde{n} + \tilde{n}_p)$ and $c_S = P_S/Pc_a$ is the saturated vapor concentration where P is the air pressure and $c_a = P/(RT)$ is the concentration of air. The rate of evaporation $-\dot{\tilde{n}}$ depends on the gradient of the concentration in gas phase above the paper filter, which in turn depends on the thickness λ of the boundary layer imposed by the air flow over the surface of the paper:

$$\dot{\tilde{n}} = DA_S(\mathbf{m} \cdot \nabla \tilde{c}_1) \cong DA_S/\lambda(c_S \gamma(x)x - \tilde{c}_1)$$

where \mathbf{m} is the outward-pointing normal to the surface of the paper filter. For simplicity we neglect diffusion in the liquid phase and average the concentrations over the entire tube. The evaporation rate

therefore becomes $k_S A_S (c_s \gamma(x)x - \tilde{c}_1)$ where $k_S \propto D/\lambda$ is a kinetic constant that captures the dependency of the rate of evaporation on the diffusion coefficient D of the odorant molecules in air, and on the thickness of the boundary layer λ . k_S also depends on the molecular forces between the paper filter and the molecules of odorant.

The ODEs that govern this system are given by

$$\begin{aligned} \frac{d\tilde{c}_1}{dt} &= -\frac{q(t)Q_1}{V_1}\tilde{c}_1 + \frac{k_d A_1 w}{V_1}\theta_1 - \frac{k_a A_1 w}{V_1}\tilde{c}_1(1-\theta_1) + \frac{k_S A_S}{V_1} \begin{cases} c_s \gamma(x) - \tilde{c}_1 & n > 0 \\ 0 & \text{else} \end{cases} \\ \frac{d\theta_1}{dt} &= -k_d\theta_1 + k_a\tilde{c}_1(1-\theta_1) \\ \frac{d\tilde{n}}{dt} &= -k_S A_S \begin{cases} c_s \gamma(x)x - \tilde{c}_1 & n > 0 \\ 0 & \text{else} \end{cases} \\ \frac{d\tilde{c}_2}{dt} &= -\frac{q(t)Q_1 + Q_2}{V_2}\tilde{c}_2 + \frac{k_d A_2 w}{V_2}\theta_2 - \frac{k_1 A_2 w}{V_2}\tilde{c}_2(1-\theta_2) + \frac{q(t)Q_1}{V_2}\tilde{c}_1 \\ \frac{d\theta_2}{dt} &= -k_d\theta_2 + k_a\tilde{c}_2(1-\theta_2) \end{aligned}$$

For simplicity, we assume that the paraffin oil does not evaporate. If pure odorant is used on the filter paper, the equations can be simplified since $x = 1$. In this case the equation for \tilde{n} does not play a role in the dynamics of the odor profile until $\tilde{n} = 0$. If we assume that the amount of odorant at the source is much larger than the amount that evaporates during a typical puff, $x \cong \text{constant}$, and we can normalize these equations by the initial concentration $c_0 = c_s \gamma(x_0)x_0$ and rewrite them in terms of these new variables:

$$c_1 = \frac{\tilde{c}_1}{c_0}, \quad c_2 = \frac{\tilde{c}_2}{c_0}, \quad \theta_1, \quad \text{and } \theta_2$$

Since we assume that the internal radii of the two tubes are the same, we have

$$\frac{A_1}{V_1} = \frac{A_2}{V_2} = \frac{2}{R}$$

and we can define the following known parameters whose values can be calculated from the geometry of the device:

$$q_1 = \frac{Q_1}{V_1} \quad q_2 = \frac{Q_2}{V_2} \quad \text{and} \quad L_{12} = \frac{L_1}{L_2}$$

and the following unknown parameters:

$$q_d = k_d \quad q_a = k_a c_0 \quad q_s = \frac{k_s A_S}{\pi R^2 L_1} \quad \text{and} \quad W = \frac{2w}{c_0 R} \quad (2.1)$$

This lets us rewrite the ODE system as:

$$\begin{aligned} \dot{c}_1 &= -qq_1c_1 + q_dW\theta_1 - q_aWc_1(1 - \theta_1) + q_s(1 - c_1) \\ \dot{\theta}_1 &= -q_d\theta_1 + q_a c_1(1 - \theta_1) \\ \dot{c}_2 &= -(qq_1L_{12} + q_2)c_2 + q_dW\theta_2 - q_aWc_2(1 - \theta_2) + qq_1L_{12}c_1 \\ \dot{\theta}_2 &= -q_d\theta_2 + q_a c_2(1 - \theta_2) \end{aligned} \quad (2.2)$$

In practice, the time between subsequent pulses (~ 10 s) is long, compared to the duration of the whiff (~ 0.5 s). We can therefore assume that the pipette is at equilibrium before the valve is opened, yielding the following initial conditions:

$$c_1(0) = 1 \quad \theta_1(0) = \frac{1}{1 + \frac{q_d}{q_a}} \quad c_2(0) = 0 \quad \text{and} \quad \theta_2(0) = 0$$

We fit this model (eq. 2.2) to PID measurements of 500 ms pulses of 27 different odorants (Fig. 2.4). This model was able to reproduce the full range of kinetics in the dataset, with just four unknown parameters (eq. 2.1).

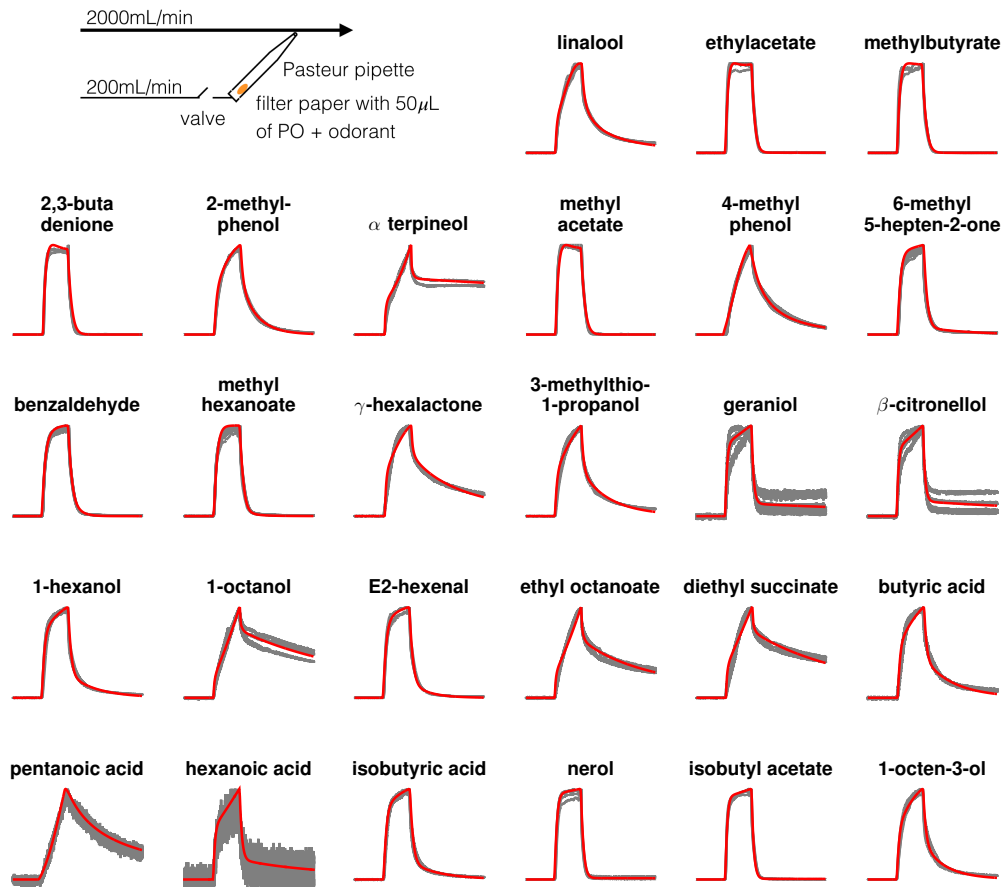


Figure 2.4: *The diversity of odorant pulse kinetics.* A common way of delivering odorants is to prepare “cartridges” from Pasteur pipettes containing $50\text{ }\mu\text{L}$ of odorant diluted in Paraffin Oil, and to force a small volume of air through the cartridge. Odorants delivered this way exhibit a broad range of stimulus kinetics, that depend on the chemical identity of the odorant [113]. Each panel shows five measurements of the kinetics of stimulus using a PID, normalized by the peak. In each panel, red curves are the model fits (eq. 2.2). The pulse duration is 500 ms. Data here is the same as in Fig. 1b in [113].

METHOD	REFERENCE
Did not calibrate	[113, 125, 146] and others
Calibration using another device	[1, 38]
Assume that odorant headspace is saturated.	[16, 131]
Assume that odorant headspace is saturated, and use a tracer gas of known concentration.	[55, 56, 95, 96]

Table 2.1: PID calibration techniques used in the literature.

2.2.2 A simple procedure to calibrate the PID to any odorant

Photo Ionization Detectors (PIPs), advantageous for their ease of use, sensitivity and speed, do not report an absolute value of the gas phase concentration of odorants. Since different odorants have different ionization potentials, identical gas phase concentrations of different odorants can lead to different measurements from the PID, and different gas phase concentrations of different odorants can lead to the same measurement from the PID. Calibration of the PID, the process of converting the reported voltage into an absolute number of molecules of odorant, is thus important if the scale of the stimulus applied is to be taken into account. Many studies that use PIDs to monitor gas phase concentrations of odorants do not calibrate the PID [113, 125, 146], due to the difficulties of established calibration techniques. Some studies have calibrated the PID by coupling the PID with another device that can measure absolutely concentrations, like Gas Chromatography - Mass Spectroscopy (GC-MS) devices or flame ionization detectors [1, 38]. However, these are expensive, and shift the problem of calibration to another device. Another approach is to assume the odorant headspace in the olfactometer is saturated, and use Raoult's and Henry's Law to estimate the gas phase concentration of the odorant, and then extrapolate to fast changes reported

by the PID. Such an approach has been used as is [16, 131] or in conjunction with a tracer gas of known concentration [55, 56, 95, 96]. It is not known how valid the assumption of saturated headspace is, and using another gas of known concentration does not contribute to the accuracy of the estimation of the absolute gas phase concentration of the test odorant.

Here, we propose a simple method to calibrate the PID to any odorant that it can detect. This method is easy to perform, does not require additional equipment or gases of known concentration, nor does it make any assumptions about the saturation of headspace in the olfactometer. It works by depleting a known volume of pure odorant, and integrating the total PID signal over the course of depletion. Since the number of molecules in the pure odorant sample can be estimated precisely (from its volume and published formula weight and density), the PID signal per unit time can be converted into the number of molecules leaving the olfactometer per unit time.

To calibrate our PID to ethyl acetate odorant, we placed 100 μL of pure odorant in a 30 mL scintillation vial with a screw top lid with two tubes. One tube was fed into a clean airstream with a 2000 mL/min flow rate, and the other led to a Mass Flow Controller (MFC) that forced air through the scintillation vial at a constant rate that could be varied. A PID measured the gas phase concentration at the outlet of the olfactometer, and data was collected when the air started flowing over the odorant. The schematic of the olfactometer is shown in Fig. 2.5a. We flowed air through the scintillation vial till all odorant in the vial was completely depleted (which was when the PID reading returned to the pre-stimulus level), and repeated this measurement for a number of fixed flow rates through the scintillation vial. The total volume of air required to evaporate the odorant decreased with the flow rate (Fig. 2.5b), reflecting nonlinear relationships between

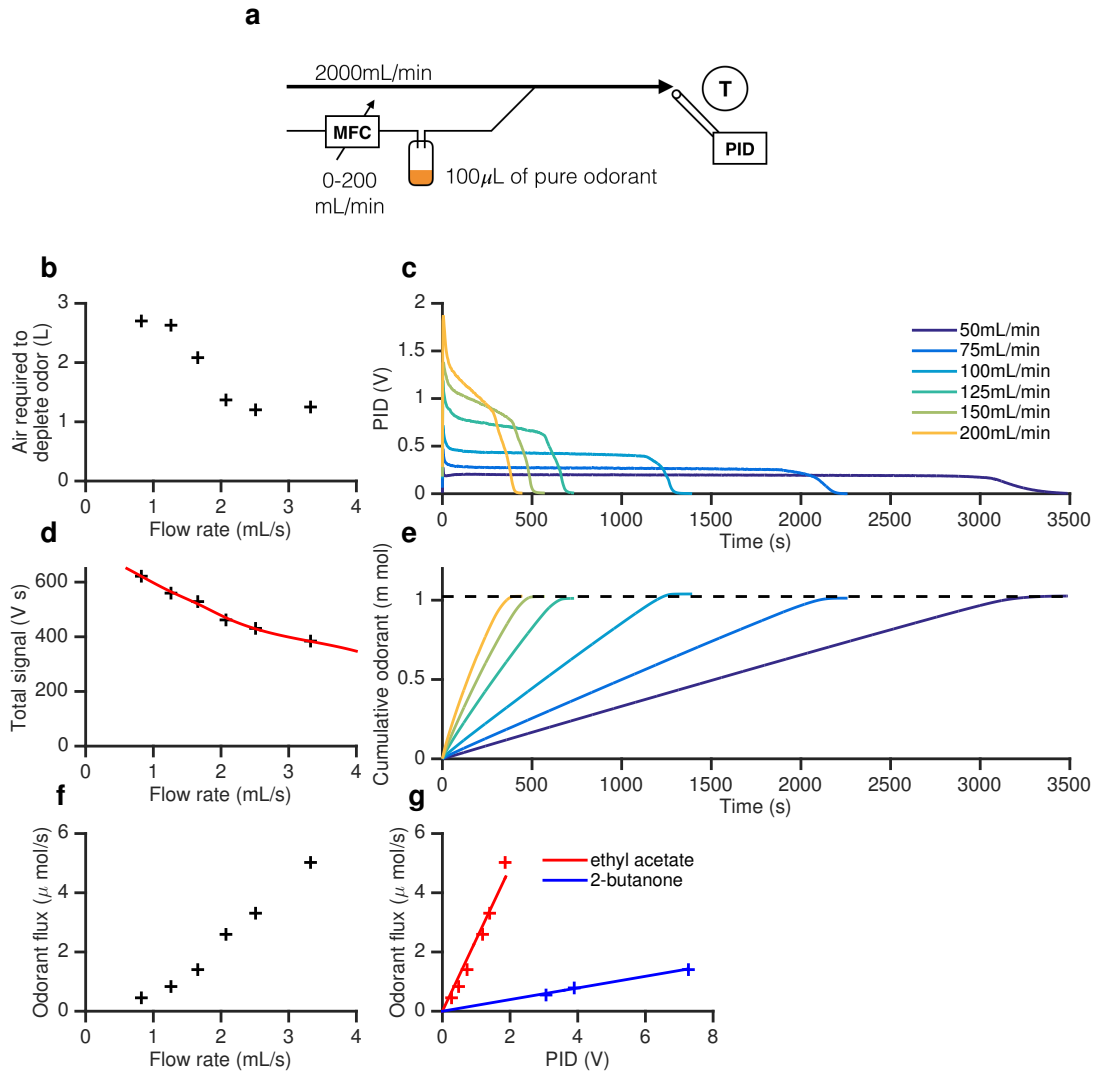


Figure 2.5: *PID calibration for arbitrary odorants.* (a) Schematic for PID calibration. 100 μL of a pure odorant is placed in a scintillation vial, and air is blown over it at a fixed flow rate. A PID is placed the outlet tube close to the target (T). (b) Air required to completely deplete the odorant as a function of flow rate. (c) PID traces from start to complete depletion of odorant for various flow rates. (d) Integrated PID signal as a function of flow rate. (e) Cumulative odorant vs . time for various flow rates. (f) Odorant flux as a function of flow rate (g) Odorant flux as a function of measured PID value, for ethyl acetate (red) and for 2-butanone (blue). The odorant in (b-f) was ethyl acetate.

the rate of evaporation and the flow rate. Correspondingly, smaller flow rates took longer to completely deplete the odorant (Fig. 2.5c), and peak and steady state value of the PID signal increased with flow rate through the scintillation vial. If the PID captured all the molecules of odorant emerging from the olfactometer, and ionized all of them, the integrated PID signal would be a constant, independent of the flow rate, and correspond to the total number of molecules of odorant in the vial. However, we observed that the total integrated PID signal decreased with the flow rate (Fig. 2.5d), an effect we attributed to flow-rate dependent partial capture of odorant molecules by the PID. To compensate for this, we fit an interpolant to this data (Fig. 2.5d, red line), and used this to correct for variations in the total signal. Integrating the corrected PID curves yielded curves of cumulative odorant *vs.* time that reached approximately the same height, corresponding to the calculated number of moles of odorant (dashed line, Fig. 2.5e), confirming that mapping from PID signals to number of molecules was consistent.

We then computed the odorant flux as a function of the flow rate, by estimating the slope of the cumulative odorant curves in a relatively stable region (Fig. 2.5f). Finally, we can combine these measurements to plot odorant flux *vs.* the PID signal, to generate a function that maps PID values onto odorant flux. Odorant flux here is reported in units of mol/s, so constitutes an estimate of the absolute number of molecules of odorant emerging per unit time. We repeated this calibration process for another odorant (2-butanone), and show find that both curves are approximately linear (Fig. 2.5g).

2.2.3 How to deliver pulses of odorant with different intensities

The simplest olfactory stimuli that can be delivered is a short pulse of a single odorant. Using short pulses of odorant lets experimenters determine if neurons and receptors of interest respond to this particular odorant [73, 74], and reveal their dynamical response properties [74, 113, 168]. Using short pulses of odorant with different amplitudes estimates the dose-response curve of that neuron, permitting the quantification of its sensitivity to that odorant [19]. Typically, pulses of odorant have been delivered by forcing air through cartridges containing a filter paper with a small quantity of odorant diluted in Paraffin Oil. Stimulus duration is controlled by the length of time air is forced through the cartridge, and stimulus intensity is controlled by the liquid phase dilution of the odorant in Paraffin Oil. This means that different cartridges have to be prepared for different desired stimulus intensities, making the process potentially cumbersome. Furthermore, since odorants contaminate the entire inner surface of the cartridge, cartridges typically are discarded after a certain number of uses [103], making this method wasteful. Since considerable time may elapse between cartridge preparation and application, a previous study has found that refrigerating cartridges is required to ensure reliability [1], further complicating this process.

Pulses of odorant delivered this way can show dramatic variation from trial to trial, especially for volatile odorants with large vapor pressures (Fig. 2.6, top row). In addition, different concentrations of odorant in liquid phase can yield pulses with similar gas phase concentrations, confounding interpretations of responses to these stimuli (Fig. 2.6, top row).

Here, we propose using pure odorants contained in a scintillation vial to deliver pulses of odorant. Pulse height is controlled by varying

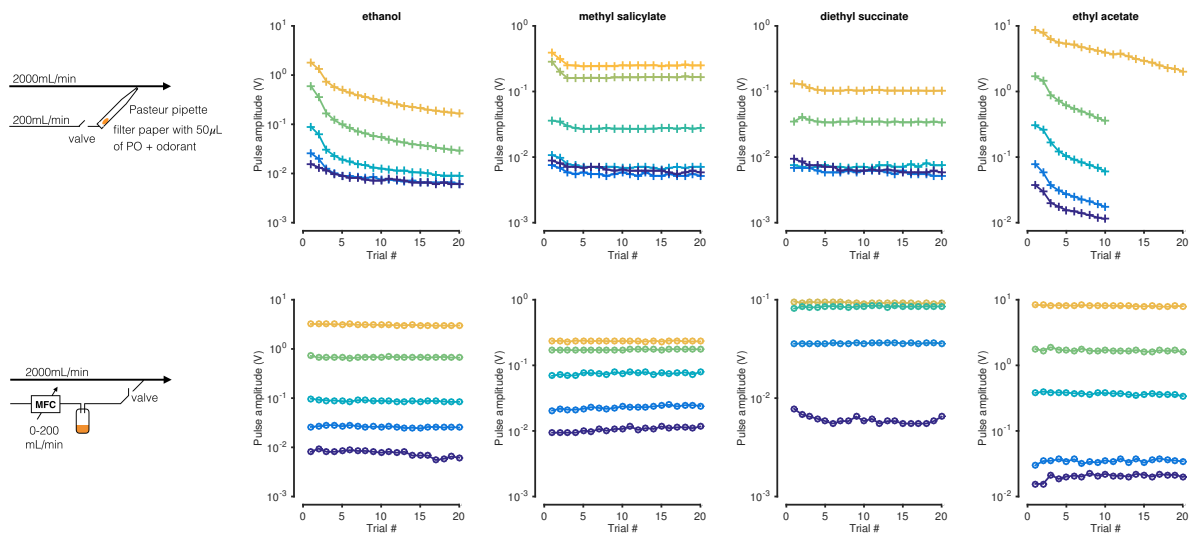


Figure 2.6: How to reproducibly deliver pulses of odorant with different intensities.

(top row) Pulses delivered using a cartridge made of a Pasteur pipette with a filter paper spotted with odorant diluted in Paraffin Oil. Pulse amplitude is controlled by varying the liquid phase concentration. (bottom row) Pulses delivered using pure odorant in a scintillation vial. Pulse amplitude is controlled by varying the flow through the vial. Plots show measured gas phase concentration using a PID vs. trial number. Colors indicate liquid phase concentration (top row) or flow rate through the vial (bottom row).

the flow through the scintillation vial using a MFC. This approach has several advantages over the earlier method. First, since pure odorant is used, evaporation of the odorant does not change the effective concentration of the odorant that remains in the scintillation vial, and the gas phase concentration of the headspace in the vial remains constant, as long as there is some odorant left in the vial. Second, it greatly simplifies the apparatus needed to deliver odorants: Pasteur pipettes, filter papers, etc. are not needed, and there is no need to accurately measure the amount of odorant in the scintillation vial, as the accuracy and precision of the pulse height is inherited from that of the MFC. Third, pulses of several intensities can be delivered with the same apparatus, enabling automation of experiments like measuring the dose-response curve of a neuron. Finally, this approach creates no waste, as all parts of the system can be re-used, including the scintillation vial. When odorant is depleted, the scintillation vial can be refilled with more pure odorant. Pulses delivered using this method are more precise than the earlier method, and do not show any significant decay in amplitude over 20 trials (Fig. 2.6, bottom row).

The primary reason to deliver odorant pulses of different intensities to a neuron is to determine its dose response curve. These results suggest that there are two approaches to this problem. First, one can embrace the intrinsic decay in pulse amplitude associated with the older method, and measure the stimulus *and* response, and use the measured stimulus to determine the dose-response curve (as shown in Fig. 2.2c). Second, one can use MFCs and pure odorants to generate reproducible pulses, and utilize the unitary nature of this hardware approach to automate the collection of data.

2.2.4 How to deliver fluctuating odorant signals

Time series of fluctuating odorant signals have been used to as an efficient way to characterize the response properties of ORNs. Paired recordings of a time series of some fluctuating odorant signal and the response of a neuron can be used to recover the linear kernel that best describes the transformation from the stimulus to the response. Such a linear kernel can be used to predict the time series of response of that neuron to a novel stimulus that the neuron has not previously been exposed to, and even to predict the response of the neuron to a stimulus from a second odorant [113]. A favorable stimuli to use for this is Gaussian white noise. This stimulus is Gaussian distributed, and is uncorrelated from any one time point to another. Its tight autocorrelation structure allows sampling all frequencies of the neuron response (see §3.1 for a discussion on linear kernel extraction). Linear filters can be estimated in an unbiased fashion even in the presence of an output nonlinearity if the stimulus is Gaussian [32].

Odorant signals that is Gaussian and white is hard to realize in practice. Interaction of the odorant with the walls of the delivery system (see §2.2.1, [113]), limits on the airspeed used in the delivery system, and finite timescales of the components of the delivery system introduce correlations into any odorant stimulus. Furthermore, since the easiest way to control an odorant signal is to use a valve to divert an odorized airstream towards or away from the preparation, early work using fluctuating odorant signals to identify linear kernels from ORN responses used binary odorant stimuli where the stimulus was either on or off [56, 113, 125, 150, 151]. This creates a typically a bimodal stimulus distribution, with the lower peak close to 0, and the larger peak at some value that can be controlled by the concentration of the odorized airstream (Fig. 2.7a-b). The correlation time of the sig-

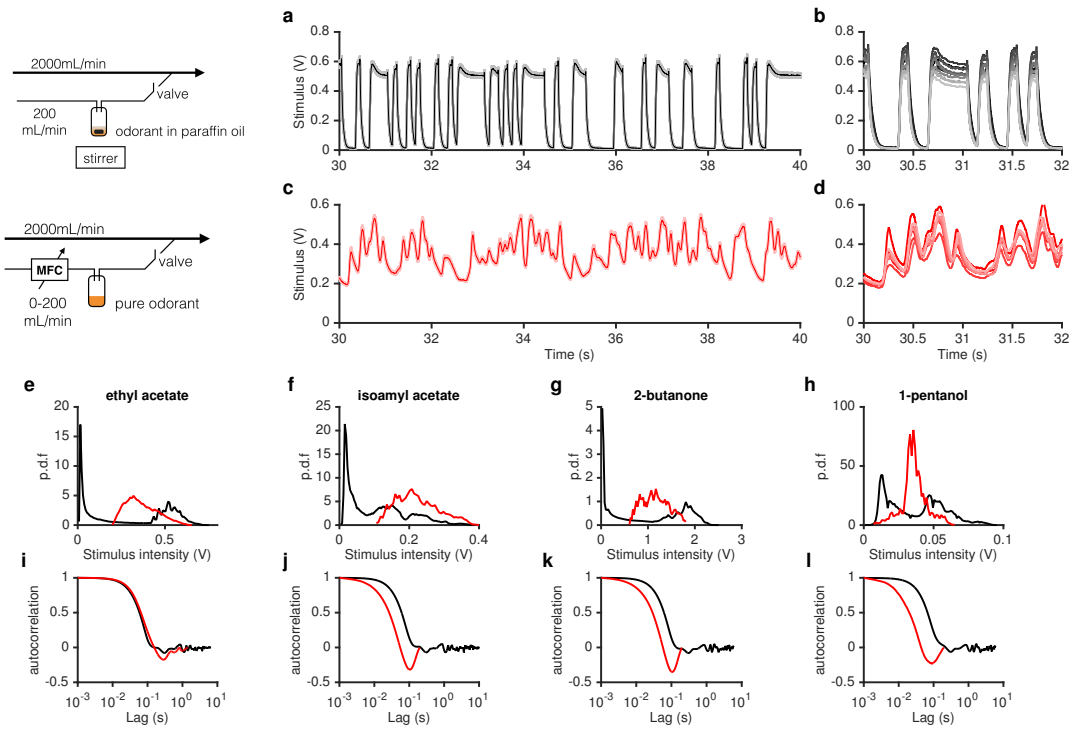


Figure 2.7: Delivering fluctuating odorant signals. (a-b) Using a valve to deliver binary random sequences of ethyl acetate odorant. (a) Mean ethyl acetate concentration (shading is standard error of mean). (b) Individual traces. (c-d) Using a MFC to deliver ethyl acetate with approximately Gaussian statistics. (c) Mean ethyl acetate concentration (shading is standard error of mean). (d) Individual traces. (e-l) Distributions and autocorrelation functions of stimulus time series for various odorants. Black traces are binary random sequences delivered using a valve and red traces and Gaussian sequences delivered using a MFC.

nal can be controlled by varying the switching time of the valve, and for volatile odorants that do not interact strongly with the surfaces of the olfactometer, correlation times as fast as 30 ms can be realized [113]. In these binary stimuli, the mean stimulus is typically rarely realized, and the responses of the neuron are dominated by the large, rapid increases of odorant on valve opening.

Using a MFC permits delivering odorants with more varied distributions [95, 96]. Specifically, mono-modal distributions can be easily realized. Fluctuating odorant signals can be delivered by varying the flow rate of the MFC, and therefore the flow rate of an airstream through a vial containing odorant (Fig. 2.7c-d). The autocorrelation time of a stimulus delivered this way is limited by update rate of the MFC, though multiple MFCs can be chained together in parallel, driven by uncorrelated control signals, to achieve faster signals. Odorants delivered this way typically need not “bottom out” at zero stimulus (Fig. 2.7c-d) and have distributions that are mono-modal (2.7e-h).

2.2.5 How to deliver Gaussian odorant signals with different means and variances

Adaptation is a process by which the amplitude and kinetics of the responses of a system change with the statistics of the signal presented. In principle, any moment of the stimulus distribution could induce adaptive changes. The visual system has been shown to adapt strongly to the first two moments of stimulus distributions – the mean and the variance – with much smaller changes in response arising from changes in stimulus kurtosis and skew. Here, we demonstrate how odorant stimuli that are dominated by changes in only one

moment of the distribution can be generated, while keeping other features of the stimulus unchanged.

The simplest way to generate odorant stimuli with varying means is to use a MFC to vary airflows through a vial containing pure odorant. We started with the ansatz that the flux of odorant in the odorized airstream scales with the fraction of odorized air in the main airstream, or the PID signal

$$S \sim \frac{Q_{\text{odor}}}{Q_{\text{odor}} + Q_{\text{main}}} \quad (2.3)$$

where Q represents the flow rate. We can therefore construct a set of control signals to the MFC using eq. 2.3 and measure the resulting signals. Deviations in the signals can be corrected by scaling and shifting the MFC control signals iteratively till a stimulus distribution sufficiently close to the desired distribution is achieved. A set of odorant signals generated this way using ethyl acetate is shown in Fig. 2.8a. Note that the time series appear correlated across intensities. Fig. 2.8b shows the distributions of these odorant stimuli, that are approximately Gaussian. In these stimuli, the mean changes by a factor of 10, with much smaller changes in the variance (Fig. 2.8c). Since the temporal structure of the control signals driving the MFC is the same across all intensities, the autocorrelation structure of the signal is similar across intensities (Fig. 2.8d).

Experiments where the variance of the stimulus is modulated, with a fixed mean, typically involve switching between epochs where the variance is low and where the variance is high. A simple way to achieve odorant signals where signal variance alternates between high and low values is to duplicate the apparatus used previously, but drive the two MFCs with signals identical except for their variance. A valve can be used to switch between the two airstreams, creating epochs with high variance (from the MFC driven with control signals

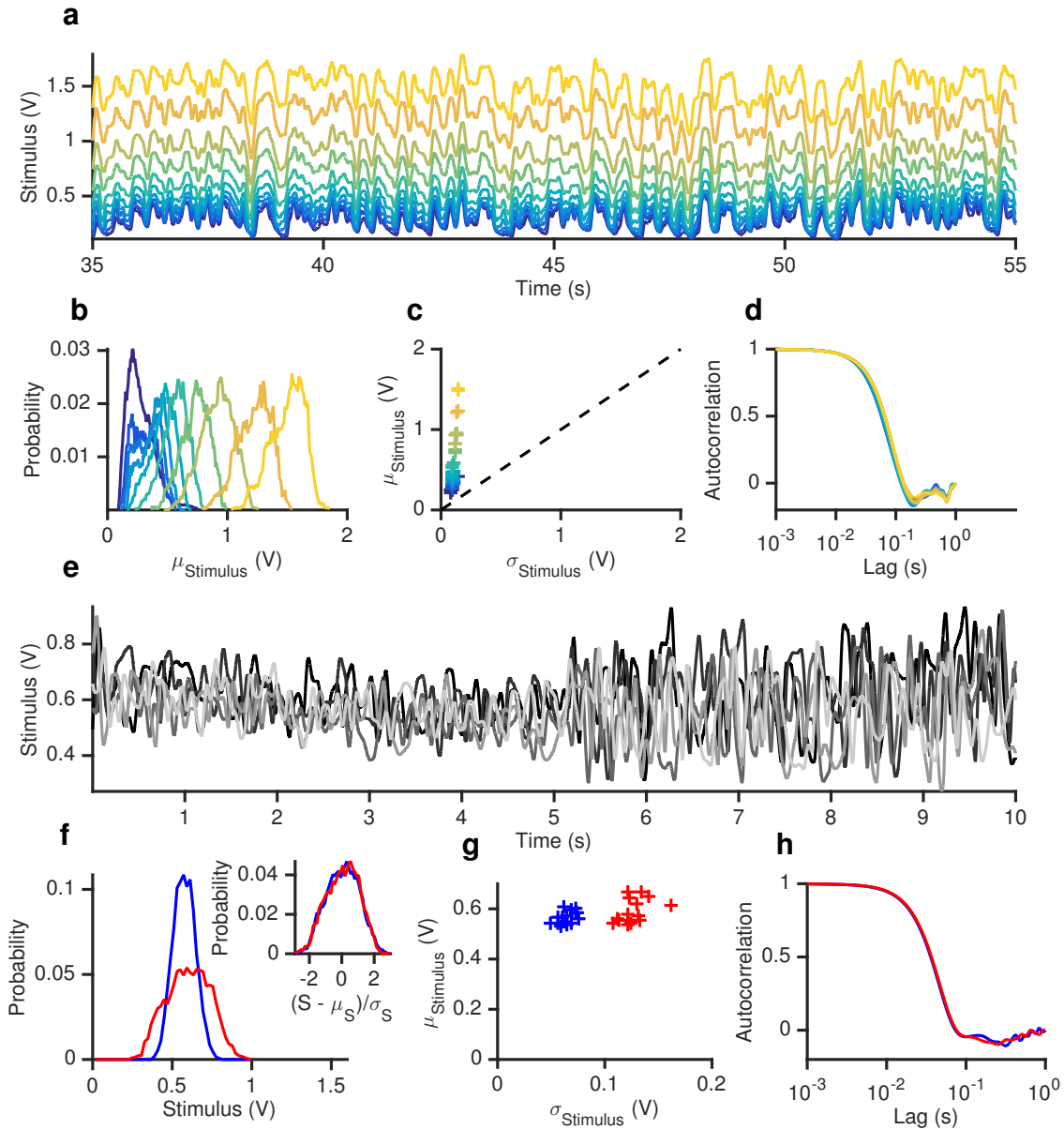


Figure 2.8: *Gaussian odorant signals with controlled means and variances.* (a-d) Gaussian ethyl acetate stimulus with varying mean. (a) Time series of stimuli with varying mean. (b) Probability distributions. (c) Mean stimulus vs. standard deviation of stimulus for each trial. (d) Autocorrelation functions of the stimulus for various mean values. (e-h) Gaussian ethyl acetate stimulus with two different variances. (e) Time series of the stimulus. Several trials are shown superimposed. (f) Distributions of the stimulus during high variance epochs (5-10 s, red) and low variance epochs (0-5 s, blue). (f, inset) Distributions normalized by their standard deviation, showing that they are rescaled versions of each other. (g) Mean stimulus vs. standard deviation of stimulus for each trial. (h) Autocorrelation functions of the stimulus during the high and low variance epochs.

with large variance) and epochs with low variance (from the other MFC). An example of such a stimulus is shown in Fig. 2.8e, where the low-variance epoch lasts from 0 – 5 s and the high variance epoch lasts from 5 – 10 s. The distribution of the stimulus during the two epochs shows that the variance is clearly different (Fig. 2.8f). If the stimuli during the high and low variance epochs are rescaled by their variance, the distributions collapse onto each other, showing that the low- and high-variance stimuli are similar in distribution (Fig. 2.8f inset). Comparing the mean and variance of the stimuli during the two epochs (Fig. 2.8g) reveals that the means are not significantly different ($p = 0.07$), but the variances differ significantly. Since the two MFCs are driven by control signals that are only rescaled versions of each other, the temporal structure of the stimulus in the low- and high-variance epochs is similar (Fig. 2.8h).

2.3 DISCUSSION

The goal of this work was to describe how a wide variety of olfactory stimuli can be generated reliably, using only two off-the-shelf components. In this study we:

- A. proposed a simple model derived from the physical interactions odorants have with surfaces to reproduce, with only 4 parameters, the wide variety of stimulus kinetics that arise from the intrinsic chemical identity of odorants under identical conditions of delivery (Fig. 2.4).
- B. developed a simple method to calibrate PIDs to any odorant that it can detect, using no additional equipment (Fig. 2.5)

- c. proposed methods to deliver pulses, intermittent stimuli and Gaussian stimuli with controlled means and variances with a high degree of reproducibility (Figs. 2.6, 2.2.4, 2.7 and 2.8)

2.3.1 *Flux or concentration detectors?*

Olfactory neurons are considered to be either concentration detectors, where receptors are directly exposed to the external stimulus concentration, or flux detectors, where stimulus molecules are accumulated in a peri-receptor compartment [91]. Are PIDs flux or concentration detectors? The calibration technique we proposed converts PID values into a flux, since (i) in the conditions described here, a constant flux of odorant molecules is maintained at the outlet of the delivery tube; and (ii) the PID sucks in air at a constant rate, and constantly removes air from the detection chamber at the same rate. Previous studies that have calibrated PIDs have reported PID values converted into a instantaneous gas phase concentration [95, 96, 152]. While a constant flux of odorant molecules emerging from the delivery tube may lead to a constant concentration of odorant at a fixed point from the outlet (assuming steady state), the translation from flux to concentration is not without assumptions, and probably varies with the geometry of the setup, and other factors. Moreover, since conservation of odorant implies that the invariant physical quantity of interest is the flux, our calibration procedure naturally converts PID readouts into units of flux.

2.3.2 *Delivering and measuring mixtures of odorants*

Odorants do not typically exist in isolation in nature. Odors consist of mixtures of odorants, and the specific fractional composition of

different odorants in an odor mixture can carry important information. The measurement and delivery of mixtures of odorants is beyond the scope of this study, primarily because there is no unambiguous method to independently measure the amount of different components of an odor mixture using a PID. Since the PID sucks in all molecules in the airstream, and sums across all the ions in the detection chamber, it is incapable of distinguishing between varying amounts of different odorants. Recent work, however, attempts to work around these challenges and presents techniques to deliver mixtures of odorants [69].

BLACK BOX ANALYSIS OF ORN RESPONSES

In this chapter, I describe numerical methods I use to analyze the responses of Olfactory Receptor Neurons (ORNs) to odorant stimuli. These analysis methods treat the ORN as a black box, and do not explicitly model the internal states of the ORN. This black box approach is advantageous since the precise mechanisms of ORN response are not quantitatively understood, and this approach generates minimal models that reproduce ORN response phenomenology quantitatively. These methods parametrize the transformation of the time series of the stimulus (the odorant) into the time series of the output using a set of linear filters and nonlinear blocks. The goal of this approach is to build phenomenological models that can describe the rules that ORNs use to transform inputs into outputs, and to quantify features of ORN responses.

3.1 LINEAR KERNEL EXTRACTION

3.1.1 *Spike triggered average and linear filters*

The typical neuron receives inputs through its dendrites, either in the form of synaptic contacts with other neurons, or through transducers in sensory neurons. These inputs may lead to inward currents in the neuron, that when large enough, lead to the generation of discrete, all-or-none action potentials in the spike initiation segment, usually on the axon hillock. Neurons fire action potentials or spikes in response

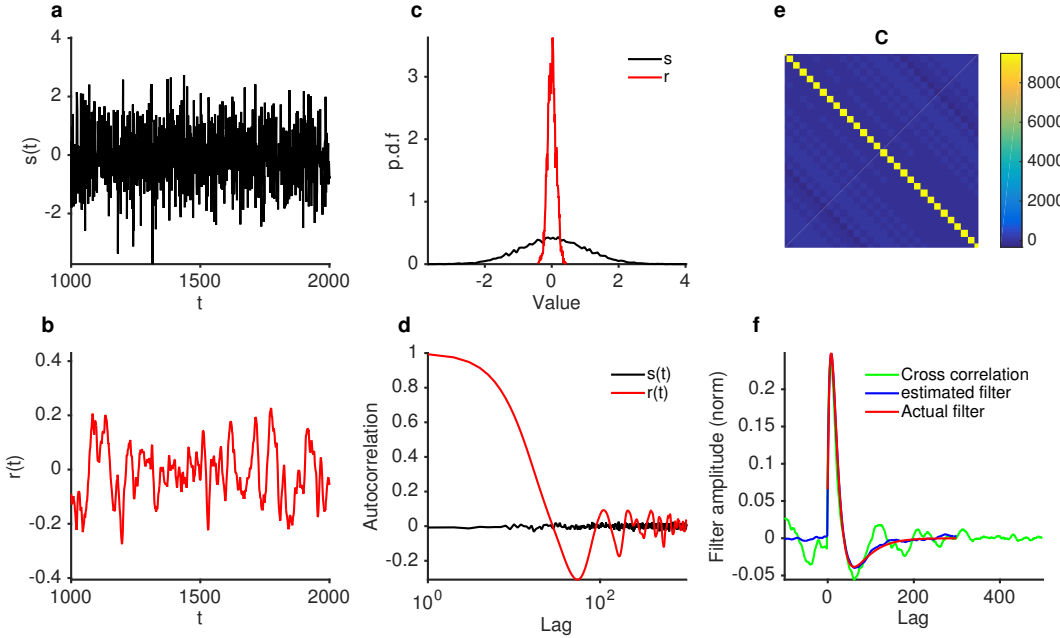


Figure 3.1: *Extracting linear filters from input and output time series data* (a) Gaussian white inputs (b) Responses generated by a linear model (c) Distributions of input and output (d) Autocorrelation functions of the input and the output. Note that the input is white. (e) Covariance matrix of the time-shifted stimulus. It resembles a diagonal matrix. (f) Comparison of actual filter, reconstructed filter, and cross correlation.

to a continuous time series input of stimuli. What features of the stimulus induce a neuron to fire spikes? One way to determine this is to systematically play all possible stimulus inputs to the neuron, and determine which stimuli are most effective in eliciting a spike. However, since neurons integrate over time, the space of all possible stimuli is extremely large, and this approach is impractical. An alternative is to present Gaussian white noise to the neuron, and trigger and average the stimulus whenever a spike is elicited. This approach is called a *spike-triggered-average* of the stimulus. A generalization of this technique allows us to work with continuous outputs, such as the firing rate of spiking neurons, or the potential of its membrane or the local field.

Consider a system that responds to a continuous input time series $s(t)$ with a continuous output time series $r(t)$. We assume that the

system is linear, i.e., $r(t)$ is generated by some linear operation on $s(t)$:

$$r(t) = K \otimes s(t) = \int_{-\infty}^t K(t-t')s(t')dt' \quad (3.1)$$

Our task then is to find the linear filter \hat{K} from the time series of $s(t)$ and $r(t)$ that best predicts $r(t)$ given $s(t)$. In other words, we want to minimise

$$\|\hat{K} \otimes s(t) - r(t)\|_2$$

Assuming that \hat{K} decays to zero after time τ , we can estimate \hat{K} by deconvolving $s(t)$ from $r(t)$. Since $s(t)$ and $r(t)$ are discretely sampled, this problem can be thought of as an overdetermined linear algebra problem. First we reshape $s(t)$ into overlapping chunks τ elements long, to get a matrix \hat{S} with dimensions $L \times \tau$ where L is the length of the time series $s(t)$. \hat{K} can be solved for using

$$\hat{K} = C \setminus (\hat{S}^T r) \quad (3.2)$$

where C is the covariance matrix of \hat{S} , and \hat{S}^T is the transpose of \hat{S} .

Fig. 3.1 shows estimation of a filter from synthetic data using this technique.

3.1.2 Regularization

The method described above works well for white inputs (with δ correlations). What happens if correlations exist in the input? This is of practical importance as physically achievable stimuli typically are not perfectly white, but are correlated on timescales that relate to the underlying physical process that generates them. For odorant stimuli,

correlation times of the input can be large, based on the chemical identity of the odorant and the details of the delivery system (see Chapter 2 for a detailed discussion).

Using white stimuli permits reliable estimation of the linear kernel that transforms stimuli to response (Fig. 3.2a-d). Note that the autocorrelation function of the stimulus is close to zero for all non-zero lags, as would be expected for white noise (Fig. 3.2b). When we examine the covariance matrix of the time-shifted stimulus C (as in eq. 3.2), we observe that it resembles a diagonal matrix, with a large numerical difference between the diagonal elements and the off-diagonal elements (Fig. (Fig. 3.2c)).

What happens when we repeat the procedure using correlated stimulus? This approximates stimuli that can be realized in the lab, and an example is shown in Fig. 3.2e. The autocorrelation function of this stimulus is not a delta function, and approaches zero only for relatively large lags (Fig. 3.2f). The covariance matrix of the time shifted version of this stimulus resembles a diagonal matrix less closely, with a smaller difference between diagonal and off-diagonal terms (Fig. 3.2g, cf. Fig. 3.2c). Solving eq. 3.2 to recover the filter K yields a poor estimate, with the filter contaminated by high frequency artifacts (Fig. 3.2h, cf. 3.2d). To estimate the filter under these conditions, we regularize C using

$$\hat{C} = C + rI \quad (3.3)$$

where I is the identity matrix and r is a regularization factor in units of the mean eigenvalue of C . Regularizing the covariance matrix this way makes it appear more diagonal (Fig. 3.2i), resembling the covariance matrix of the white stimulus more closely (Fig. 3.2c). The filter extracted using this regularized covariance matrix approximates the actual filter more closely, and is less contaminated by high-frequency artifacts (Fig. 3.2j).

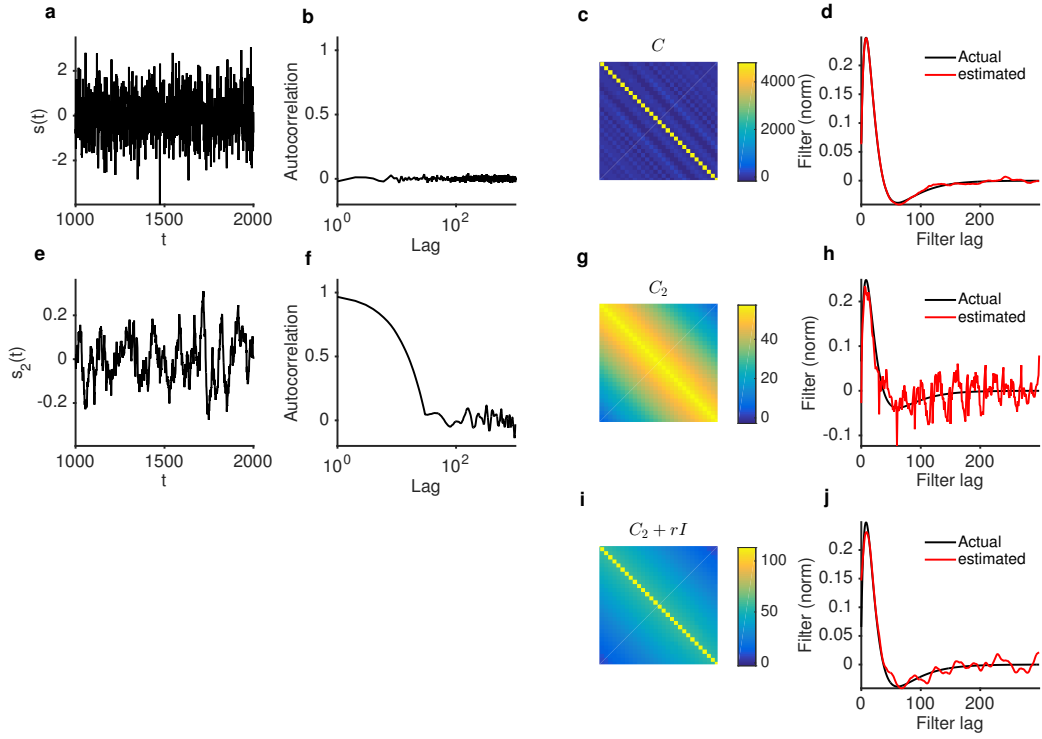


Figure 3.2: *Extracting linear filters from correlated stimuli* (a-d) Extracting linear filters from uncorrelated stimulus. (a) Gaussian white stimulus (b) Autocorrelation function of the stimulus shown in (a). Note that it is close to zero for all non-zero lags. (c) Covariance matrix of time shifted stimulus C (see eq. 3.2) (d) Actual filter (black) vs. estimated filter (red). (e-j) Extracting linear filters from correlated stimuli. (e) Correlated stimulus. (f) Autocorrelation function of this stimulus. Note that it is non-zero for many non-zero lags. (g) Covariance matrix of time shifted stimulus. (h) Actual filter (black) vs. estimated filter (red) (i) Adding a scaled diagonal matrix to the covariance matrix makes it look more diagonal. (j) Filter estimated from the regularized covariance matrix.

3.2 LN MODELING AND GAIN ESTIMATION

The Linear-Nonlinear (LN) model is a simple phenomenological model where responses to stimuli are given by

$$r(t) = N(K \otimes s(t))$$

where K is a linear filter, \otimes represents convolution, and N is a static nonlinearity. Since N acts on the stimulus after it has been convolved

with the filter, it is called an output nonlinearity, and the LN model comprises of two blocks: a linear filter, followed by a static output nonlinearity. LN models are commonly used in neuroscience as they provide a simple analogy to many neurons, and theoretical work has shown that linear filters can be reliably estimated even with strong output nonlinearities, if the stimulus is Gaussian white noise [32].

We define gain as the change in response due to a unit change in the stimulus:

$$\text{gain} = \frac{\Delta R}{\Delta S}$$

and is a measure of how sensitive the system is to stimuli, or how much it amplifies a signal in its response. For systems that respond instantly, the gain is easily estimated by presenting pulses of stimulus, and measuring the amplitude of the response to each pulse. However, the response of systems that integrate over time is more complicated, and is harder to interpret. The LN model presents a clear separation of the kinetic properties of a system from its gain: while the kinetics of the model are captured by the linear filter K only, normalizing K appropriately [6] can make all its gain manifest in its output nonlinearity N .

In the following, I demonstrate how LN modeling can be used to estimate gain of models given time series data of the input and the output, and no additional knowledge of the system that generated these responses. To do this, I use two models, the Dynamical Adaptation (DA) model [36] and a Nonlinear-Linear-Nonlinear (NLN) model to generate synthetic datasets and fit LN models to them, estimating gain in each case. The DA model is a feed-forward model, where the stimulus is convolved with two different filters and the response is a nonlinear combination of the two signals:

$$r_{\text{DA}}(t) = \frac{\alpha K_y \otimes s(t)}{1 + \beta K_z \otimes s(t)}$$

where K_y and K_z are two filters and α and β are two parameters. The gain of the DA model depends nonlinearly on the parameter β . In the NLN model, an input nonlinearity acts on the stimulus, which is then convolved by a filter, and finally passed through an output nonlinearity:

$$r_{\text{NLN}}(t) = N(K \otimes a(t))$$

where $a(t)$ is parameterized by a simple Hill function:

$$a(t) = \frac{s(t)}{s(t) + K_D}$$

where K_D is the half-maximum of the input nonlinearity. In the NLN model, K_D sets the sensitivity of the model, and determines the range of stimuli it can respond to.

Varying β in the DA model generates responses that differ in magnitude to the same stimulus (Fig. 3.3a). However, filters extracted for all the models are similar (Fig. 3.3b), since the kinetic parameters of all the models used here do not change. To visualize the effective nonlinearity of the LN model that best fits this DA model, I plot the response of the DA model vs. the stimulus projected through the best-fit filters (Fig. 3.3c). These output nonlinearities resembled curves with different slopes, each corresponding to the response of a different DA model with a different value of β . Gain in this definition is simply the slope of the output nonlinearity (Fig. 3.3c). Comparing gain computed this way to the β parameter of the DA model reveals a strong correlation (Fig. 3.3d), suggesting that LN analysis is able to estimate gain in this synthetic data.

Can LN analysis also estimate a meaningful gain in synthetic data generated by a NLN model? Here, models with different sensitivities are constructed by varying K_D (Fig. 3.3e). Does the gain of best-fit LN models recapitulate this changing K_D ? To determine this, I generate synthetic data using scaled stimuli that fluctuates around the K_D for each model shown in Fig. 3.3e. The NLN model (filter shown in Fig. 3.3f) produces identical responses to these different stimulus (Fig. Fig. 3.3g), since changes in the stimulus scale are exactly compensated for by changes in K_D (by construction).

The presence of the input nonlinearity means that the estimated filters (colored curves in Fig. 3.3h) do not exactly correspond to the actual filter (black curve in Fig. 3.3h). Nevertheless, they are similar. Comparing the response of the NLN model to the stimuli projected through each estimated filter shows that the nonlinearities of best-fit LN models are different for the different NLN models with different K_D s. In particular, responses from models with large K_D s produce shallow nonlinearities, and responses from models with small K_D s produce steep nonlinearities (Fig. 3.3i). Comparing the gain (the slope of the nonlinearities in (i)) to $1/K_D$ reveals a strong correlation, suggesting that LN analysis can be used to estimate gain even when the underlying model has significant front-end nonlinearities.

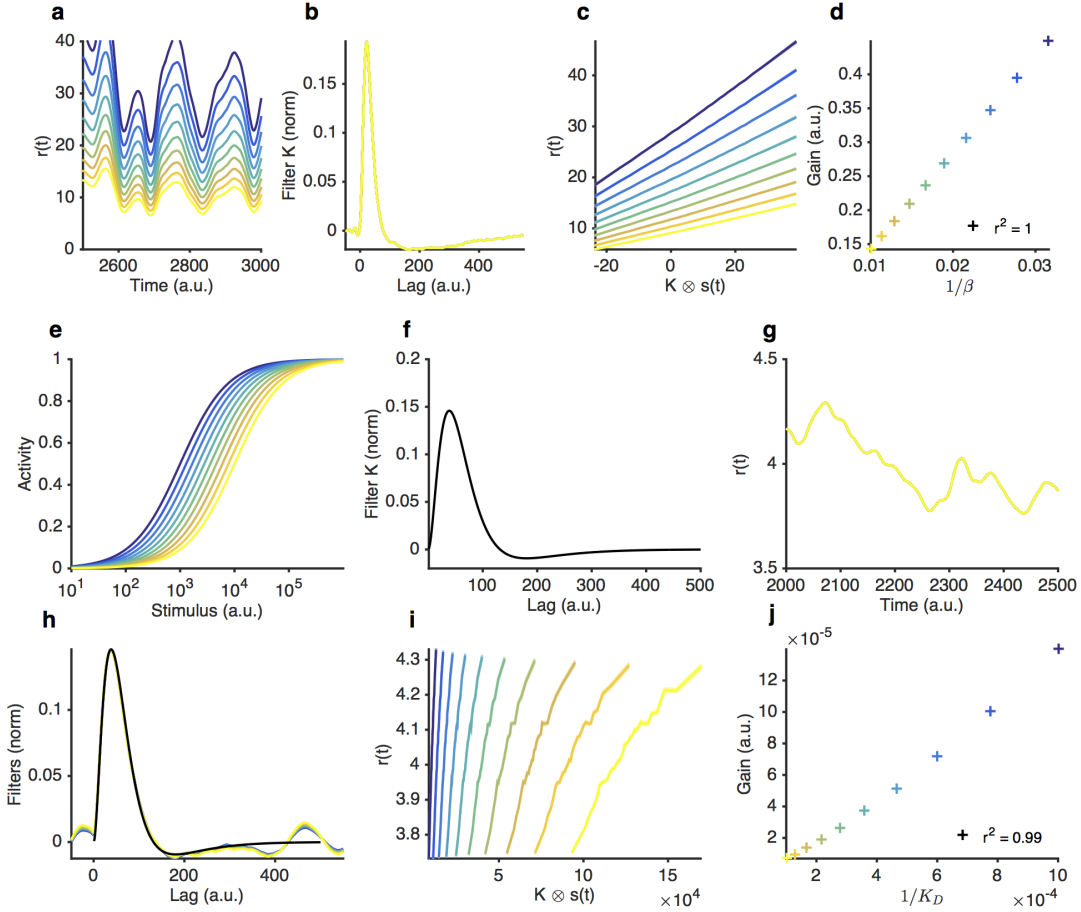


Figure 3.3: *Using a LN model to determine gain from input-output data.* (a-d) Gain estimation using synthetic data generated by a **DA** model [36]. (a) Responses of a set of DA model with different β parameters to the same stimulus. (b) Linear kernels fit to stimulus and response data. (c) DA model responses *vs.* linear projections of the stimulus using the estimated filters in (b). (d) Gain (the slope of the curves in (c) *vs.* $1/\beta$ for each model. (e-j) Gain estimation using synthetic data generated by a Nonlinear-Linear-Nonlinear (**NLN**) model. (e) The half maximum K_D of the input nonlinearity is varied in this model. (f) Linear filter of NLN model. (g) Responses of NLN models with varying K_D are identical because the input stimulus is scaled by K_D . (h) Estimated linear kernels (colors) cf. actual filter (black). (i) NLN model responses *vs.* linear projections of the stimulus using the estimated filters in (h). (j) Gain (slopes of curves in (i)) *vs.* $1/K_D$ of the various models shown in (e).

Part III

EXPERIMENTS

OLFACtORY RECEPTOR NEURONS USE GAIN CONTROL AND COMPLEMENTARY KINETICS TO ENCODE INTERMITTENT ODORANT STIMULI

4.1 INTRODUCTION

Odor landscapes that insects navigate are often not smooth gradients [29, 142]. Instead, turbulent airflows shape odor plumes into intermittent whiffs randomly separated by periods of background air (blanks). In the absence of reliable spatial gradients, navigating insects may use the timing of whiff encounters [174], combined with other sensory modalities such as mechanosensation to detect wind direction [21, 29, 48], to navigate odor plumes towards mates and food. Insect olfactory systems face dual challenges in detecting natural odor plumes. First, the intensity of whiffs is typically distributed according to a power law [119], with intense whiffs interleaved unpredictably with weak ones [142]. This requires the insect to represent a very large domain of stimulus intensity using a relatively narrow response range of its sensors. Second, whiff durations and blank durations are also distributed as a power law over a wide range of time scales [30]. This lack of characteristic scale in the intensity and timing of whiffs makes it challenging to precisely detect and encode individual odor whiffs. The encoding problem is aggravated by shifting local statistics of odor encounters, which change with wind speed [123, 125], position [89], or environment [121]. How does the olfactory system manage to en-

code whiffs of odors whose intensities and timing can vary over such wide ranges?

Several features of the olfactory system contribute to encoding odor stimuli of different intensities. A single odorant can be detected by multiple receptor types, with different sensitivities [73] and static compressive nonlinearities at both Olfactory Receptor Neuron (ORN) and their post-synaptic targets, the Projection Neuron (PN), selectively amplify weak signals and suppress responses to large signals [12, 19]. Glomerular mechanisms implement a type of divisive gain control that maintains PN sensitivity within the range of changing ORN responses [12, 110, 128, 129]. Finally, transduction currents in response to odor pulses scale inversely with the intensity of the background signal, consistent with the Weber-Fechner Law [26]. However, whether ORN firing follows a similar scaling is unclear [25, 113]. Thus, although the input-output curve of ORNs to odor stimuli changes with odor background, the precise scaling of ORN gain control from stimulus to firing rate has not been characterized.

Olfactory responses in insects can be fast. Transduction can be initiated within milliseconds of odor reaching the antenna [170]. The speed of the response is enhanced by ORN spike generation, which emphasizes changes in transduction currents [125], and by PNs [95], which maintain fast information transmission from ORNs to PNs [124, 135]. In contrast, adaptation to high intensity stimuli slows down transduction [26, 92, 125], a property that might make it difficult to reliably encode the timing of odor encounters.

We investigated *in vivo* how *Drosophila* ORNs encode encounters with naturalistic odor plumes, which possess the dual complication that both whiff intensities and whiff timing are broadly distributed. To address this question, we first developed an odorant delivery system that reproducibly delivered odorants with naturalistic statistics,

or approximately Gaussian statistics with controlled means and variances. We simultaneously recorded the odorant stimulus (using a fast Photo Ionization Detector (PID)) and recorded extracellularly from identified ORNs. In these studies, we focused on the phenomenology of odorant encoding, which can help to constrain the potential molecular mechanisms that implement them. We found that in response to naturalistic stimuli, ORNs employed front-end nonlinearities inherent in receptor saturation to encode broadly distributed signals. In addition, ORNs could rapidly desensitize following encounters with odorant whiffs, dynamically adjusting gain while responding to intermittent odorant stimuli. On increasing the mean stimulus background, ORNs decreased gain inversely with stimulus intensity, consistent with the Weber-Fechner Law. This phenomenon could be explained if the disassociation constant K of odorant binding scaled with the mean stimulus intensity. Supporting this model, we found that gain control to changes in mean was localized to LFP signals, suggesting that adaptation occurs at transduction in the ORNs, with little contribution from spiking machinery. ORN gain also changed in response to changes in stimulus variance, with gain changes distributed equally across transduction and spiking. Even though the transduction response time slowed down with increasing stimulus intensity, the spiking machinery sped up to compensate. The result of these complementary kinetic changes was that the firing rate response time remained invariant with stimulus intensity, revealing a mechanism that could allow ORNs to preserve information about the precise timing of odor encounters over a wide range of rapidly changing signal intensities.

4.2 RESULTS

4.2.1 ORN responses to broadly distributed naturalistic stimuli.

Odorant signals used to study ORN adaptation typically consist of long pulses or constant backgrounds of various intensities [25, 26, 113, 125]. However, airborne stimuli encountered by flying insects can be intermittent with both the intensities of encounters and durations between encounters broadly distributed as power laws [30]. Since ORN transduction can be adapted by odorant pulses as brief as 35 ms on timescales as fast as 500 ms [26], we asked if ORNs could change their gain dynamically during responses to naturalistic stimuli, amplifying responses to isolated whiffs of odorant, and suppressing responses to whiffs following dense clumps of whiffs.

We measured the responses of *ab3A* and *ab2A* ORNs to naturalistic stimuli of ethyl acetate and 2-butanone, odorants that elicit spikes in these neuron types [73], and are easy to control and measure [113]. We used *in vivo* extracellular recording with simultaneous measurement of the stimulus to record both the Local Field Potential (LFP) and spikes from a single sensillum. Previous results have shown that LFP responses are unaffected by the addition of Tetrodotoxin (TTX), which eliminates neural spiking, and are unaffected when the neuron's partner cell in the sensillum is genetically ablated, when that partner does not sense the odorant [125]. This means that the LFP signal is generated by the sensing neuron, and is upstream of spiking machinery under the conditions tested. We therefore used LFP recordings as an imperfect but useful proxy for transduction activity in ORNs [87, 93, 125, 169].

The naturalistic stimulus we used was intermittent and consisted of brief odor whiffs of varied amplitude (Fig. 4.1a-b). Durations of

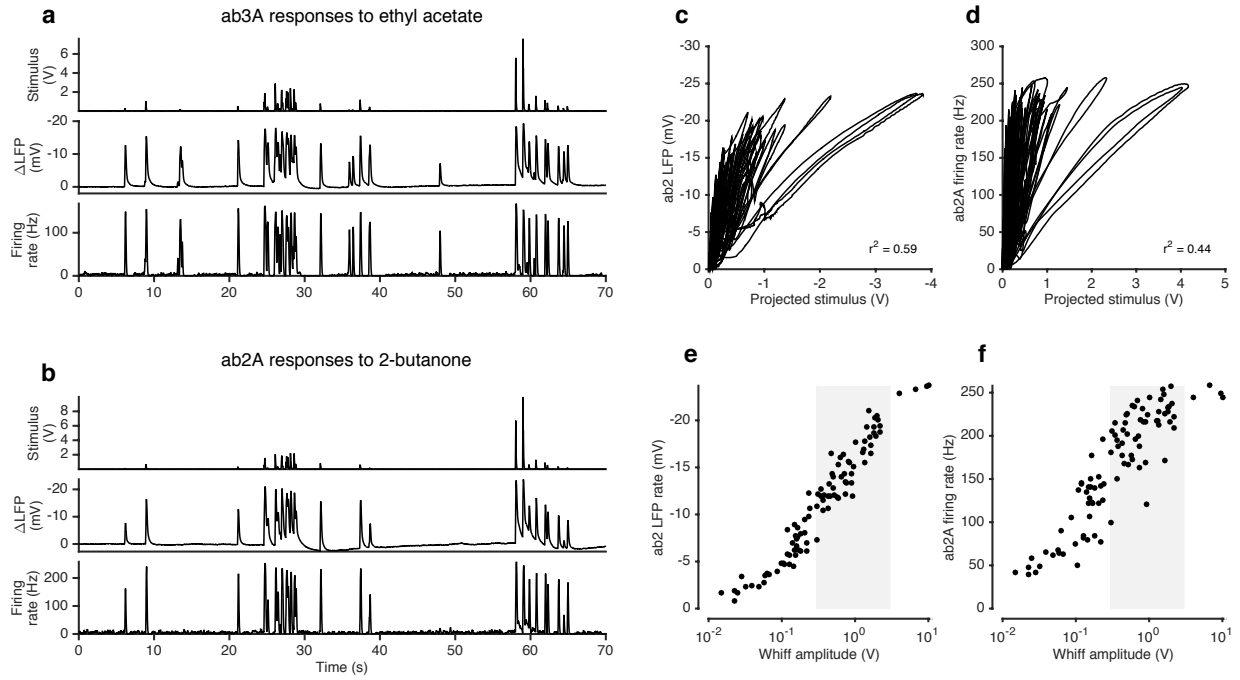


Figure 4.1: Adaptation and saturation modulate ORN responses to broadly distributed naturalistic stimuli. (a) Ethyl acetate odorant (top) elicits LFP (middle) and firing rate (bottom) responses from a ab3A ORN. (b) (a) 2-butanone odorant (top) elicits LFP (middle) and firing rate (bottom) responses from a ab2A ORN. (c) ab2 LFP responses *vs.* projected stimulus. (d) ab2A firing rate *vs.* projected stimulus. (c) and (d) show that ORN responses differ significantly from linearity. (e) ab2 LFP responses *vs.* whiff amplitude. (f) ab2A firing rate *vs.* whiff amplitude. $n = 15$ trials from 2 ORNs. 101 whiffs shown in (e-f).

whiffs and blanks were broadly distributed, with a power law of exponent $-3/2$ to match natural intermittent statistics of odor plumes [30] (Fig. 4.2a-c). ab2A and ab3A ORNs responded to whiffs with transient decreases in the local field potential (LFP) and corresponding increases in the firing rate (Fig. 4.1a-b).

Even though individual whiff intensities were broadly distributed (1st lines in Fig. 4.1a-b) ORN responses to these whiffs were more even, so that responses to faint whiffs were amplified more than those to intense whiffs. To quantify these differences, we defined the gain of the neuron to be the change in the response for a unit change in the stimulus. Since ORNs do not respond instantaneously to odorant stimuli [19, 20], we fit linear filters to best predict the LFP and firing

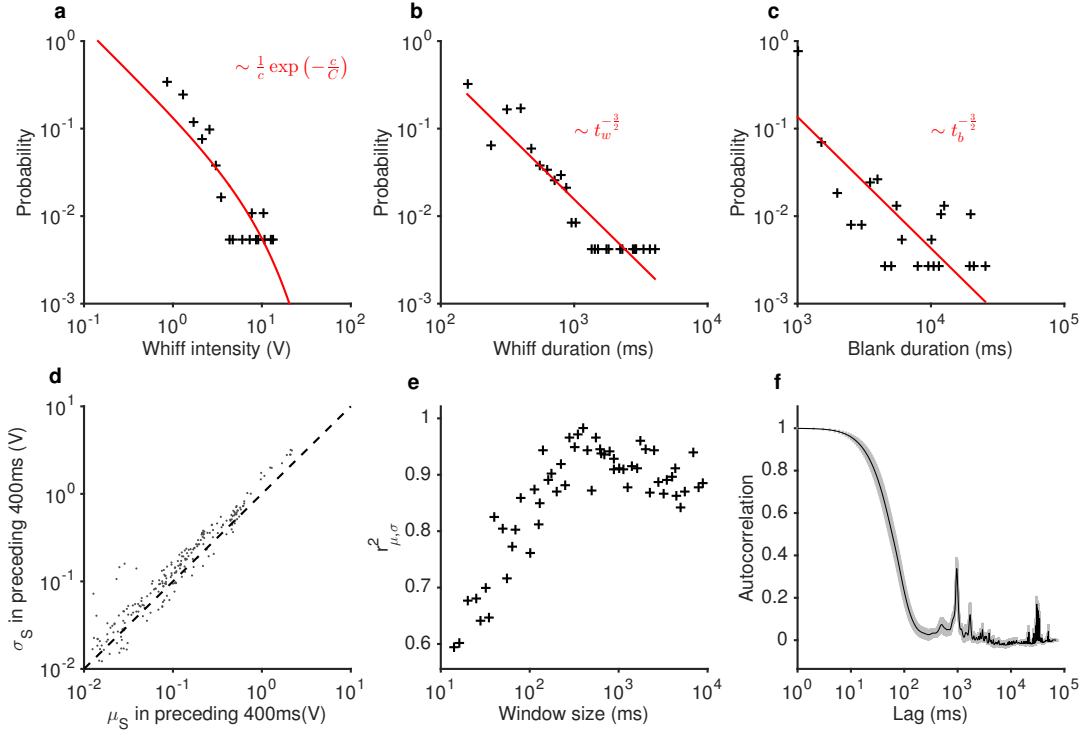


Figure 4.2: Statistics of the ethyl acetate stimulus with naturalistic temporal structure. (a) Distribution of whiff intensities. (b) Distribution of whiff durations. (c) Distribution of blank durations. Predicted distributions from [30] are shown in red lines (a-c). c is the odor concentration (whiff intensity). t_w and t_b are whiff and blank durations. (d) Mean vs. standard deviation of stimulus, computed in 400 ms non-overlapping blocks. (e) Correlation between mean and standard deviation of stimulus as a function of window length. Peak correlation observed for timescales ~ 400 ms. (f) Autocorrelation function of the stimulus. Shading indicates standard deviation across trials.

rate from the stimulus. We used these filters to make linear predictions of the responses from the stimuli (Fig. 4.3). Changes in gain were therefore defined as deviations from the linear prediction of response from the stimulus, similar to [6, 97]. We visualized these gain changes by plotting the LFP responses against linear prediction of the LFP (Fig. 4.1c) and the firing rate against the linear prediction of the firing rate (Fig. 4.1d). Each excursion in these plots corresponds to the ORN’s response to a single whiff. Excursions occurred with different slopes, suggesting that ORN gain changed frequently in time. Deviations from linearity persisted even when filters computed from Gaussian inputs were used to project the stimulus, suggesting that the existence of these deviations do not depend on the exact shape of the filter, but rather reflect a property of the ORN response not captured by the linear model (Fig. 4.3).

Variations in the gain clearly do not arise from a static output nonlinearity, such as one associated with a static linear-nonlinear transformation [42] (Fig. 4.1c-d). We reasoned that changes in the gain could arise from input nonlinearities due to odor-receptor binding and channel opening. To visualize the nonlinearity between the stimulus and response, we plotted LFP and firing rate responses to each whiff in the naturalistic stimulus as a function of the amplitude of that whiff (Fig. 4.1e-f). A clear sigmoidal function is visible in the plot of LFP responses against whiff intensity, consistent with a front-end nonlinearity arising from receptor-odorant binding. However, in both the LFP and firing rates, responses to whiffs with similar intensities varied significantly, deviating from a single sigmoidal dose-response curve (Fig. 4.1e-f).

What causes these deviations from the dose-response curve? The simplest explanation is that these deviations are due to random variability in the responses of the neuron. Another possibility is that these

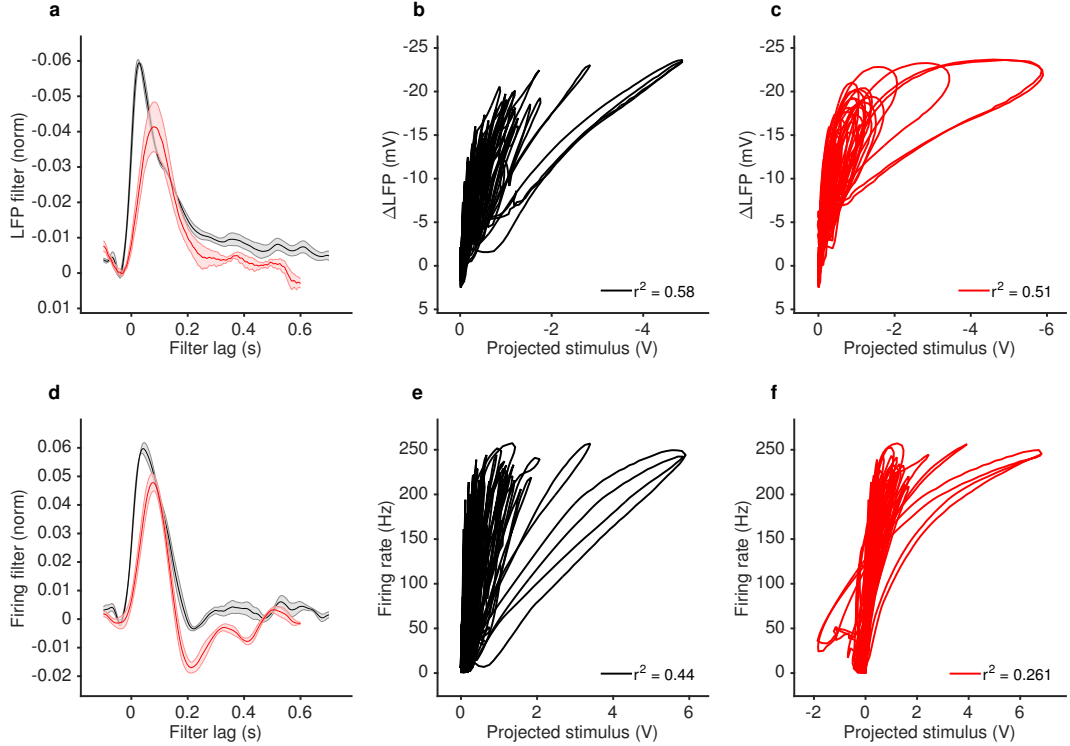


Figure 4.3: Deviations from linearity persist even when filters extracted from Gaussian stimuli are used to project naturalistic stimulus. (a) LFP filters for ab2A ORNs responding to 2-butanone, extracted either from naturalistic stimuli (black) or from Gaussian stimuli (red). (b) LFP responses to naturalistic stimulus vs. stimulus projected through filter computed from naturalistic stimulus (Black filter in (a)). (c) LFP responses to naturalistic stimulus vs. stimulus projected through filter computed from Gaussian stimulus (red filter in (a)). (d) Firing rate filters for ab2A ORNs responding to 2-butanone, extracted either from naturalistic stimuli (black) or from Gaussian stimuli (red). (e) Firing rate responses vs. stimulus projected through filter computed from naturalistic stimulus (black filter in (d)). (f) Firing rate responses vs. stimulus projected through filter computed from Gaussian stimulus (red filter in (d)).

deviations are due to variations in the stimulus history preceding each whiff. To test this hypothesis, we collected whiffs that had similar amplitudes, and examined the LFP and firing rate responses they evoked (Fig. 4.4a-b). The amplitude of LFP and firing rate responses elicited by these whiffs varied inversely with the amplitude of the preceding stimulus: whiffs that occurred in isolation (purple) elicited the largest responses, while whiffs that followed earlier, large whiffs (blue, red) elicited the smallest responses, suggesting that ORN responses can be modulated by stimulus history.

To quantify this context-dependent modulation, we estimated deviations of the LFP and firing rate response to each whiff from the median response. Deviations in LFP response to each whiff decreased with mean stimulus in the preceding 300 ms (Fig. 4.4c, $\rho = -0.39, p = 0.01$, Spearman test), and were uncorrelated with the amplitude of the whiff that elicited them (Fig. 4.4c, inset, $p = 0.9$, Spearman test). Similarly, deviations in the firing rate responses to each whiff decreased with mean stimulus in the preceding 300 ms (Fig. 4.4d, $\rho = -0.68, p < 10^{-5}$, Spearman test), and were uncorrelated with the amplitude of the whiff that elicited them (Fig. 4.4d, inset, $p = 0.37$, Spearman test).

To generalize beyond a particular timescale of the stimulus history, we parametrized the stimulus history of each whiff by the amplitude and time since the preceding whiff, and grouped estimated deviations from the median response into positive or negative (Fig. 4.4e-f). When response deviations were negative (smaller than median responses, blue dots), the amplitude of the preceding whiffs tended to be larger, and the time since the previous whiff tended to be shorter. When response deviations were positive (red dots), the amplitude of preceding whiffs tended to be smaller, and the time since the previous whiff tended to be longer ($p = 0.01$, 2-dimensional KS test on

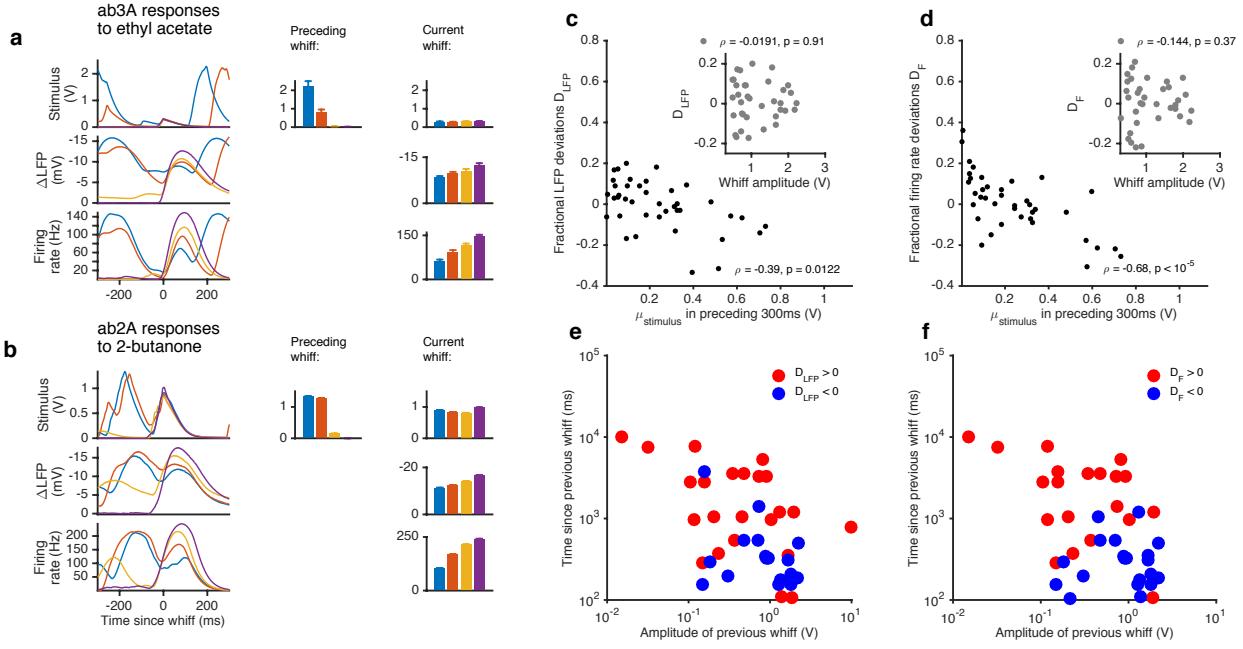


Figure 4.4: Adaptation and saturation modulate ORN responses to broadly distributed naturalistic stimuli. (a) Ethyl acetate whiffs of similar size (top) elicit ab₃ LFP responses (middle) and ab₃A firing rate responses (bottom) with different amplitudes. (b) 2-butanone whiffs of similar size (top) elicit ab₂ LFP responses (middle) and ab₂A firing rate responses (bottom) with different amplitudes. Bar graphs in (a) and (b) show that ordering in LFP and firing rate response does not correlate with whiff amplitude, but correlates with the intensity of the preceding whiff. Deviations in LFP (c) and firing rate responses (d) from the median response *vs.* mean stimulus in the preceding 300 ms. Deviations in LFP (c, inset) and firing rate responses (d, inset) from the median response *vs.* whiff amplitude. (e) LFP response deviations (positive: red, negative: blue) as a function of the amplitude of the previous whiff and the time since previous whiff. Positive and negative deviations are significantly different ($p = 0.01$, 2-dimensional KS test). (f) Firing rate response deviations (positive: red, negative: blue) as a function of the amplitude of the previous whiff and the time since previous whiff. Positive and negative deviations are significantly different, ($p = 0.001$, 2-dimensional KS test on firing rate deviations).

LFP deviations, $p = 0.001$, 2-dimensional KS test on firing rate deviations).

What causes this context dependent suppression of responses following preceding whiffs? One possibility is a bilobed filter, with one positive and one negative lobe. Such a filter is partly differentiating, and would lead to attenuated responses to the second of two closely spaced whiffs, and has been measured in linear models of the firing rate [96, 113, 125]. Such a mechanism may partly account for context dependent variation in firing rates. However, stimulus to LFP filters, computed for this stimulus and others, are mono-lobed (Fig. 4.5), and purely integrating [125], ruling out contributions to dynamic modulation of LFP responses by this mechanism. A model with a static frontend nonlinearity and a mono-lobed filter fit to the LFP also cannot reproduce context-dependent adaptation observed in the LFP (Fig. 4.5), suggesting that this context-dependent variation in response arises at least in part from ORNs dynamically varying gain in response to naturalistic stimuli.

Since the mean and variance of naturalistic stimuli are correlated over many timescales, (Fig. 4.2), it is unclear whether adaptation in this context is sensitive to the mean or the variance (or to some other statistic) of preceding whiffs. To determine how changing one moment of the stimulus distribution changed ORN gain, and to disambiguate the effect of receptor saturation from adaptation, we proceeded to other experiments using Gaussian stimuli with changing means (Fig. 4.6) and variances (Fig. 4.9).

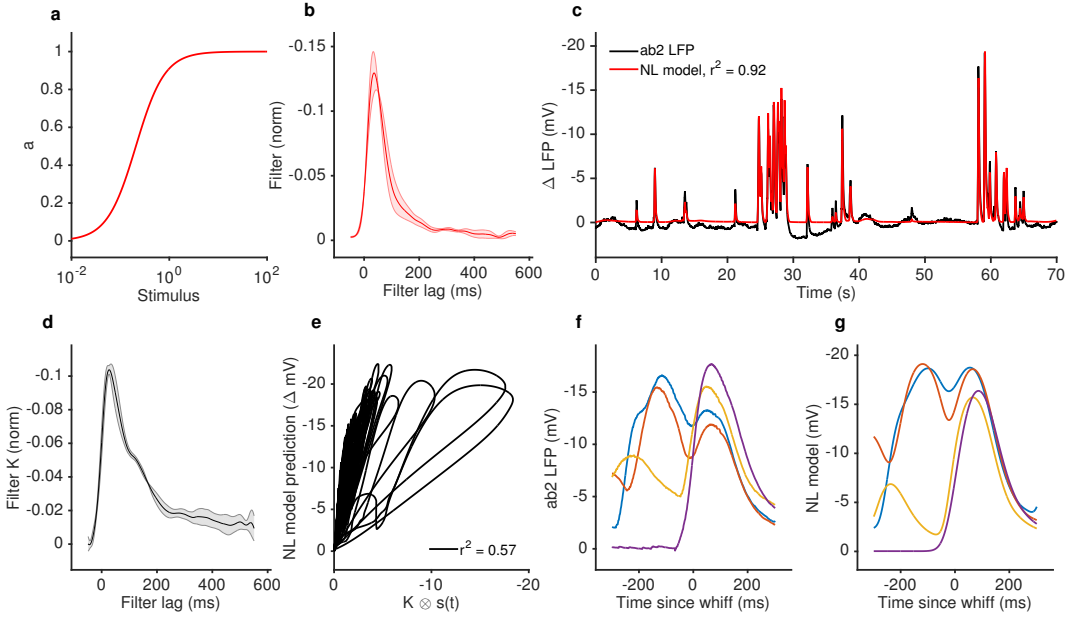


Figure 4.5: An NL model (static input nonlinearity followed by a linear filter) cannot reproduce context-dependence of LFP responses to similar-sized whiffs. Input nonlinearity (a) and filter (b) fit to ab2 LFP responses to 2-butanone naturalistic stimulus. The input nonlinearity is a Hill function ($\frac{S}{S+K_D}$) where S represents the input, and K_D the half maximum value. The nonparametric filter and parametric nonlinearity are fit simultaneously in an iterative manner (see Methods). (c) Comparison of ab2 LFP responses and NL model predictions. (d) Linear filter extracted from the stimulus and the NL model prediction. Note that the filter is not the same as in (b); a filter extracted from an NL model is not guaranteed to be an unbiased estimate of the true one. (e) NL model responses vs. naturalistic stimulus projected through filter in (d), showing that the NL model shows deviations from linearity similar to what is observed in the data (cf. Fig. 4.1c). (f-g) Context dependence of response in the ab2 data and model. (f) ab2 LFP responses to whiffs of similar size (same data as in Fig. 4.4). Note that the responses to isolated whiffs (purple, yellow) are larger than the responses to repeated whiffs (red, blue). (g) NL model responses to these whiffs. Note that the responses to isolated whiffs (purple, yellow) are smaller than the responses to repeated whiffs (red, blue), the opposite of the trend visible in the data.

4.2.2 ORNs adapt to stimulus background by decreasing gain according to the Weber-Fechner Law

A common strategy used by sensory systems to encode signals over a broad range of background intensities is to scale the response according to Weber-Fechner's Law [165], i.e. to control gain inversely with stimulus mean. In ORNs, transduction currents elicited by odorant pulses are reduced by preceding pulses [125] and scale inversely with background intensity, consistent with Weber-Fechner's law [25, 26]. It remains unclear whether the ORNs' ultimate output — the firing rate — follows the same Weber-Fechner scaling [25, 113]. We therefore stimulated ab₃A ORNs with a set of fluctuating ethyl acetate stimuli with increasing means (Fig. 4.6a) but roughly constant variances (Fig. 4.6b, 4.7a). ORNs responded to the stimulus with the smallest mean by modulating firing rates between 0-60Hz (Fig. 4.6c). This response range progressively decreased on increasing mean stimulus intensity (Fig. 4.6d), though the mean response remained at ~30 Hz. To estimate ORN input-output curves, we plotted ORN responses *vs.* the stimulus projected through the normalized best-fit linear filter for each stimulus, estimated through least-squares fitting [32, 43, 140] (Fig. 4.6e). Input-output curves grew shallower with increasing mean stimulus. We defined the ORN gain to be the slope of the input-output curve at that mean stimulus [6].

ORN gain in each trial varied with the mean stimulus in that trial as an approximate power law with exponent -1 (Fig. 4.6f). ORN gains could also be estimated by the ratio of standard deviation of the response to the standard deviation of the stimulus. This measure yielded similar values of ORN gain, and also decreased as a power law with exponent -1 (Fig. 4.7b). This exponent is consistent with the Weber-Fechner Law, which postulates that the just noticeable differ-

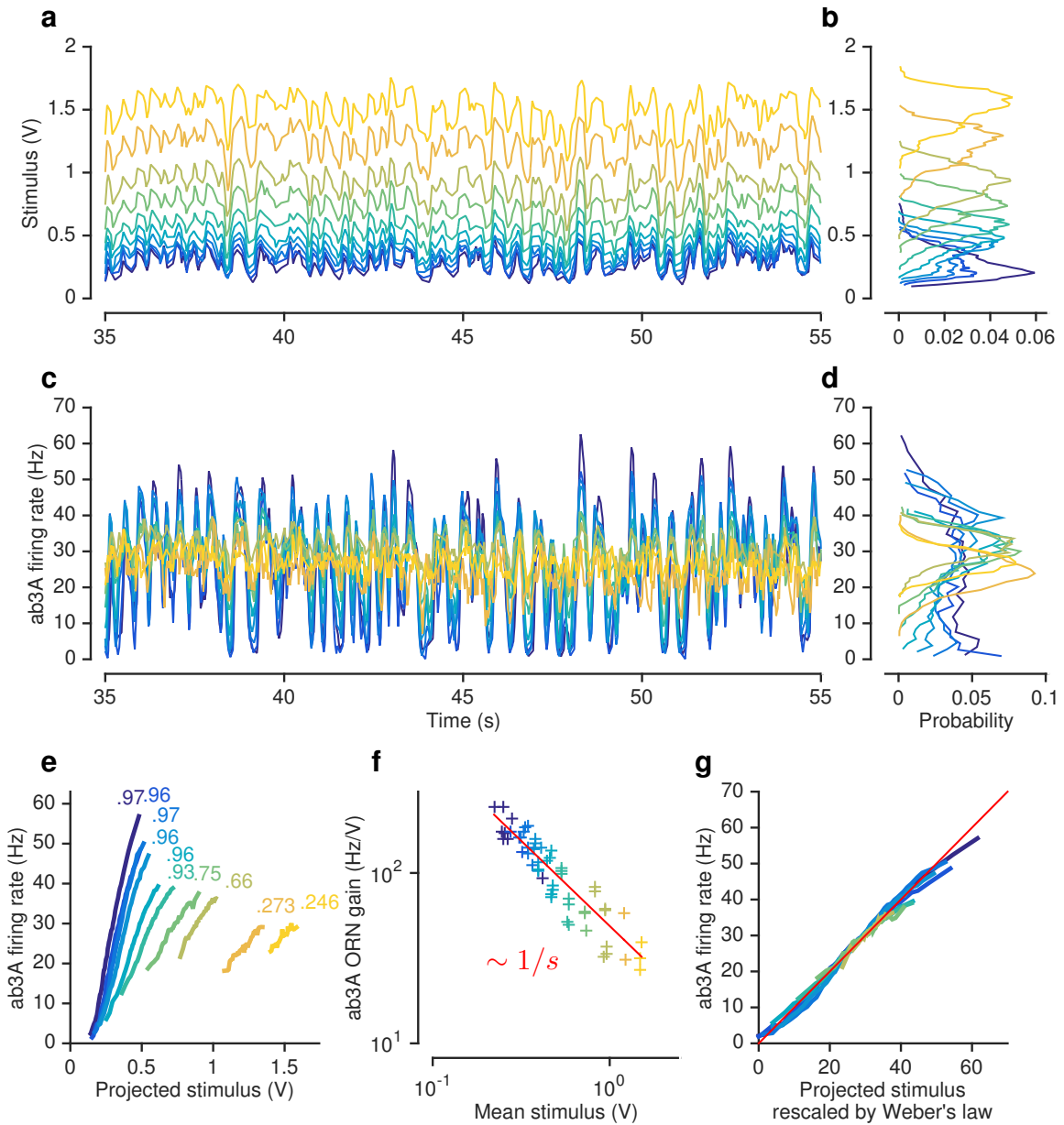


Figure 4.6: ORNs decrease gain with stimulus mean, consistent with the Weber-Fechner Law. (a) Ethyl acetate stimuli with different mean intensities but similar variances. Stimulus intensity measured using a PID, units in Volts (V). Colors indicate mean stimulus intensity. (b) Corresponding stimulus distributions. (c) ab3A firing rate responses to these stimuli. (d) Corresponding response distributions. (e) ORN responses vs. stimulus projected through linear filters. Colored numbers indicate r^2 between linear projections and ORN response. (f) ORN gain vs. mean stimulus for each trial. Red line is the Weber-Fechner prediction (g) After rescaling the projected stimulus by the gain predicted by the red curve in (f), and correcting for an offset, ORN responses collapse onto one line. $n = 55$ trials from 7 ORNs in 3 flies. All plots except (f) show means across all trials. (f) shows individual trials.

ence between two stimuli is inversely proportional to the stimulus magnitude [165]. Rescaling the projected stimulus by the gain predicted by Weber's Law collapsed all input-output curves onto a single curve (Fig. 4.6g).

Can front-end or back-end nonlinearities reproduce the observed change of input (stimulus)-output (firing rate) curves (Fig. 4.6e)? Clearly, no single output nonlinearity can fit the data shown in (Fig. 4.6e). Since a front-end nonlinearity is present (Fig. 4.1), we asked whether a nonlinear-linear (NL) model could reproduce this data, with the input nonlinearity parameterized by a Hill function where s represents the input, and K the half maximum value. (Fig. 4.8a-c). NL model responses increased with mean stimulus (Fig. 4.8c), unlike in the data (Fig. 4.6d-e). However, if the half maximum value of the Hill function was allowed to vary with the mean stimulus, the model could qualitatively reproduce the data, suggesting adaptation at the front-end nonlinearity (Fig. 4.8d-f).

To determine if similar gain-control relative to mean signal intensity was broadly observed, we tested additional ORNs from the two major olfactory organs of the fly, the antenna and the maxillary palp (ab2A, pb1A), and used ecologically relevant odorants from three different functional groups (ketones: 2-butanone, alcohols: 1-pentanol, esters: isoamyl acetate) in various combinations. In all five cases, the neurons decreased gain with increasing odorant concentration, and obeyed a roughly inverse scaling (Fig. 4.7c-f). Thus *in vivo*, for various neurons and odorants, ORN firing rate followed the Weber-Fechner Law.

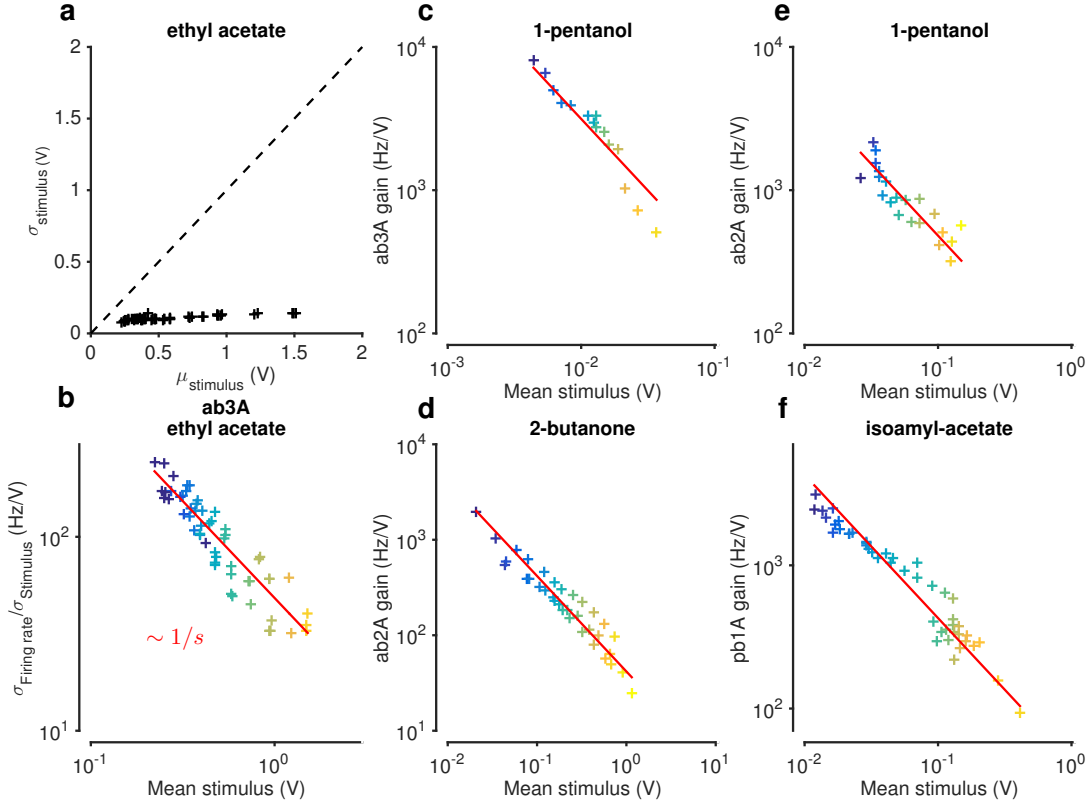


Figure 4.7: *Weber-Fechner Law broadly observed across odor-receptor combinations.* (a) Standard deviation vs. mean of ethyl acetate stimulus in Fig. 4.6. (b) ORN gain estimated by the ratio of standard deviation of firing rate to standard deviation of stimulus, vs. mean stimulus in each trial. This model-free estimate of ORN gain ignores kinetics of response, but returns similar estimates of the gain (cf. Fig. 4.6f). Note that the units of gain estimated this way are the same. (c-f) ORN gain as a function of mean stimulus for various odor-receptor combinations. In all plots, the red line is a power law with slope -1 (the Weber-Fechner Law). Data in panel a and b is the same as in Fig. 2. n = 121 trials from 16 ORNs in 6 flies.

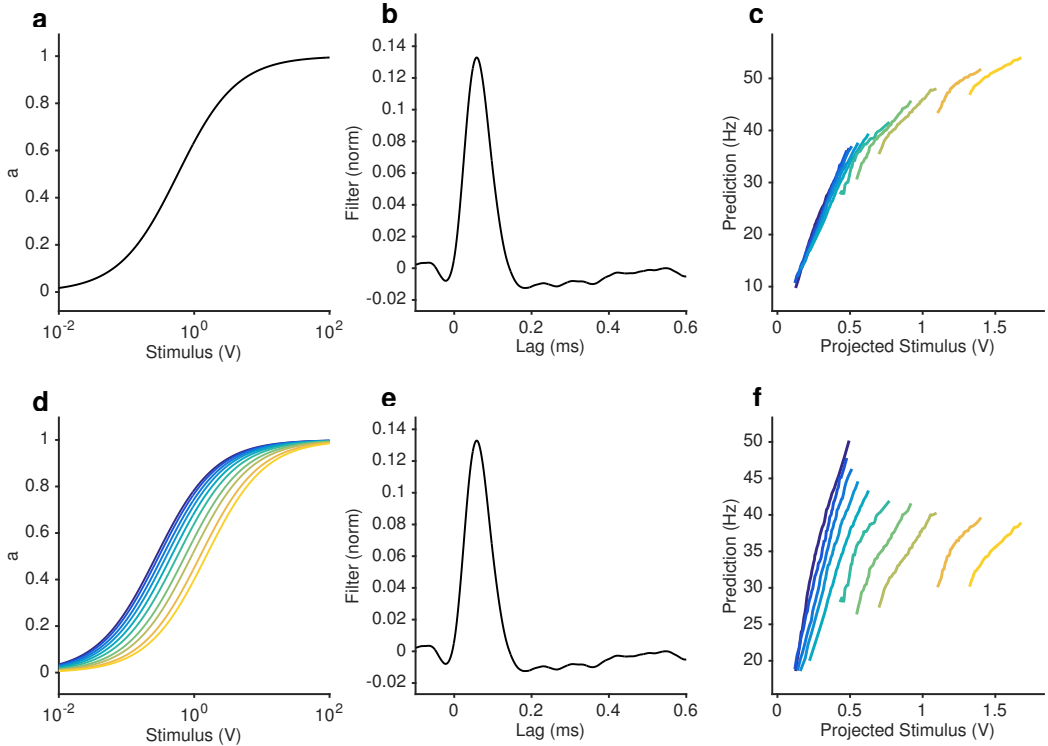


Figure 4.8: Ability of NL models to reproduce observed change in input-output curves. (a-c) static NL model responses. (a) The input nonlinearity of NL model is chosen to be a Hill function with $n = 1$. (b) Filter of NL model, measured directly from the data. (c) NL model responses *vs.* projected stimulus. While these curves appear to change slope with increasing mean stimulus, mean responses also tend to increase (purple ... yellow). (d-f) Varying NL model responses, where the K_D of the input nonlinearity is allowed to vary with the mean stimulus. (d) Input nonlinearities for stimuli with different mean (colors). The KD of each curve is set to the mean stimulus of that trial. (e) Filter of NL model, same as in (b). (f) Model responses *vs.* projected stimulus. Note that, like in the data (cf. Fig. 4.6e), the mean response remains relatively invariant with mean stimulus, and that curves get shallower with increasing mean stimulus.

4.2.3 Fast variance-dependent gain control in ORNs

In other sensory modalities, such as vision, some neurons adapt not only to the mean but also to the variance of the signal [6, 140]. We therefore asked whether ORNs adjust their gain in response to changes in the variance of the signal. We stimulated ab₃A ORNs with fluctuating ethyl acetate stimuli in which the variance of the signal changed every 5 s (Fig. 4.9a), switching back and forth between high to low values, around a nearly constant mean (Fig. 4.9b; 4.10a), a protocol used to study gain control in visual neurons [6, 54, 140].

As expected, ORNs responded to input fluctuations by modulating their firing rate. Interestingly, ORN firing rate variance did not vary as much as the stimulus variance between epochs of high and low stimulus variances, suggesting that ORNs actively changed their gain to compensate for such input differences (Fig. 4.9c-d). ORN input-output curves during high variance epochs (red) were shallower than during low variance (blue) epochs (Fig. 4.9e). Trial-wise ORN gain decreased with the variance of the stimulus (Fig. 4.9f). ORN gains estimated by dividing the standard deviation of the response by the standard deviation of the stimulus showed a similar decrease in ORN gain with stimulus variance (Fig. 4.10b).

A simple coding strategy maximizes a neuron's information capacity by matching its input-output curve to the cumulative distribution function (c.d.f) of the stimulus [104]. Like the c.d.f.s (dashed lines), the input-output curves (solid) are steeper during the low variance epoch. On a trial-by-trial basis, ORN gain was correlated with the c.d.f slope ($r^2 = 0.7$) (Fig. 4.9g). However, as the input variance changed by a factor of 2.5, the gain in the neuron only changed by a factor of 1.7, not as much as would be required for optimal information encoding.

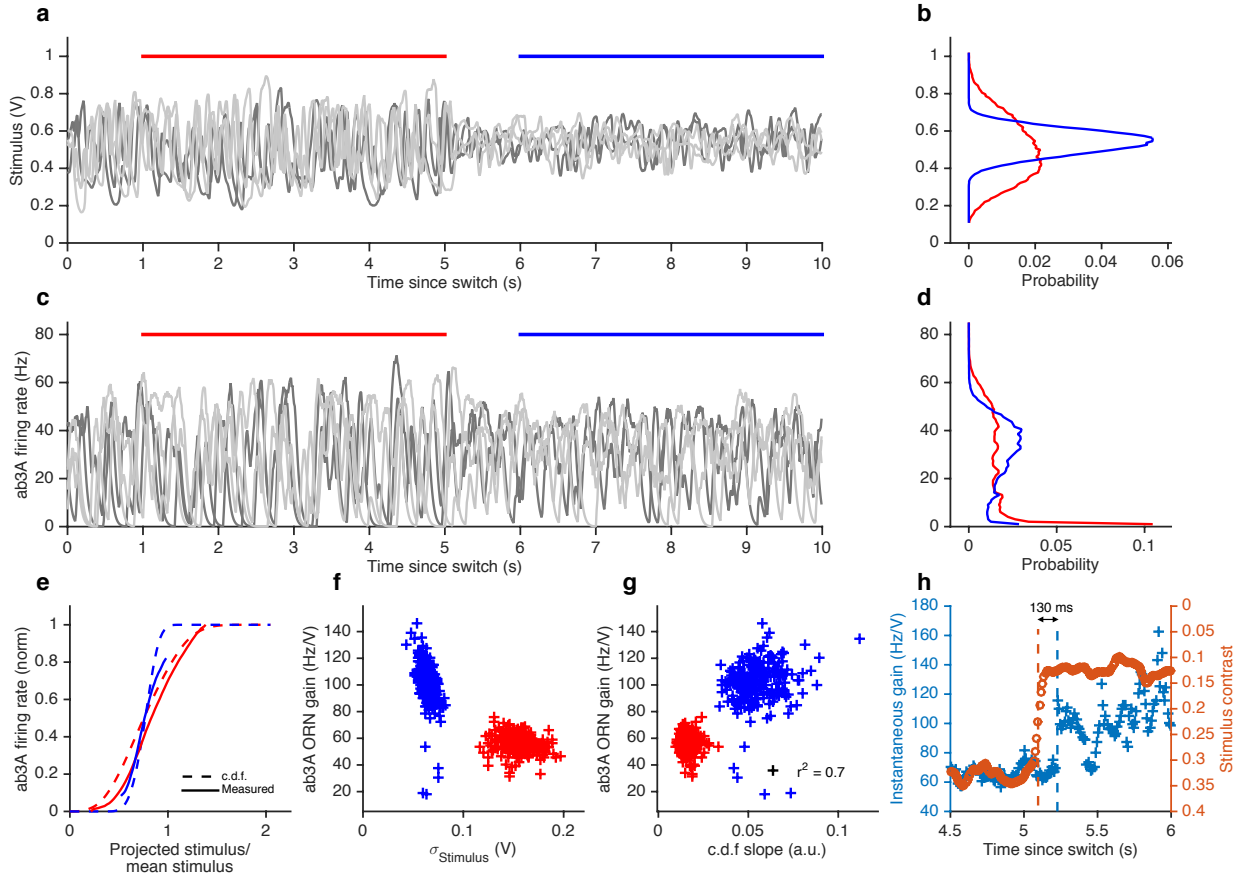


Figure 4.9: ORNs decrease gain with stimulus variance. (a) Stimulus intensity of a fluctuating ethyl acetate stimulus with nearly constant mean but a variance that switches between high and low every 5 seconds. 5 independent trials (out of 248) are plotted. (b) Distributions of stimulus intensity for the epochs of low (blue) and high (red) variance. (c) ab3A firing rate responses corresponding to the trials shown in (a) following the switch from low to high variance, which takes place at $t = 0$ s and from high to low, which takes place at $t = 5$ s. (d) Probability distributions of the response. (e) Solid lines are ORN input-output curves computed from a single filter from both low (blue) and high (red) variance epochs. Dashed lines are the cumulative distribution functions (c.d.fs) of the projected stimulus. (f) ORN gain as a function of the standard deviation of the stimulus, measured per trial for each epoch. (g) Measured gain plotted against the slope of the cumulative distribution function for each trial. (h) Instantaneous gain (blue) and stimulus contrast (orange) as a function of time since switch. Dashed lines indicate crossover times of stimulus contrast and instantaneous gain. The delay is ~ 130 ms. $n = 248$ trials from 5 ab3A ORNs in 2 flies.

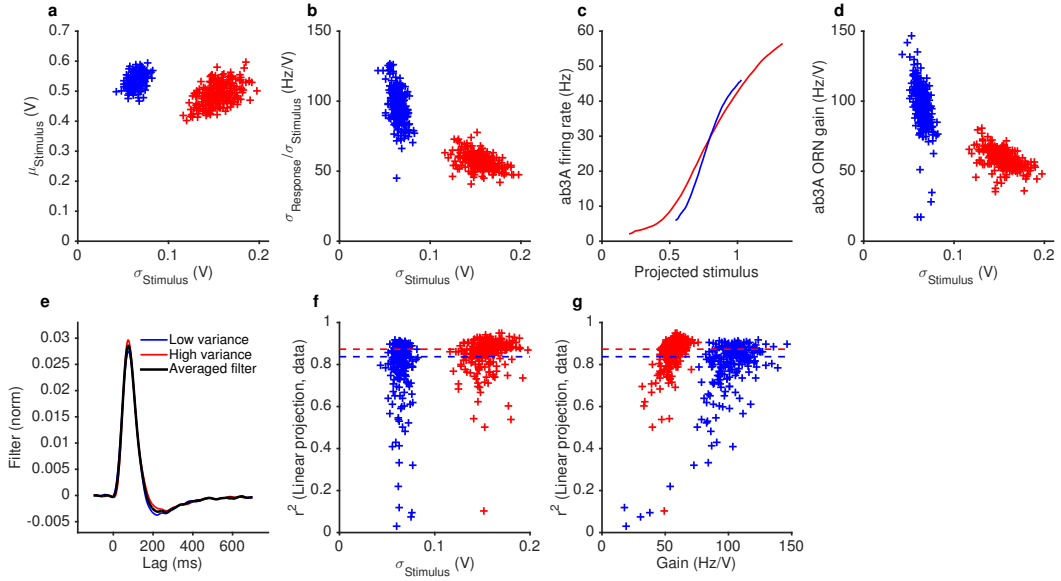


Figure 4.10: Variance gain control in Gaussian stimuli. (a) While the dominant change between the two epochs is the change in variance (by construction), the low variance trials also tend to have slightly higher means. (b) ORN gain estimated by dividing the standard deviation of the response by the standard deviation of the stimulus, for each trial, *vs.* the standard deviation of the stimulus (cf. Fig. 4.9f). (c) Input-output curves for the ab3A ORN uncorrected for the change in the mean stimulus. The blue curve intersects the red curve, and is steeper than the red curve, suggesting that gain during the low variance epoch is higher than the gain during the high variance epoch. (d) ORN gain during high and low variance epochs, without correcting for the change in the mean stimulus. Each trial appears in the plot as one blue point (for the low variance epoch) and one red point (for the high variance epoch). (e) Filters used in this analysis. Filters backed out of low variance (blue) or high variance (red) epochs alone are very similar. Therefore, we averaged all filters (black) and used that averaged filter to project all the stimulus in this dataset. (f) Coefficient of determination (r^2) *vs.* the standard deviation of the stimulus. ~80% of trials had $r^2 > 0.8$. (g) Coefficient of determination (r^2) *vs.* trial-wise ORN gain in the high and low variance epoch. Dashed lines in (f-g) indicate the median during the high and low variance epoch.

Gain control to the stimulus variance was fast, with gain changing as fast as ~ 130 ms following the change in stimulus variance (Fig. 4.9h).

4.2.4 *Mean and variance gain control occur at different stages of odor encoding, and are mechanistically distinct*

ORN responses arise through two sequential steps: odor transduction followed by spike generation [125]. Does each step possess separate gain control mechanisms, or is gain control achieved solely at one step? Previous studies place the mechanism of adaptation to mean stimulus at the level of signal transduction [25, 26, 125]. How the spiking machinery might influence gain control, and where adaptation to signal variance takes place, remain unknown.

We reanalyzed the responses of ab β A to ethyl acetate signals (Figs. 4.6&4.9) and measured “transduction gain” (stimulus to LFP) and “firing gain” (LFP to firing rate). Changing the stimulus mean alone modified gain in LFP (Fig. 4.11a-b). However, gain at the spiking machinery was invariant to the ten-fold change in the mean stimulus. ($p = 0.41$, Spearman rank correlation), with a 1 mV change in LFP leading to a ~ 10 Hz change in the firing rate, consistent with earlier studies[125] (Fig. 4.11c-d). Transduction gain, like ORN gain, scaled with the Weber-Fechner Law, for a variety of odor-receptor combinations (4.12a-d), consistent with previous studies [25, 26]. In contrast, adaptation to the stimulus variance changed gain both at transduction and at spiking (Fig. 4.11e-h). Both gains changed by a factor of ~ 1.3 from the high to the low variance epoch ($p < 10^{-4}$, Wilcoxon signed rank test), contributing roughly equally to variance gain control (Fig. 4.12f). In other systems such as vision, variance gain control has been traced down to the spiking machinery and single neuron Hodgkin-Huxley models have been shown to exhibit variance gain

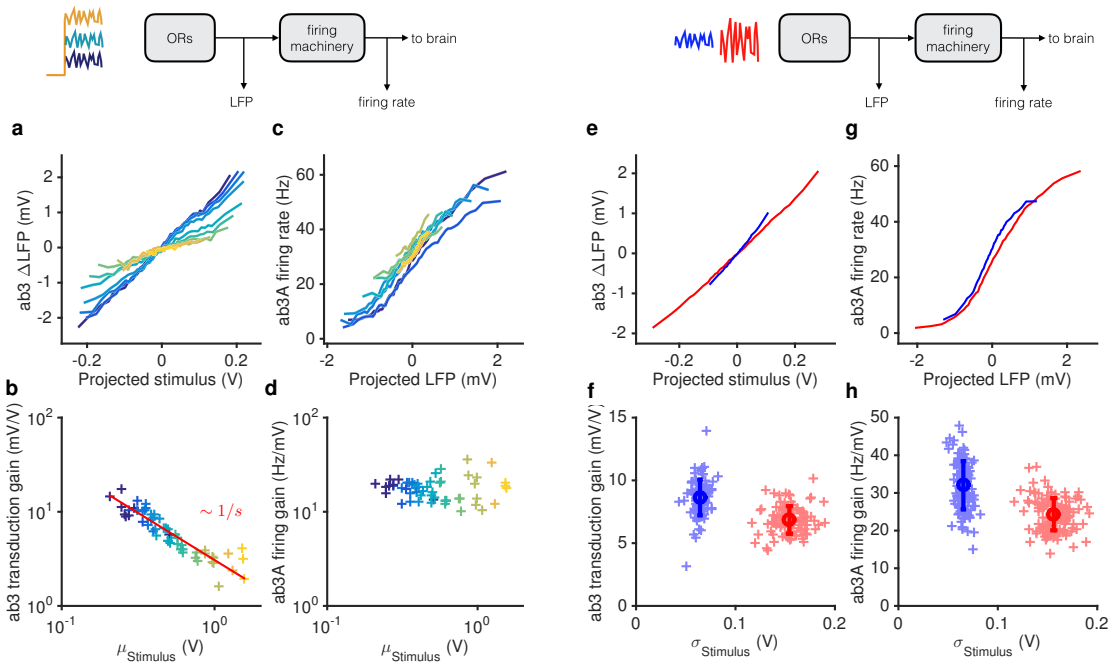


Figure 4.11: *Mean gain control occurs primarily at transduction, and variance gain control occurs both at transduction and at the firing machinery.* (a) Transduction input-output curves from stimulus to LFP. Colors indicate increasing mean stimulus. Filters and projections are computed trial by trial. (b) Transduction gain, measured from the slopes of these input-output curves, decreases with the mean stimulus. The red line is a power law with exponent -1, (Weber's Law). (c) Input-output curves for the firing machine module. (d) Firing gain does not change significantly with mean stimulus. (e) Transduction input-output curves for low (blue) and high (red) variance stimuli. (f) Transduction gains in the low variance epoch are significantly higher than transduction gains in the high variance epoch ($p < 0.001$, Wilcoxon signed rank test) (g) Input-output curves of firing machinery during low variance stimuli. (g) Firing gain during low variance epochs are significantly higher than firing gains during high variance epochs ($p < 0.001$, Wilcoxon signed rank test). Projections of stimulus are divided by the mean stimulus in each trial to remove the small effect Weber-Fechner gain scaling. Data in this figure is same as in Figs. 4.6 and 4.9. (a,c,e,g) Mean across all trials. (b,d,f,h) Individual trials.

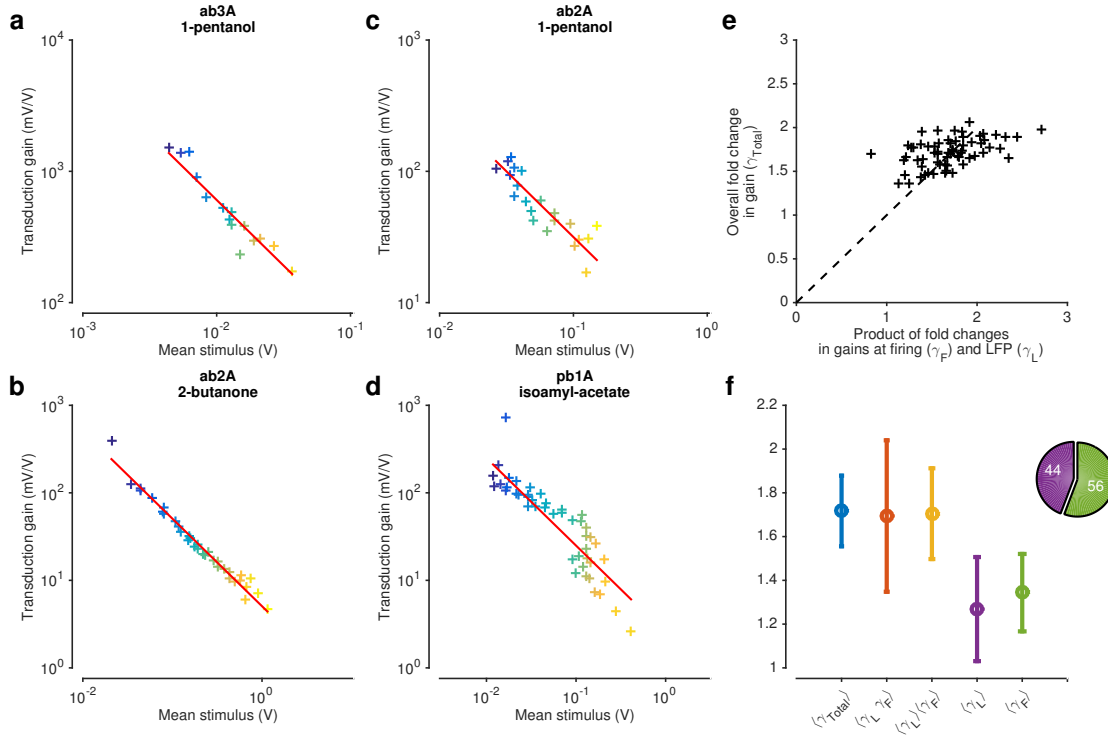


Figure 4.12: Mean and variance gain control at transduction and spiking. (a-d) Gain due to changing the mean stimulus. Transduction gain as a function of mean stimulus for different odor-receptor combinations. Red lines are power laws with exponent -1 (Weber-Fechner prediction). (e-f) Comparison of gain changes at transduction and firing due to changes in stimulus variance. (e) Trial-wise overall gain fold change ($\gamma_{\text{total}} = \text{ORN gain at low variance}/\text{ORN gain at high variance}$) vs. trial-wise product of gain fold changes at transduction (γ_L) and firing (γ_F). (f) Comparison of average fold change in gain due to changing stimulus variance. Pie chart shows relative contribution (in percent) of transduction gain change (purple) and firing gain change (green) to overall gain change.

control to current injection. It is interesting that in ORNs transduction gain changes are also involved in contrast adaptation.

Adaptation of ORNs to the mean stimulus and their Weber-Fechner gain control may be mediated by a feedback mechanism involving a slow diffusible factor such as calcium, which has been suggested to be involved in other types of adaptation [125]. Decreasing extracellular calcium has been shown to abolish ORN adaptation to steps of odorant and cause deviations away from the Weber-Fechner Law [26], suggesting that ORN activity can cause an influx of calcium that

leads to ORN adaptation. To test this hypothesis, we measured intracellular calcium concentrations by measuring fluorescence changes in ab₃A ORNs expressing the calcium reported GCaMP6 [31]. We found that GCaMP6 fluorescence increased with increasing odorant stimulus, supporting a role of calcium influx in ORN adaptation to the mean stimulus (Fig. 4.13). In contrast, changing stimulus variance but keeping the stimulus mean the same did not significantly change GCaMP6 fluorescence between high- and low-variance epochs (Fig. 4.14), suggesting that mean and variance gain control are mechanistically distinct.

4.2.5 Modularity of gain control at transduction and spiking

Since spiking occurs downstream of transduction, Weber-Fechner gain scaling at transduction ensures that fluctuations in the input to the spiking machinery occur at the same scale, independent of the scale of the stimulus. Can spiking gain change to amplify or suppress transduction responses? To decouple the overall drive to the neuron from Weber-Fechner gain control at transduction, we expressed Chrimson channels [98] in ab₃A ORNs and activated them using red light.

First, we used a fluctuating ethyl acetate stimulus to probe transduction and ORN gain while increasing the neuron's firing rate using increasing backgrounds of red light (Fig. 4.15a-b). While increasing light levels elicited increasing firing rates (Fig. 4.15b inset), ORN and transduction gain did not vary with the intensity of supplemental light (Fig. 4.15a-b). This suggests that constitutive spiking activity does not feed back onto LFP adaptation, or overall ORN gain.

Second, we used a fluctuating light stimulus to probe the spiking gain while stimulating the ORN and its receptors with increasing backgrounds of ethyl acetate odorant (Fig. 4.15c-d). While ethyl ac-

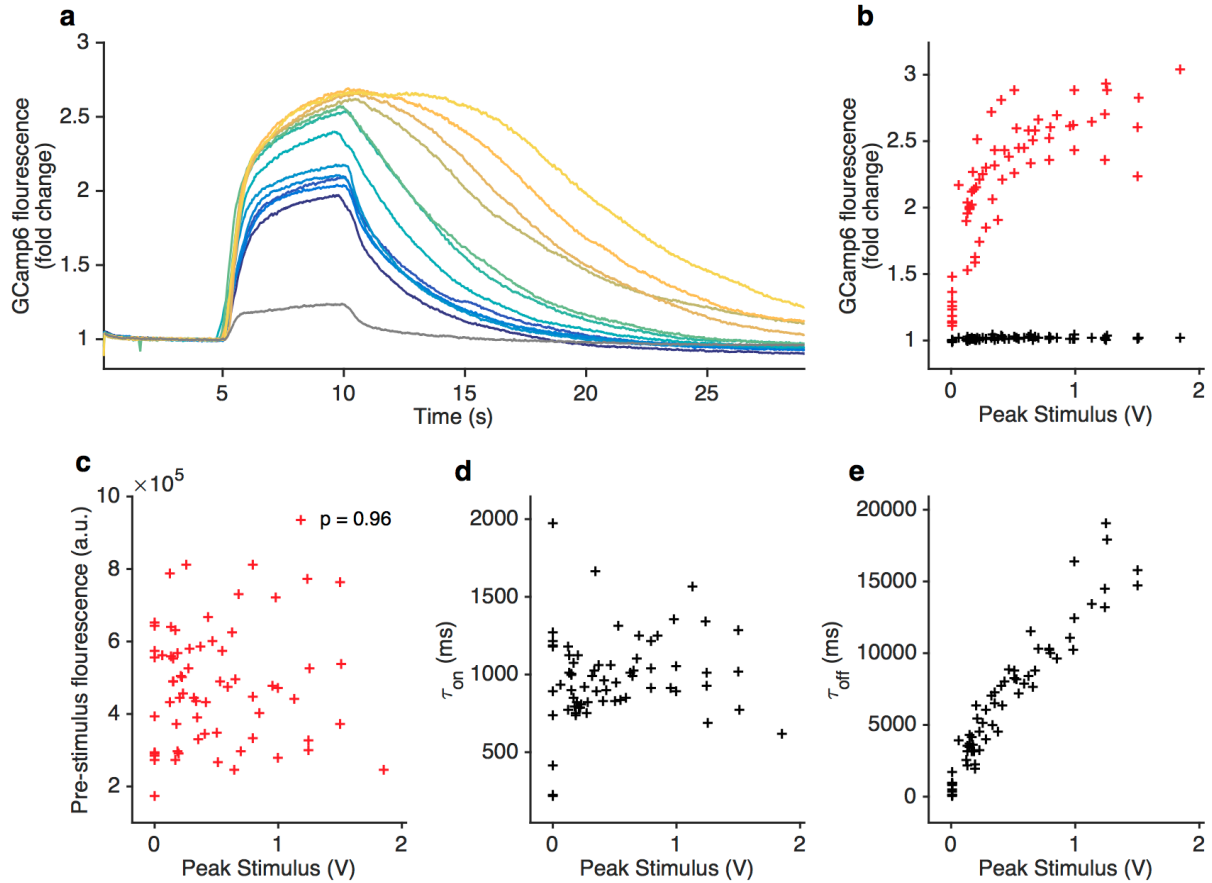


Figure 4.13: *Intracellular Calcium increases with odor concentration.* (a) Fold change in fluorescence from regions of interests (ROIs) over ab₃ sensilla in w; 22a-GAL4/+; UAS-GCamp6f/+ flies. Colors indicate odorant concentration applied (purple...yellow). Gray trace is from a control application with no odorant. Odorant was applied for 5 second from $t = 5$ s to $t = 10$ s. (b) GCamp6 fluorescence fold change as a function of peak stimulus, for ROIs over ab₃ sensilla (red) and for control ROIs (black). (c) Pre-stimulus fluorescence vs. peak stimulus of odorant stimulus. (d) Rising timescale of Calcium signals in (a) vs. peak stimulus (see Methods). (e) Off timescale of Calcium signals in (a) vs. peak stimulus (see Methods).

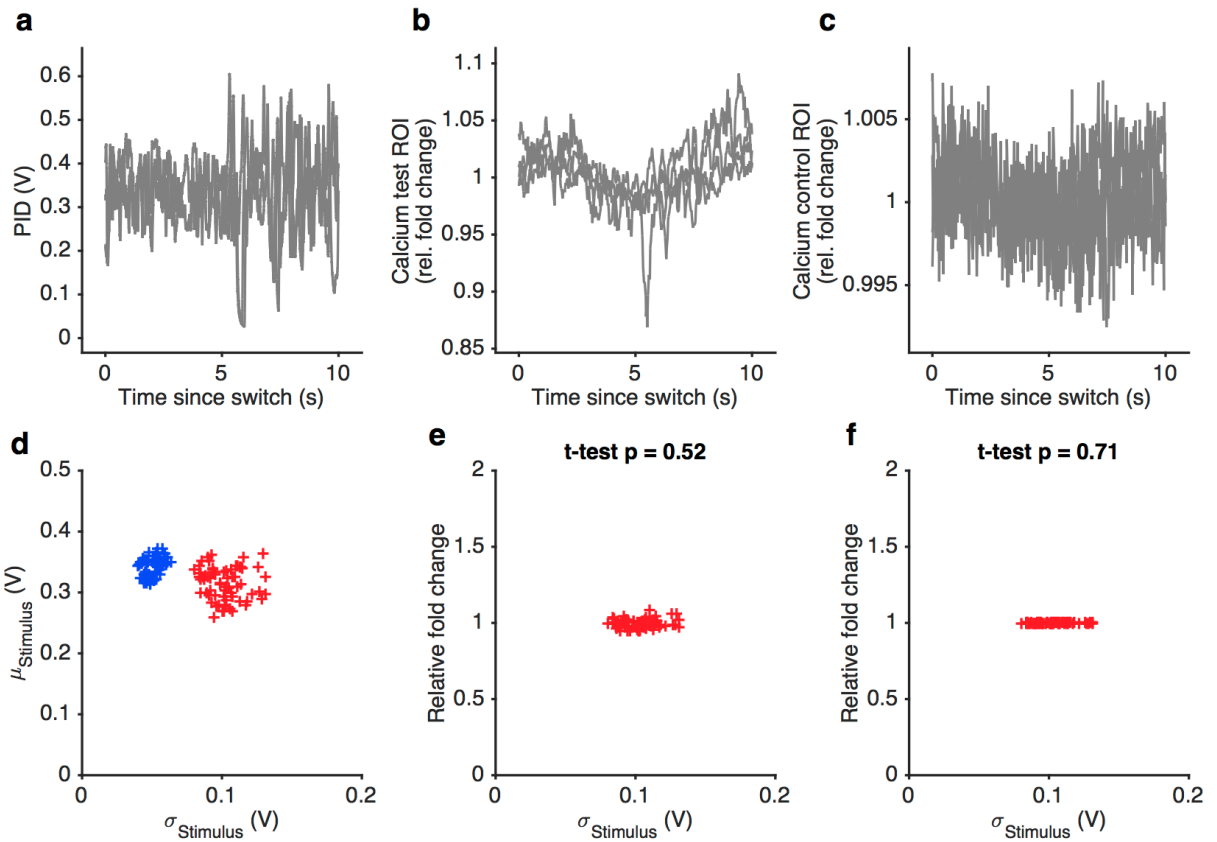


Figure 4.14: Intracellular Calcium does not change with stimulus variance. (a) Odorant stimulus applied, consisting of alternating 5 s epochs of low variance (0 - 5 s) and high variance (5 - 10 s). (b) Relative fold change of GCamp6f fluorescence from ROIs over ab₃ sensilla in w; 22a-GAL4/+; UAS-GCamp6f/+ flies. (c) Relative fold change of GCamp6f fluorescence from ROIs over control regions outside sensilla in w; 22a-GAL4/+; UAS-GCamp6f/+ flies. (d) Mean stimulus *vs.* standard deviation of stimulus for low variance epochs (blue) and high variance epochs (red). (e) Relative fold change in GCamp6f fluorescence from ROIs over ab₃ sensilla between high-variance epochs and low-variance epochs. No significant change was observed (*t*-test, $p = 0.52$). (f) Relative fold change in GCamp6f fluorescence from control ROIs between high-variance epochs and low-variance epochs. No significant change was observed (*t*-test, $p = 0.71$).

estate backgrounds of increasing intensity increased ORN firing rate (Fig. 4.15d inset), they failed to change gain in the spiking machinery. Increasing odor backgrounds moved input-output curves along the y-axis (Fig. 4.15c), consistent with increasing firing due to background odor, but failed to change the slope of these curves, suggesting that ORN gain to the fluctuating light probe was not changed. This suggests that adaptation at transduction does not affect gain of the spiking machinery, consistent with our result that increasing odor backgrounds decreased gain at transduction, but not spiking (Fig. 4.11a-d). Thus, Weber-Fechner scaling in ORN gain control to stimulus mean is insulated from activity of the spiking machinery.

Variance gain control exists in a wide range of neurons [6, 46, 122, 140, 179, 186] and in models of spiking neurons [60, 81, 184, 185], suggesting that variance gain control could be an intrinsic property of spiking neurons. To determine if the spiking machinery alone could give rise to variance gain control, we stimulated ab3A ORNs that express Chrimson with fluctuating light stimuli of different variances at fixed mean. ORN input-output curves were steeper when the variance of the light stimulation was smaller (Fig. 4.15e-f), similar to the curves observed with odor stimulation (cf. Fig. 4.9e). We observed that gain changed by a factor of ~1.5 when the standard deviation of the light stimulus changed by a factor of ~3, consistent with variance gain control occurring partly in the spiking machinery (Fig. 4.11e-h), though Chrimson channels might exhibit their own adaptation to inputs.

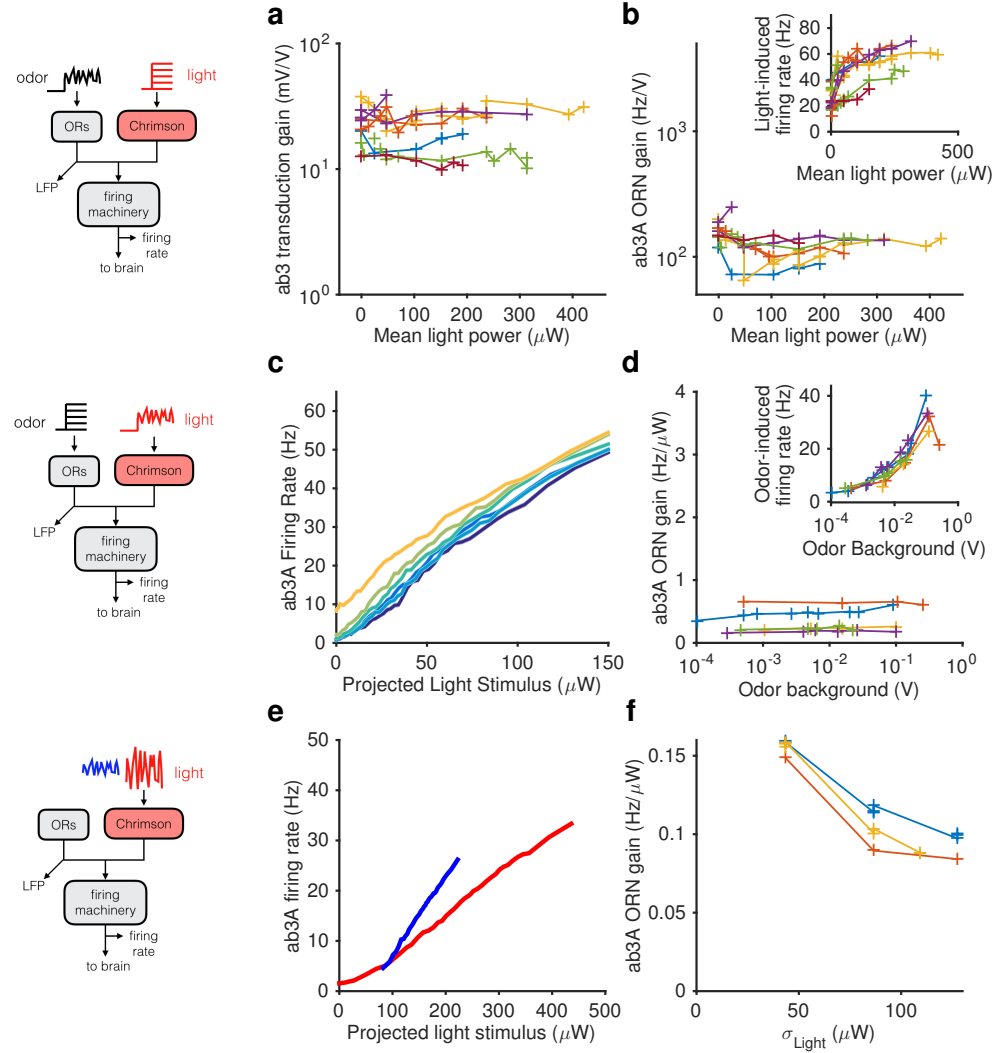


Figure 4.15: Modularity of gain control revealed by optogenetic stimulation. ab3A ORNs in *w; 22a-GAL4/+; UAS-Chrimson/+* flies can be activated by ethyl acetate odorant or by red light. (a-b) Fluctuating odor foreground and constant light background. (a) Transduction gain to fluctuating odor . background light stimulation intensity. (b) Overall ORN gain to fluctuating odor stimulus vs. background light stimulation intensity. (b, inset) ORN firing rate vs. background light intensity. (c-d) Fluctuating light foreground and constant odor background stimulus. (c) Input-output curves to fluctuating light stimulus for increasing background odor (lighter colors indicate larger odor background). (d) ORN gain is invariant with background odor concentration. (d, inset) Odor-induced firing gain vs. background odor concentration. (e-f) Fluctuating light stimulus with different variances. (e) Input-output curves for high (red) and low (blue) variance light stimuli. (f) ORN gain as a function of the standard deviation of the light stimulus. (a-b) $n = 75$ trials from 13 ORNs. (c-d) $n = 64$ trials from 5 ORNs. (e-f) $n = 21$ trials from 3 ORNs. Lines link trials from a single ORN.

4.2.6 Despite slowdown in transduction, ORN firing rate preserves timing of odor encounters

When navigating odor plumes, the precise timing of the encounter with the plume carries important information, which may be lost if adaptation changes the lag between signal and response in a concentration-dependent manner. The kinetics of ORN spiking in response to pulses of odorant are invariant to the pulse intensity and to the background intensity over a range of odorant concentrations [113]. Paradoxically, adaptation to background odorants slows transduction current responses to odor pulses [26, 92, 125]. We hypothesized that these seemingly contradictory results might be resolved if the ORN spiking machinery speeds up to compensate for the intensity-dependent slowdown in the LFP.

We characterized responses to odorant stimuli on increasing backgrounds by measuring both ORN spike rates and LFP. We computed cross correlation functions between the stimulus and the LFP for various stimulus backgrounds. For stimuli on low backgrounds, LFP cross-correlation functions peaked earlier, while for stimuli on larger backgrounds, LFP cross-correlation functions peaked later (Fig. 4.16a), consistent with [26, 92, 125]. Surprisingly, cross-correlation functions from the stimulus to the firing rate were similar between stimuli on low and high backgrounds (Fig. 4.16b), consistent with [113]. This selective change in the kinetics of the LFP, but not the firing rate, occurred even though there was no change in the stimulus autocorrelation function from low to high stimulus (Fig. 4.16c). We defined the LFP and firing rate lags relative to the stimulus by the location of the peak of the cross-correlation function, and found that while LFP response lags increased with increasing odorant concentration ($p < 10^{-2}$, Spearman test), firing rate lags remained relatively invari-

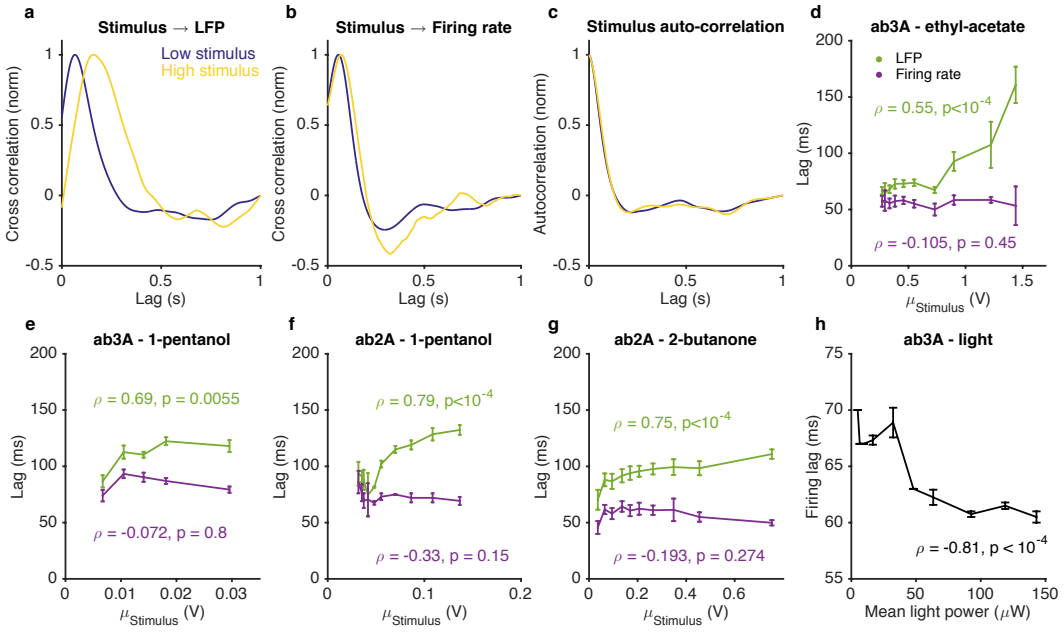


Figure 4.16: Adaptation to the mean slows down LFP, but not firing rate. (a-d) Response of ab3A ORNs to Gaussian ethyl acetate stimuli on increasing backgrounds. (a) Cross correlation functions between ethyl acetate stimulus and ab3 LFP responses for low (purple) and high (yellow) background stimuli. (b) Cross correlation functions between ethyl acetate stimulus and ab3A firing rate responses for low (purple) and high (yellow) background stimuli. (c) Stimulus autocorrelation functions for low (purple) and high (yellow) background stimuli. (d-g) LFP and firing rate lags w.r.t to the stimulus *vs.* the mean stimulus for various odor-receptor combinations. LFP lags increase with mean stimulus, while firing rate lags do not. (h) Firing lags of ab3A ORNs expressing Chrimson channels *vs.* applied light power. In (c-g), ρ is the Spearman correlation coefficient, and p is the corresponding *p*-value.

ant with odorant concentration ($p > 0.1$, Spearman test) (Fig. 4.16d-g).

For firing rate lags to remain invariant with odorant concentration despite a slowdown in transduction, the kinetics of the spiking machinery need to speed up with increasing input to the cell. To test if this is the case, we stimulated ab3A ORNs expressing Chrimson with Gaussian red light stimuli with increasing means, and measured lags between the applied light stimulus and firing rate. Firing lags decreased with increasing light power concentration ($p < 10^{-4}$, Spear-

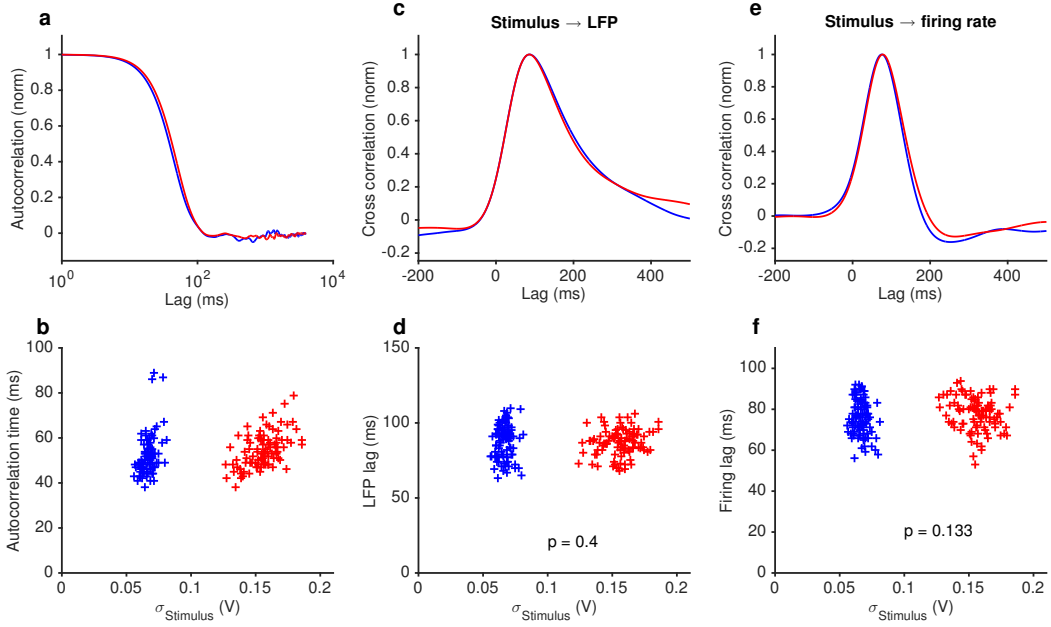


Figure 4.17: Variance gain control does not change response kinetics. (a) Stimulus autocorrelation functions, computed during high variance epochs (red) and during low variance epochs (blue). (b) Autocorrelation time (defined as the time the autocorrelation function first drops to $1/e$) vs. the standard deviation of the stimulus, for each trial. (c) Cross correlation functions from stimulus to LFP. The cross correlation functions are very similar between high (red) and low (blue) variance epochs. (d) LFP lag w.r.t the stimulus, estimated from the location of the peak cross-correlation, vs. standard deviation of the stimulus. No significant change in lag was observed ($p = 0.4$, t -test). (e) Cross correlation functions from stimulus to firing rate. The cross correlation functions are very similar between high (red) and low (blue) variance epochs. (f) Firing rate lag w.r.t the stimulus, estimated from the location of the peak cross-correlation, vs. standard deviation of the stimulus. No significant change in lag was observed ($p = 0.133$, t -test).

man test), suggesting that the ORN spiking machinery can speed up with increasing input currents (Fig. 4.16h).

If adaptation to the mean slows down transduction, which is corrected for at spiking, does adaptation to the stimulus variance also lead to similar compensatory kinetics? We found that a three-fold change in the stimulus variance, despite leading to changes in LFP and firing gains (Fig. 4.9-4.11), did not significantly change kinetics either at LFP or firing rate (Fig. 4.17), consistent with our earlier re-

sults suggesting that mean and variance gain control are etiologically distinct.

4.2.7 An adaptive two-state receptor-complex model reproduces Weber-Fechner scaling, slow down of LFP kinetics, and responses to intermittent and Gaussian stimuli.

How do adaptive mechanisms at transduction preserve both the Weber-Fechner Law and lead to response slowdowns? In the following we show that a minimal two-state model of the olfactory receptor-olfactory co-receptor (Or-Orco) complex with an adaptation architecture similar to that of the bacterial chemotaxis system [2, 7, 53, 157] can reproduce the LFP responses to naturalistic and Gaussian stimuli, as well as Weber-Fechner Law and its accompanying response slow down. In our model, Or-Orco complexes can be active or inactive (C and C^* in Fig. 4.19a) and the active complex binds odorant S with higher affinity than the inactive complex. We assume that ligand (un)binding is fast compared to (in)activation rates (w_+ and w_- in Fig. 4.19a). The fraction of active complexes therefore obeys the equation

$$da/dt = (1 - a)w_+(S, \varepsilon) - aw_-(S, \varepsilon) \quad (4.1)$$

where the rates of activation $w_+(S, \varepsilon)$ and inactivation $w_-(S, \varepsilon)$ are nonlinear functions of the odor concentration S and of the free energy difference ε between the unbound active and inactive states (Eqs. 3-4 in Methods). The LFP is modeled as a linear filter acting on the activity (Fig. 4.19a, eq. 5 in Methods). At steady state, Eq. 4.1 reduces to

$$\bar{a}(S, \varepsilon) = 1/(1 + w_-(S, \varepsilon)/w_+(S, \varepsilon)) \quad (4.2)$$

where the bar indicates steady state. $\bar{a}(S, \varepsilon)$ is a monotonically increasing function of the odor concentration S . Increasing the free energy difference shifts this function towards higher values of S , therefore reducing the sensitivity of the system. We model adaptation by assuming that activity of the Or-Orco complex controls the activity of factors that act on the complex to modify the free energy difference :

$$\frac{d\varepsilon}{dt} = \beta(a - a_0) \quad (4.3)$$

where β is the rate of adaptation. Importantly, the rate of change of ε only depends on the activity a but not on the free energy difference ε . The architecture of this feedback is similar to that of the bacterial chemotaxis system and ensures that for increasing values of S , the changes in compensate for changes in free energy due to ligand binding [7]. Thus, adaptation eventually returns a to the adapted value providing Weber-Fechner scaling [157] (as in Fig. 4.6). We assume that the free energy of the complex can only be changed within a finite range, and that the lower bound ε_L is reached for small values of S . Thus, in the absence of ligand, the steady state activity can be smaller than a_0 . For non-zero values of S , the steady state activity first increases with background signal intensity [113], before it becomes independent of background intensity once it reaches (Fig. 4.18), as seen in Fig. 4.6c.

An important intrinsic property of this model is that adaptation to increasing background of odorant decreases the rates of activation and inactivation and of the Or-Orco complex decrease, providing a self-consistent explanation for the slowdown of the response kinetics of the LFP upon adaptation. It is interesting to note that this kinetic property emerges because (1) the switching rates are decreasing functions of the free energy difference and (2) the requirement of Weber-

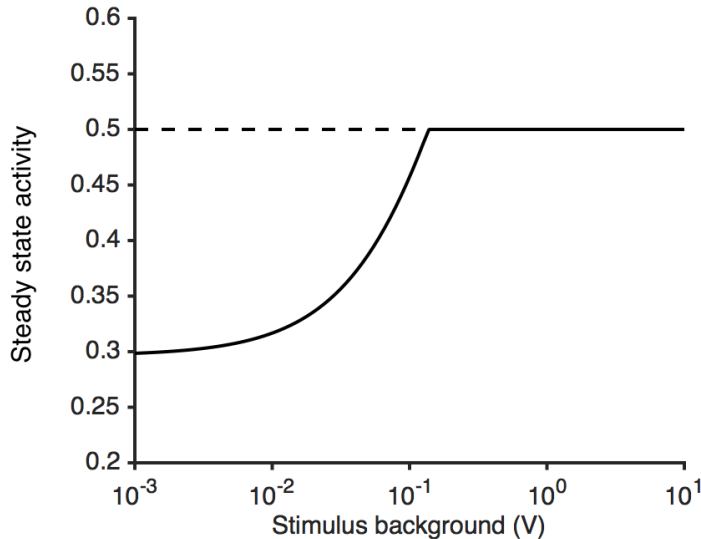


Figure 4.18: *Steady state activity as a function of the stimulus background.* At high stimulus background, the steady state activity of the receptor complex is (here, $a_0 = 0.5$). The model is unable to adapt perfectly to lower stimulus backgrounds, since ε is bounded by ε_L . This causes the steady state activity to decrease.

Fechner scaling, which causes the adapted value of to scale with the logarithm of the mean signal intensity (see Methods).

The resulting model (Eqs. 4.1-4.3) contains six parameters plus another 3 for converting the signal from activity to LFP. We fit this model to LFP responses to the Gaussian and naturalistic stimuli. The model decreased gain with the mean stimulus background, consistent with Weber-Fechner Law (Fig. 4.19b), and predicted the observed decrease in the LFP gains well (Fig. 4.19c, $r^2 = 0.84$). In addition, response lags of this model with respect to the stimulus increased with the mean stimulus (Fig. 4.19d), similar to the slowdown observed in the LFP responses (cf. Fig. 4.16). Finally, this model can also reproduce LFP responses to naturalistic, intermittent signals, approximating well the time trace (Fig. 4.19e, g) and the dependence on previous whiffs (Fig. 4.19f, compare to Fig. 4.4).

Since the spiking machinery compensates for the slowdown in LFP responses to preserve the timing of odorant encounters, we wondered

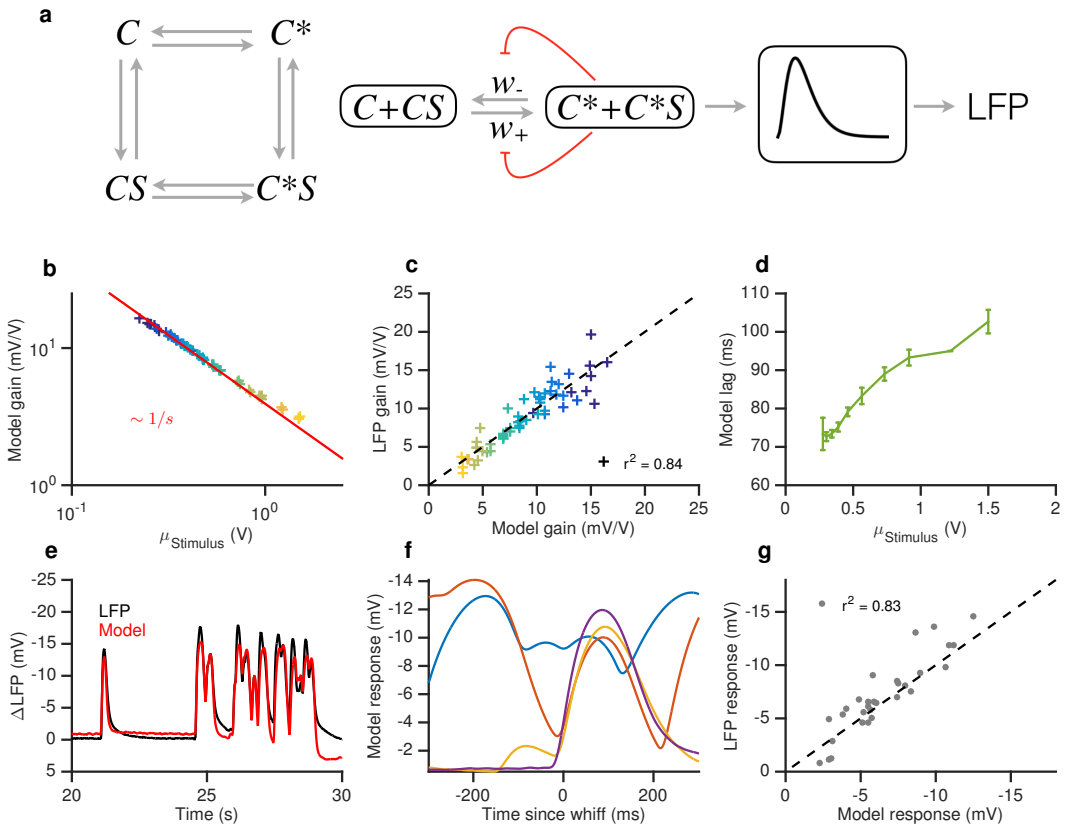


Figure 4.19: A modified two state receptor model reproduces Weber's Law and adaptive slowdown in LFP responses. (a) Or-Orco complexes (C) can be bound or unbound and active or inactive. We assume (un)binding rates are much faster than (in)activation rates. Activity of the complex feeds back onto the free energy difference between active and inactive conformations, which also decreases the activation and inactivation rates of the complex (Eqs. 1-4). A mono-lobed filter converts receptor activity into LFP signals (Eq. 5). We fit the model to Gaussian (Fig. 3,5) and naturalistic data (Fig. 1-2). In these fits, and . (c) Model gain *vs.* mean stimulus. Red line is the Weber-Fechner prediction ($\Delta R / \Delta S \sim 1/S$). (c) LFP gain *vs.* model gain. (e) Model response lag with respect to stimulus *vs.* mean stimulus. (f) LFP and model responses to naturalistic stimuli. (g) The model reproduces LFP responses to similar-sized whiffs that vary inversely with the size of preceding whiffs. (cf. Fig 2). (h) LFP responses *vs.* model responses for every whiff in the naturalistic stimulus.

if a simplification of this model that ignores the slowdown of the LFP kinetics upon adaptation could be used to predict firing rate: $R_F = N(K_F \otimes \bar{a}(S, \varepsilon))$ where N is a static nonlinearity, K_F a partially derivative taking linear filter (\otimes indicates convolution), and $\bar{a}(S, \varepsilon)$ is the steady state solution (eq. 4.2) with ε obeying eq. 4.3. This simplification reduces this model to a type of adaptive nonlinear linear-nonlinear (NLN) model, which preserves Weber-Fechner Law and reproduces the firing rates of ORN in response to both naturalistic and Gaussian Stimuli (Fig. 4.20). Thus it could be a useful tool in modeling ORN responses received by PNs, or in constructing computational models of the antennal lobe [3, 8, 11, 27, 33, 82, 94, 99, 147, 148, 164]. The model reproduced the change in the input-output curves on increasing the mean stimulus (Fig. 4.20a, cf. Fig. 4.6e) and decreased gain inversely with the mean stimulus, consistent with the Weber-Fechner Law (Fig. 4.20b). The model reproduced the observed decrease in the ORN gains (Fig. 4.20c,), and responses to naturalistic stimuli (Fig. 4.20d-f).

4.3 DISCUSSION

The goal of this work was to study how ORNs encode naturalistic odor signals, characterizing how gain control in ORNs is modulated dynamically in response to stimuli. By using precisely controlled, repeatable odorant stimuli, and linear modeling, we found that:

- A. ORN gain varies dynamically during responses to naturalistic stimuli, suppressing responses to whiffs following earlier whiffs (Figs. 4.1,4.4).
- B. Gain varies inversely with the mean stimulus (Weber-Fechner Law) and can also decrease with increasing stimulus variance (Figs. 4.6, 4.9).

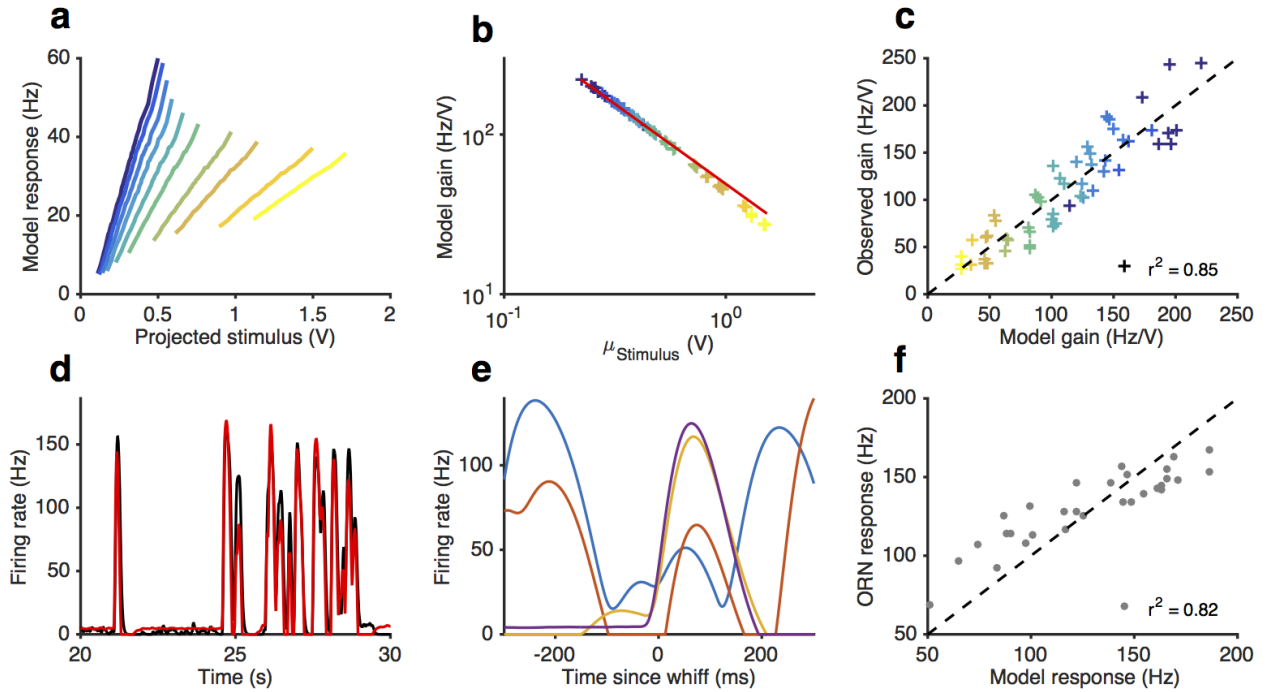


Figure 4.20: *Front-end adaptation followed by a LN model reproduces firing rate responses to Gaussian and naturalistic stimuli.* (a-f) Model from stimulus to firing rate (see Methods) fit to Gaussian and naturalistic stimuli. (a) Model responses *vs.* projected stimulus with increasing mean stimulus (cf. Fig. 4.6). (b) Model gain *vs.* mean stimulus. Red line is the Weber-Fechner prediction ($\Delta R / \Delta S \sim 1/S$). (c) Firing rate gain *vs.* model gain. (d) Firing rate and model responses to naturalistic stimulus. (e) The model reproduces variation in the firing rate responses to similar-sized whiffs (cf. Fig 4.4). (f) Firing rate responses *vs.* model responses for every whiff in the naturalistic stimulus.

- c. Variance gain control occurs at both transduction and spiking, while mean gain control occurs only at transduction (Fig. 4.11, 4.15).
- d. While gain control slows stimulus-to-transduction kinetics, this is compensated for by a corresponding speed up of transduction-to-spiking kinetics, therefore maintaining the stimulus-to-firing rate kinetics relatively unaffected (Fig. 4.16).
- e. Finally, we proposed a simple model based on the two-state receptor model that reproduce several key features of LFP and firing rate response and gain control (Figs. 4.19, 4.20).

4.3.1 *The Weber-Fechner Law in olfaction*

The Weber-Fechner Law has been observed in several sensory systems, including vision [23, 105, 126], audition [141], and somatosensation[79]. However, a clear identification of the law in the firing rate of ORNs has remained elusive, due to difficulties in controlling and measuring odor stimuli in gas phase simultaneously with ORN firing rate [25, 113]. Here we directly measured ORN firing rate and stimulus intensity and found that the ORN firing rate exhibited Weber-Fechner gain scaling relative to the mean stimulus intensity for five different odor-receptor combinations (Fig. 4.6, 4.7). These data suggest that olfaction shares the Weber-Fechner Law with other sensory systems.

What is the purpose of front-end Weber-Fechner gain scaling? ORNs are capable of spiking up to ~300Hz [73]; however, we found that with their compressive gain control, ORNs maintained firing rates between 0 - 50 Hz to fluctuating odor stimuli, even with a ten-fold increase in the mean stimulus. The ORNs' postsynaptic partners, the projection neurons (PNs) [128], are most sensitive to ORN firing rates of below

~ 50 Hz [85]. Thus, gain scaling at ORNs could act to maintain ORN firing rates in the range that PNs are most sensitive to for a wide range of concentrations.

4.3.2 Variance gain control in olfaction

In principle, gain control in sensory systems could be affected by several moments of the stimulus distribution, measured over many timescales. In the visual system, gain control depends on stimulus mean and variance, but not strongly on higher moments like the skew and the kurtosis [14, 173]. Cell-intrinsic variance gain control exists in a variety of systems, including the retina [9, 186], lateral geniculate nucleus [107], auditory neurons [122], and cortex [46, 145]. Photoreceptors do not exhibit variance gain control, and variance adaptation arises only in the subsequent processing in bipolar cells and ganglion cells [6, 97, 140].

What could be the functional role of variance gain control in olfaction? One possibility is to ensure that ORN responses occupy their full dynamic range [104]. While we quantified our stimulus in terms of the first and second moments of the stimulus statistics in this study, these moments may not map simply onto the salient features that are most relevant to the fly's encoding scheme. Variance gain control could therefore be a consequence of an adaptive representation that is important to the coding properties of the ORN. Nonetheless, because i) variance gain control is distributed between transduction and spiking machinery (Fig. 4.11), ii) mean gain control is linked to calcium influx and variance gain control is not (Figs. 4.13, 4.14) [26], and iii) mean gain control slows down transduction (Fig. 4.16) [26, 125] but variance gain control does not (Fig. 4.17), adaptation to the stimu-

lus variance is mechanistically distinct from adaptation to stimulus mean.

4.3.3 *Models and mechanisms of ORN response and gain control*

The results presented here, and the models that reproduce them, focus on the phenomenology of gain control in ORNs. Do these phenomenological results constrain possible mechanisms that could implement gain control in ORNs? Weber-Fechner gain scaling (Fig. 4.6) can be reproduced by models using feed-forward loops [36, 64], integral feedback [84] or both [152]. A detailed biophysical model of odor-receptor binding and channel opening has been proposed to account for transduction responses to odors [125]. While this model can change gain via a negative feedback mechanism, it does not reproduce the Weber-Fechner law, or the slowdown of LFP kinetics upon adaptation. Here we showed that these features emerge if we assume that: (i) the activity a of the Or-Orco complex feeds back onto the free energy difference between the active and inactive state of the unbound Or-Orco complex, which in turns affects both the rates of activation and inactivation of the complex; (ii) the rate at which is modified only depends on the activity a .

Such an architecture reproduces the Weber-Fechner law and is similar to that of the bacterial chemotaxis system [7]. There, adaptation is mediated by two antagonistic factors, one that acts on inactive complexes only, and another one that acts on active complexes [7]. While the molecular architecture of the signaling pathway in ORNs has not been fully characterized, several studies have implicated calcium as a slow diffusible factor that could mediate adaptation to the mean stimulus [45, 166]. Decreasing extracellular calcium levels, or internal free calcium breaks Weber-Fechner gain scaling at transduction

[26] and increasing stimulus amplitude leads to increasing levels of intracellular calcium (Fig. 4.13). Other mechanisms have also been implicated in adaptation of ORNs, like auto-regulation of Orco via cAMP signaling [63]. While slower adaptive processes also exist, our data on responses to naturalistic stimuli (Fig. 4.1, 4.4), and data from paired-pulse experiments [26], suggest that these potential mechanisms can also act on fast timescales of several hundred milliseconds.

Many models that decrease gain with increasing mean stimulus also speed up response kinetics [36, 44, 125, 152, 153] describing well the phenomenology of other sensory systems where gain and response speed trade off [39, 50, 122, 132]. However, in olfactory systems, transduction kinetics slow down with increasing stimulus background, both in insect ORNs (Fig. 4.16, [26, 125]) and in vertebrate ORNs [138]. It is not trivial to devise systems in which kinetics slow down with increasing stimulus background. To exhibit this property, a system must increase its effective timescale of response with stimulus intensity, for example, by decreasing all reaction rates uniformly. Interestingly, our model also exhibits a slowdown in the LFP kinetics upon adaptation. This feature emerges intrinsically from the model architecture because: (i) the feedback of the activity onto the free energy difference affects both the activation and deactivation rates of the complex (w_+ and w_-); and (ii) the Weber-Fechner gain control causes ε to scale logarithmically with the stimulus, which in turn causes w_+ and w_- to decrease.

Earlier work modeled the transformation from LFP to firing rates using a derivative-taking kernel [125]. Here, we show that the temporal structure of these kernels depends on the adaptation state of the ORN, and must take derivatives on shorter timescales at higher stimuli to compensate for slowing transduction kinetics. While the mechanism of this speed up is not known, the neuron's ability to

spike with shorter latencies could depend on the adapted state of its receptors, the level of intracellular calcium, or the distance of its membrane potential from firing thresholds.

What cellular mechanisms could give rise to gain control that is variance dependent? (Fig. 4.9). We found that both the transduction machinery and the spiking machinery of the ORNs exhibit variance-sensitive gain-control (Fig. 4.11, 4.15). Variance gain control after transduction could arise from the spike generating machinery. Hodgkin Huxley (HH) model neurons exhibit variance gain control [80, 109, 185]. Simpler neuron models, like the FitzHugh-Nagumo model [81], and the linear integrate-and-fire (LIF) model [185] also exhibit variance-dependent gain control. In the visual system, non-spiking bipolar neurons show variance gain control [6, 140] so mechanisms for variance gain control in the absence of spike generation might be similar between these systems.

4.3.4 Dynamic gain control could aid in naturalistic odor detection

Previous studies of olfactory adaptation employed conditioning and probe stimuli [25, 113, 125], which typically adapt neurons over many seconds or minutes before testing response properties with a short probe. Other studies using paired pulse protocols [26] found that responses to brief pulses of odorant reduced gain on timescales as brief as 500 ms, which is close to the timescale of the neural response to odors [96, 113, 125]. Similar fast timescales of gain control have been observed in the visual system [24, 39]. We found that this fast gain control was employed by ORNs to dynamically control gain during responses to naturalistic odorant stimuli (Fig. 4.4).

Fast gain control allows ORNs to respond to the rapidly changing statistics of natural odor plumes, letting gain decrease quickly in

response to a large whiff and then ramp up again to a subsequent small whiff. Dynamic inhibition in the antennal lobe [124, 135] would permit PNs to remain sensitive to these rapid changes in ORN firing rate, ensuring propagation of information about odor encounters to the brain.

4.3.5 *Invariant firing rate kinetics could improve odor-guided flight behavior*

Insects follow odor plumes to their source to find food or reproductive mates [119]. For flies, this task is challenging since they fly fast (~30 cm/s) [172] and odor filaments are narrow [119]. Even for relatively broad and static odor plumes, flies are within odor plumes so briefly that they experience plume contact and plume loss in quick succession (10-250 ms) [16]. Olfactory search behavior in this setting consists of rapid flight surges on encountering odor plumes, and stereotyped crosswind casts on losing odor plumes [16]. Navigation based on odor intensities alone may not be possible, as odor intensities are not informative about the direction to the odor source at length scales longer than 10 cm [119]. Indeed, there is a growing body of evidence underlining the importance of timing in olfaction [113, 136, 158, 161, 162].

In this context, it may be important for the fly to know precisely when it encountered an odor filament. This task is made difficult by the fact that olfactory adaptation to large stimuli slows transduction [26, 125]. Adaptation could change the kinetics of the transduction from whiff to whiff, so that downstream neurons would have to know the adaptation state of the ORN to precisely determine encounter timing.

Our results reveal that flies solve this problem by using transduction and firing machinery that possess complementary kinetic properties. This maintains ORN firing rate lags at a constant value in the face of slowing transduction. Our results suggest that ORNs can encode the precise timing of odor encounters, for a wide range of odor concentrations. Such an encoding scheme could aid insects in navigating odor plumes to their source.

When a system responds identically, in amplitude and in kinetics, to stimuli that are different only in scale, the system is said to show Fold Change Detection (FCD) [65]. FCD thus implies the Weber-Fechner Law. In addition, the invariance of response kinetics with stimulus intensity means that FCD implies an invariant response lag with stimulus intensity. While ORNs do not adapt perfectly [113], as required for FCD, their invariance of response lag with stimulus intensity [113], (Fig. 4.16) is intriguingly similar to the response phenomenology of FCD networks [64, 65].

Interestingly, olfactory adaptation is linked to flight in insects. Olfactory Receptors (ORs) adapt and have co-evolved with flight [52, 63, 88] and occur only in flying insects [115]. In contrast, the more ancient ionotropic receptors [115] found in all insects, do not appear to adapt to prolonged odor stimuli [26]. While ORs play an important role in larval olfactory navigation [77, 114, 152, 159], the statistics of odor signals close to surfaces, and in the air, where flying insects encounter them, may be very different [119]. Receptors capable of fast adaptation may allow flying insects to detect brief whiffs of airborne odors.

4.4 METHODS

4.4.1 Electrophysiology

SINGLE SENSILLUM RECORDINGS. Single sensillum recordings from *Drosophila* antennae were performed as described previously [19, 113]. The recording electrode was inserted into a sensillum on the antenna of an immobilized *Drosophila melanogaster* and a reference electrode was placed in the eye. Electrical signals were amplified using an Iso-DAM amplifier (World Precision Instruments). The ab₃ sensillum was identified by 1) its size and location on the antenna 2) test pulses of 2-heptanone, to which the B neuron is very sensitive, 3) spike shapes (A spikes are larger than B spikes) and 4) spontaneous firing (ab₃B fires at a higher rate than ab₃A). Other sensilla were identified using test odors to which either the A or B neuron strongly responded to.

SPIKE SORTING. All sensilla recorded from in this study contained two neurons [19, 163]. Generally, spikes from the “A” neuron are larger than spikes from the “B” neuron. However, spike amplitude and spike shape changed in our experiments with strong odor or light drive, due to a phenomenon called “pinching” [130], and due to small movements of the recording electrode relative to the sensillum. To identify spikes from the A neuron under these challenging conditions, we developed a spike-sorting software package written in MATLAB (Mathworks, Inc.), available at <https://github.com/emonetlab/spikesort>. This package uses the full spike shape, with various dimensionality reduction and clustering methods to reliably identify spikes from noise, and to sort identified spikes. This spike-sorting package performed with 99.5% accuracy compared to manually sorted data on a test dataset.

LOCAL FIELD POTENTIALS. The local field potential was recorded by lowering the gain of the amplifier and switching to DC mode, where we recorded the sensillar potential without any low frequency cutoff. Spike detection and sorting was reliable in either mode. Since we were only interested in the deflections of LFP in response to a fluctuating odor stimulus, we band-passed the raw voltage in software to remove spikes and slow fluctuations.

4.4.2 Fly stocks and genetic strategies

Flies were reared at 25°C on conventional fly medium [76]. All experiments were performed on adult female flies 3-5 days post-eclosion. Unless otherwise mentioned, recordings were from ab₃A neurons in Canton-S flies. In Fig. 4.15 and Fig. 4.16h, we recorded from ab₃A ORNs in w; Or22a-GAL4/+; UAS-Chrimson/+ flies. In these flies, only ab₃A ORNs were sensitive to light, while ab₃B neurons and nearby ab₂ sensilla were not. In Figs. 4.13-4.14, we recorded from w; Or22a-GAL4/+; UAS-GCaMP6f/+ flies.

4.4.3 Stimulus measurement

We used a Photo Ionization Detector (PID) (200B, Aurora Scientific) to measure the odor stimulus during every experiment. Stimulus measurements occurred simultaneously with all electrophysiology, and the tip of the PID probe was < 1 cm of the odor delivery tube and the fly. The PID was calibrated by depleting known volumes of pure odorants, and the response of the PID was found to be approximately linear with odorant flux (Fig. 2.5). However, due to gradual changes in the sensitivity of the PID detector, odor intensity measurements are not comparable across experiments. For more details on how the

stimulus was measured, and for details on PID calibration, see Chapter 2.

We measured the intensity of red light that we used to activate Chrimson at the location of the fly using a PM160 light power meter (Thorlabs). We used this to construct a function mapping control signals to our LED to light power in μW , and transformed control signals into light power using this function.

4.4.4 *Odor stimulus generation*

Details on the odorant stimulus delivery are found in Chapter 2.

4.4.4.1 *General principle.*

Odorants in gas phase were delivered to the antenna by blowing air over pure monomolecular odorants in liquid phase. The flow rate of air over the liquid odorant determined the gas phase concentration.

4.4.4.2 *Controlling air flows.*

Mass Flow Controllers (MFCs) (Aalborg instruments & Controls, Inc. and Alicat Scientific) were used to regulate airflows. Dynamic response parameters of Alicat MFCs were chosen either for high speed, and driven with switching times of up to 20 ms (at the cost of reproducibility) or were chosen for high precision, and driven with switching times of 100 ms (at the cost of very fast stimulus control). An odorized airstream (0-200 mL/min) was fed into a main airstream (2 L/min) that was delivered through a glass tube positioned within 10mm of the fly's antenna. The secondary airstream passed through a scintillation vial with a machined plastic screw-top lid containing pure odorant. Using pure odorant and gas phase dilution permitted excellent reproducibility of the odor stimulus. All tubing was made

of chemical-resistant PTFE tubing (McMaster Carr, stock #5239K24). By varying the control signals to the MFC bank, steps, pulses, and frozen noise waveforms with arbitrary distributions could be reliably delivered. We wrote a general-purpose acquisition and control system called kontroller (available at <https://github.com/emonetlab/kontroller>) in MATLAB (Mathworks, Inc.) to control MFCs, valves and LEDs and to collect data from electrophysiology and the stimulus measurement.

NATURALISTIC STIMULUS (FIG. 4.1) To generate naturalistic odor stimuli, we randomly varied flow rates over 0-200 mL/min, and used a small solenoid valve (Lee Co.) to deliver 50 ms whiffs of odorant. We used the same frozen random sequence in subsequent trials.

STIMULUS WITH CHANGING MEAN (FIG. 4.6) To generate approximately Gaussian-distributed stimuli that differed in their mean, but with similar variances, we started with the ansatz that air flow rates were proportional to measured gas-phase stimulus. We then defined target Gaussian distributions that differed only in their mean, and a parametric distribution from which we drew control signals to the MFC. Using kontroller to automate the process, we performed a direct search on hardware to find the best distribution of control signals that was closest to the desired Gaussian distribution. Further rounds of off-line numerical optimization using nonparametric models of the delivery system ensured that the resultant stimulus distributions were as close to Gaussians and with variances as similar to one another as possible.

STIMULUS WITH CHANGING VARIANCE (FIG. 4.9) We used two MFCs driven by control signals with different variances to generate two Gaussian-distributed stimuli with differing variances. Solenoid valves (Lee Co.) were used to switch from one airstream to the other every 5 seconds. Control signals were iteratively optimized using sim-

ulations and controller till the mean stimulus intensity from the two odor lines was indistinguishable.

4.4.5 Numerical Methods

4.4.5.1 Statistics of Naturalistic Odor.

Since the intensity distribution in our naturalistic odor stimulus was very broad, we defined whiffs of odor as short excursions of the odorant signal above the noise floor. Blanks were defined as the periods of time between whiffs. Whiff intensities were broadly distributed, and were fit with a functional form proposed in [30]. Both whiff and blank duration distributions were fit with a power law with exponent $-3/2$, following theoretical calculations for a jet flow [30] (Fig. 4.2). Mean and variance of naturalistic odor stimuli were computed in non-overlapping windows of length (Fig. 4.2e, $\tau = 400$ ms). Window lengths were varied from $\tau = 10$ ms to $\tau = 10$ s (Fig. 4.2f).

4.4.5.2 Estimating deviations in response to naturalistic stimulus.

For every whiff shown in Fig. 4.1e-f, we computed the median response for all whiffs in a bin centered around that whiff's stimulus amplitude, that encompassed other whiffs if their amplitude was within 10%. The fractional deviation in response to a given whiff i is defined as $D_i = (R_i - \tilde{R})/\tilde{R}$, and is a dimensionless number that is negative when responses are smaller than the median. To determine if the time to the previous whiff and the amplitude of the previous whiff of negative deviations and positive deviations were different, we used a 2-sample two-dimensional Kolmogorov-Smirnov test, based on the method proposed by Peacock [133].

4.4.5.3 Filter extraction.

Details of filter extraction are found in §3.1.

Linear filters extracted from naturalistic stimuli (Fig. 4.1, 4.3) are not unbiased estimates of the true filter, since the stimulus is not Gaussian. Similarly, if a front-end nonlinearity precedes a linear filtering step in a system, this fitting procedure will not yield an unbiased estimate of the true filter. Nonetheless, linear filters computed by least squares fitting are the filters that best predict R given S , in the least-squares sense.

ORN INPUT OUTPUT CURVES. (solid lines in Fig. 4.6e, 4.9e etc.)

We defined ORN input-output curves to be the output nonlinearity of a LN model, which were estimated by plotting ORN response *vs.* the projected stimulus, and then computing a piecewise linear function using 50 bins along the horizontal axis. Computing piecewise linear functions allowed us to visualize the output nonlinearity without making explicit assumptions of the functional form of the nonlinearity. Dashed lines in Fig. 4.9e are the cumulative distributions of the stimulus, computed over all the data.

ESTIMATION OF GAIN. In general, for any system with a single stimulus and response, we define the gain of the system by measuring the slope of the nonlinearity in the best fit LN model, normalizing the filters to preserve the scale of the stimulus as in [6]. With Gaussian stimuli that only gently perturb the system, the nonlinearity is simply a straight line, and the gain is computed by the average slope of a linear fit to the output nonlinearity (Fig. 4.6). When output nonlinearities are strong, we estimated gain by the slope at the midpoint of the nonlinearity (Figs. 4.9-4.11). We measured three different gains: 1) transduction gains, from the stimulus to the LFP, 2) firing gains, from

the LFP to the firing rate, and 3) overall ORN gains, from the stimulus to the firing rate. Transduction gain had units of (mV/V) since deflections in LFP are measured in mV and the stimulus is measured in V. Similarly, firing gain had units of Hz/mV. Overall ORN gain had units of Hz/V when stimulating ORNs with fluctuating odor, and had units of Hz/ μ W when stimulating with light. In experiments where we changed the variance (Fig. 4.9), low-variance epochs tended to have a mean stimulus ~8% higher than high-variance epochs (Fig. 4.10), despite our best efforts to keep the stimulus mean the same. To estimate gain changes solely due to the change in stimulus variance, we divided the projected stimulus by the mean stimulus in each epoch in each trial (Fig. 4.9e). Differences in gain between high- and low-variance epochs remain significant even without this correction (Fig. 4.10b-c). A single filter was used to project stimuli in both low- and high-variance epochs; changes in gain from low- to high-variance stimuli thus appear solely in the nonlinearity (Fig. 4.10d).

MEASURING LAGS. In all our data, we measured the stimulus together with the response of ORNs. This allowed us to estimate transduction and firing lags with respect to the stimulus. In general, we estimated response lags by computing cross-correlation functions from the stimulus to the response. Lag was defined to be the location of the peak of the cross-correlation function. (Fig. 4.16a-b).

ESTIMATION OF VARIANCE GAIN CONTROL TIMESCALE. To estimate the timescale of variance gain control (Fig. 4.9), we computed input-output curves from the projected stimulus to the firing rate in 50 ms bins, pooling all trials together. This allowed us to estimate gain in 50 ms bins, together with the stimulus contrast (standard deviation/mean). We plotted time series of instantaneous gain and

stimulus contrast (Fig. 4.9h), and observed that while the stimulus contrast changed rapidly after the switch from high to low variance (at $t = 5$ s), the instantaneous gain changed more slowly, but still changed in ~ 130 ms, suggesting that timescale of variance gain control is relatively rapid.

STATISTICAL TESTS. To determine if ab₃A transduction-to-firing gain varied with the mean stimulus (Fig. 4.11d), we used a Spearman rank correlation test. To determine if gains varied significantly from low to high variance epochs (Fig. 4.9, 4.11), we first reshaped the raw data into trials 10 s long. Each trial consisted of a high variance epoch followed by a low variance epoch. Each trial was fit with three linear models, and yielded three pairs of gains, for transduction gain, firing gain, and total ORN gain. We discarded all trials where any linear model fit was poorly correlated with data, retaining only trials where all fits had high correlations with data ($r^2 > 0.8$, see Fig. 4.10f-g). We used the Wilcoxon signed rank test on these tuples to determine if the difference in gains in the low and high variance epochs was statistically significant.

4.4.6 Modeling

4.4.6.1 Stimulus binding and the activity of the Or-Orco complexes.

We assume that Or and Orco form a complex that can exist in two conformations that can bind ligand. The concentration of unbound active complexes is C^* and that of unbound inactive one is C . The corresponding concentrations for the bound complexes are C^*S and CS (Fig. 4.19a). The fraction of active Or-Orco complexes is therefore:

$$a = \frac{C^* + C^*S}{C + CS + C^* + C^*S}$$

(Un)binding of odorant is taken to be much faster than the (in)activation. Thus, the probability to be bound in the active and inactive cases are

$$P_b = \frac{S}{S + K_{\text{off}}}$$

$$P_b^* = \frac{S}{S + K_{\text{on}}}$$

Here $K_{\text{on}} < K_{\text{off}}$ are the dissociation constants for each state. Let the free energy difference in units of $k_B T$ between the active and inactive states be ε and ε^b when unbound and when bound, respectively. For simplicity, we assume detailed balance (this can easily be relaxed [160]), which constrains the free energy difference between C^*S and CS to be $\varepsilon^b = \varepsilon + \log(K_{\text{on}}/K_{\text{off}})$. The activation kinetics can then be described by

$$\frac{dC^*}{dt} = w_+^u C - w_-^u C^*$$

where the rates are

$$w_{\pm}^u = \frac{\alpha}{1 + e^{\pm\varepsilon}}$$

$$w_{\pm}^b = \frac{\alpha}{1 + e^{\pm\varepsilon^b}}$$

We constrained the energy barrier between the active and inactive conformations by making the simplifying assumption that $w_+^u + w_-^u = \alpha = w_-^b + w_+^b$, where α is an intrinsic switching rate (see e.g. [160]). From these considerations we can then derive Eq. 4.1 from the main text, which describes the dynamics of the activity:

$$\frac{da}{dt} = (1 - a)w_+(S, \varepsilon) - aw_-(S, \varepsilon)$$

with the rates

$$w_+(S, \varepsilon) = P_b w_+^b + (1 - P_b) w_+^u = \frac{S}{S + K_{\text{off}}} \frac{\alpha}{1 + e^{\varepsilon + \log(\frac{K_{\text{on}}}{K_{\text{off}}})}} + \frac{K_{\text{off}}}{S + K_{\text{off}}} \frac{\alpha}{1 + e^\varepsilon}$$

$$w_-(S, \varepsilon) = P_b^* w_-^b + (1 - P_b^*) w_-^u = \frac{S}{S + K_{\text{on}}} \frac{\alpha}{1 + e^{-\varepsilon - \log(\frac{K_{\text{on}}}{K_{\text{off}}})}} + \frac{K_{\text{on}}}{S + K_{\text{on}}} \frac{\alpha}{1 + e^{-\varepsilon}}$$

Given a steady state signal S , the activity relaxes towards

$$\bar{a}(S, \varepsilon) = \frac{1}{1 + \frac{w_-}{w_+}} = \frac{1}{1 + e^{\varepsilon \frac{1+S/K_{\text{off}}}{1+S/K_{\text{on}}}}}$$

Where the overbar indicates that equation 4.1 is solved at steady state. We model adaptation assuming that the activity feeds back onto the free energy difference with rates that depend only on the activity (the effective switching rate is constant):

$$d\varepsilon/dt = \beta(a - a_0)$$

where β is the rate of adaptation. Note that the free energy is bounded both from below and from above. In practice, we only need the lower bound $\varepsilon_L < \varepsilon$. At steady state (for values of S high enough that $\varepsilon_L < \varepsilon$) we have $\bar{a} = a_0$ which implies that

$$\bar{\varepsilon}(S) = \log\left(\frac{1 - a_0}{a_0} \frac{1 + S/K_{\text{on}}}{1 + S/K_{\text{off}}}\right)$$

Thus, at steady state, adaptation causes the free energy difference of the complex to increase with the logarithm of the background signal intensity.

4.4.6.2 Kinetic slowdown upon adaptation.

Substituting $\bar{\varepsilon}(S)$ into the definitions of the (in)activation rates, we get

$$\bar{w}_+(S) = \frac{S}{S + K_{\text{off}}} \frac{\alpha}{1 + \frac{K_{\text{on}}}{K_{\text{off}}} \frac{1-a_0}{a_0} \frac{1+S/K_{\text{on}}}{1+S/K_{\text{off}}}} + \frac{K_{\text{on}}}{S + K_{\text{off}}} \frac{\alpha}{1 + \frac{1-a_0}{a_0} \frac{1+S/K_{\text{on}}}{1+S/K_{\text{off}}}}$$

and

$$\bar{w}_-(S) = \bar{w}_+(S) \frac{1-a_0}{a_0}$$

When $K_{\text{on}} < K_{\text{off}}$, the rates are decreasing functions of S in the range

$$0 \leq S \leq \sqrt{\frac{1-a_0}{a_0} K_{\text{on}} K_{\text{off}}}$$

In our case this bound is large (~ 40 V) and in our experiments the rates are decreasing functions of S over the entire range.

4.4.6.3 Receptor activity to LFP.

The output of the model described above is a time series of the fraction of receptors that are active, a . Receptor activation can lead to the opening of other channels, which results in a transduction current that we measure as changes in the LFP. To generate LFP responses from this, we use

$$R_{LFP} = C_0(K_{LFP} \otimes a(t))$$

where \otimes represents a convolution and K_{LFP} is a linear time-invariant mono-lobed filter that is given by

$$K_{LFP} = \frac{t^m e^{-t/\tau}}{m! \tau^{m+1}} \theta(t)$$

4.4.6.4 Receptor activation to firing rates.

Since firing rates cannot be negative, and since the LFP to spiking transformation has been shown the partly differentiating [125], we generated firing rate responses from the receptor activity using

$$R_F = N(K_F \otimes a(t))$$

where N is an output nonlinearity which is a simple threshold linear function ($N(x < 0) = 0$; $N(x > 0) = Cx$). \otimes represents a convolution and K_F is a linear time-invariant filter that is given by the sum of two other kernels:

$$K_F = K_1 + \alpha K_2$$

where each kernel is parameterized by a Gamma function:

$$K_i = \frac{t^m e^{-t/\tau_i}}{m! \tau_i^{m+1}} \theta(t) \quad i \in \{1, 2\}$$

THE TETHERED FLY ASSAY

5.1 GOALS

Olfactory stimuli can be decomposed into a few basic features, like the chemical identity of the odorants in the odor, their concentration, and the kinetics of the stimulus. Olfactory Receptor Neurons (ORNs) appear to be able to capture all these features. The chemical identity of the odorant is captured by which olfactory neurons respond, since different neurons have different receptors [71, 74]. The concentration of the odorants in the stimulus is captured in part by the amplitude of neuronal response [19, 20], and also by the identity of the neurons that respond, since different receptors have different sensitivities to the same odorant [71, 74]. Finally, the temporal structure of the odorant stimulus is encoded in the response kinetics of neuron response [113]. Insects on the wing can encounter odorant stimuli with varying concentrations and durations [16, 30], and it is not clear if flies use all these features of the stimulus equally to make navigational decisions.

The Tethered Fly Assay (TFA), originally developed to study insect flight [67] was later adapted and modified to study vision, mechanosensation, and the visual control of flight [10, 22, 57, 106, 156]. Recently, the TFA has also been used to study olfaction, either in the fixed tethered configuration [13] or in rotatable tethered configuration, where flies can actively reorient into or away from an odorized airstream [58, 59, 101]. Since the fly is fixed in place in this assay, this makes it possible to deliver and measure olfactory stimuli and permits mea-

suring how these olfactory stimuli modulate olfactory flight behavior. In this assay, the behavior of the fly is quantified by changes in the Wing Beat Amplitude ([WBA](#)) and by changes in the Wing Beat Frequency ([WBF](#)), both of which are measured in real time by the “Wing Beat Analyzer” that is part of the assay.

In the next section, I detail my attempts to use this assay to determine how flies change their flight behavior with the identity, amplitude and duration of olfactory stimuli.

5.2 RESULTS

Following [[13](#)], I constructed a tethered flight assay where flies are tethered to insect pins and held in front of an airstream in the dark (see Fig. [5.1](#)for a picture). A paired olfactometer used four valves, all upstream of vials containing odorant or control, to deliver short pulses of either odorant or control. A PID behind the fly captured the odorant delivered to the fly, and allowed me to record the stimulus simultaneously with the behavior of the fly.

5.2.1 *Flight responses to pulses of different odorants*

Flies flapped their wings spontaneously when suspended in the device, creating the “hütchens” waveform on the photodetector cell (Fig. [5.2a](#)). Each wingbeat cycle produced this characteristic bilobed wave, and the height of the waveform was a proxy for the wing beat amplitude, and the frequency of this waveform was the wing beat frequency. Flies tended to gradually decrease their wing beat frequency when the airstream was turned on (Fig. [5.2b](#), left panel), though the wing beat amplitude did not change as much ((Fig. [5.2b](#), right panel). Switching airstreams in the absence of odorant did not evoke a strong

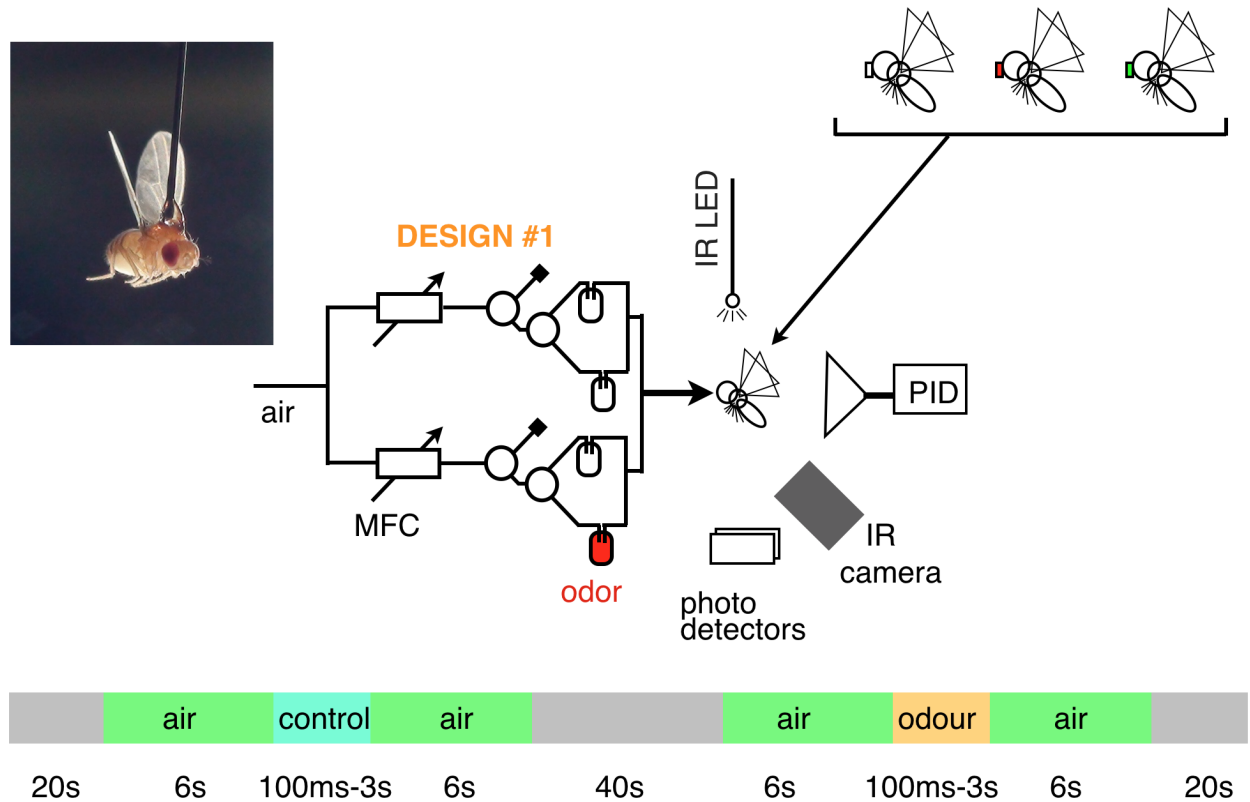


Figure 5.1: *Schematic of the tethered flight assay*. A fly is tethered to a fine insect pin and suspended below a Infra red (IR) Light Emitting Diode (LED) (see top left for a picture). The wings of the fly cast a shadow on two photo detectors below the fly, whose signals can be used to measure the frequency and amplitude of the fly's wing beats. An odorant delivery system (labelled “design #1” can deliver either pulses of odorant or pulses of clean air to the fly. Valves switch between two symmetrical airstreams, one with odor (red) or one without, to deliver odorant to the fly with minimal changes in airflow. A Photo Ionization Detector (PID) sucks all the air and odorant delivered to the fly, allowing simultaneous monitoring of the behavior and the stimulus. Finally, genetic strategies can be used to delete or replace receptors in the fly. The time-series at the bottom shows the typical experimental block, where a control pulse (with no odorant) is presented first, followed by a test pulse with odorant.

response, either with the control airstream (Fig. 5.2b, blue), or with the “odor” airstream (Fig. 5.2b, red).

Having established that flies do not increase their WBF or WBA in the absence of odorant, I then delivered 3 s pulses of four different odors (Apple Cider Vinegar, ethyl butyrate, methyl salicylate and ethyl acetate). Flies’ behavior to these odor pulses were measured interleaved with responses to control pulses with no odorant. PID measurement of odor stimuli, control stimuli with no odor, and WBF responses of flies to these odors are shown in Fig. 5.2c. In all traces, red curves correspond to test trials with odors, and blue trials correspond to control trials with no odor. For all four odors tested, WBF decreased in control trials where there was no odorant (Fig. 5.2c, blue curves) and WBF increased transiently when odor was presented to the flies (Fig. 5.2c, red curves). These results suggest that flies can detect these odors, and respond to encounters with these odors by increasing WBF.

5.2.2 *Flight responses to pulses with different amplitudes*

How does fly behavior vary with the amplitude of odorant signal presented? One possibility is that flies execute the same motor program independent of the concentration of the odor detected, and that the concentration of odorant detected triggers a navigational behavior, but does not affect the details of that behavior. Another possibility is that flies modulate their behavioral response based on the amplitude of the stimulus they detect. To distinguish between the two, I delivered pulses of ethyl acetate with varying concentrations to flies and recorded their flight behavior.

I generated three different amplitudes of ethyl acetate pulses by diluting serially in Paraffin Oil (1/10, 1/100 or 1/1000). This serial

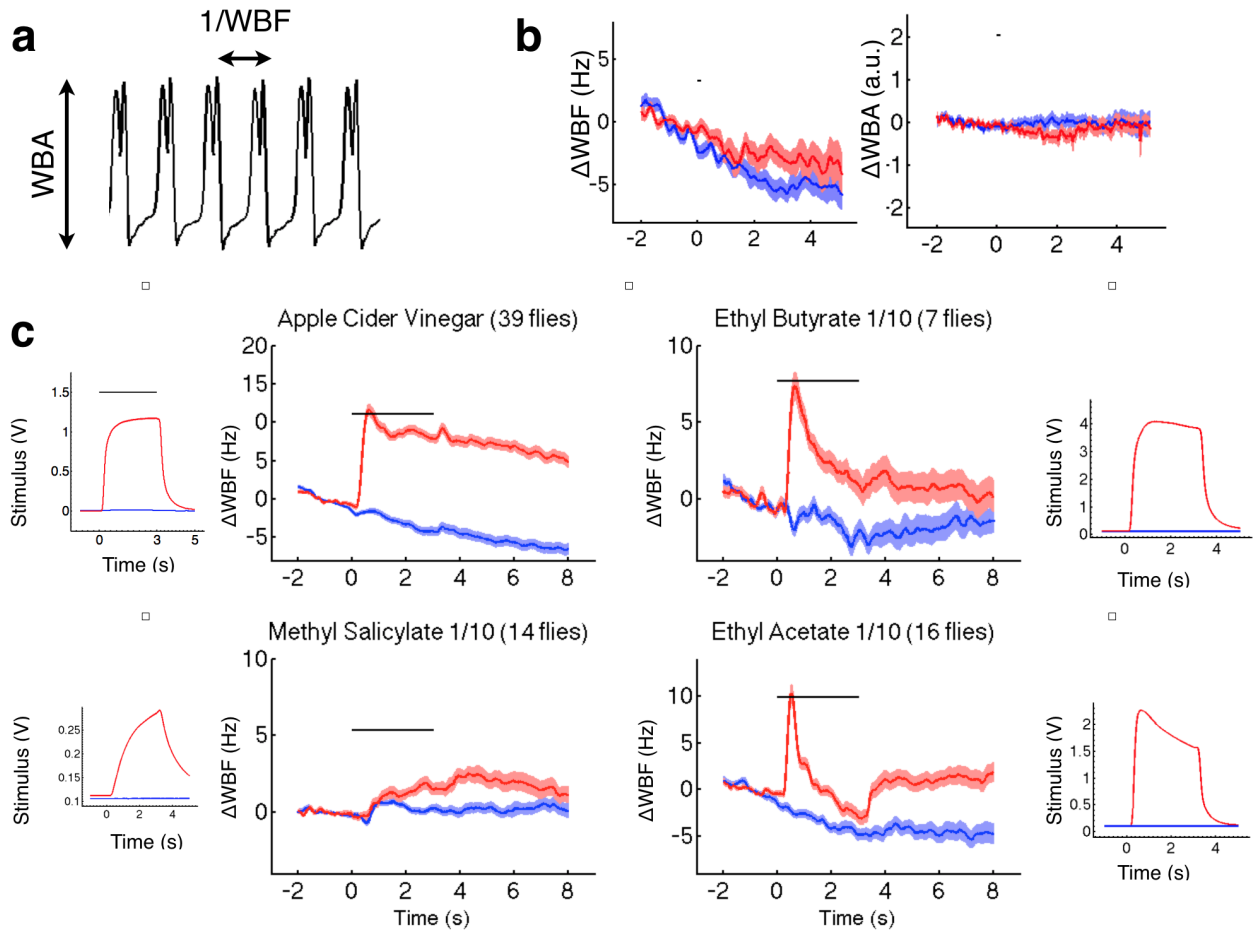


Figure 5.2: Flight responses to different odorants. A fly is tethered to a fine insect pin and suspended below a Infra red (IR) Light Emitting Diode (LED) (see top left for a picture). The wings of the fly cast a shadow on two photo detectors below the fly, whose signals can be used to measure the frequency and amplitude of the fly's wing beats. An odorant delivery system (labelled “design #1” can deliver either pulses of odorant or pulses of clean air to the fly. Valves switch between two symmetrical airstreams, one with odor (red) or one without, to deliver odorant to the fly with minimal changes in airflow. A Photo Ionization Detector (PID) sucks all the air and odorant delivered to the fly, allowing simultaneous monitoring of the behavior and the stimulus. Finally, genetic strategies can be used to delete or replace receptors in the fly. The time-series at the bottom shows the typical experimental block, where a control pulse (with no odorant) is presented first, followed by a test pulse with odorant. In time traces of ΔWBF vs. time, the mean WBF before the pulse (at $t = 0$ s) is subtracted from every trace, and the mean ΔWBF is plotted with solid lines. Shading indicates the standard error of the mean.

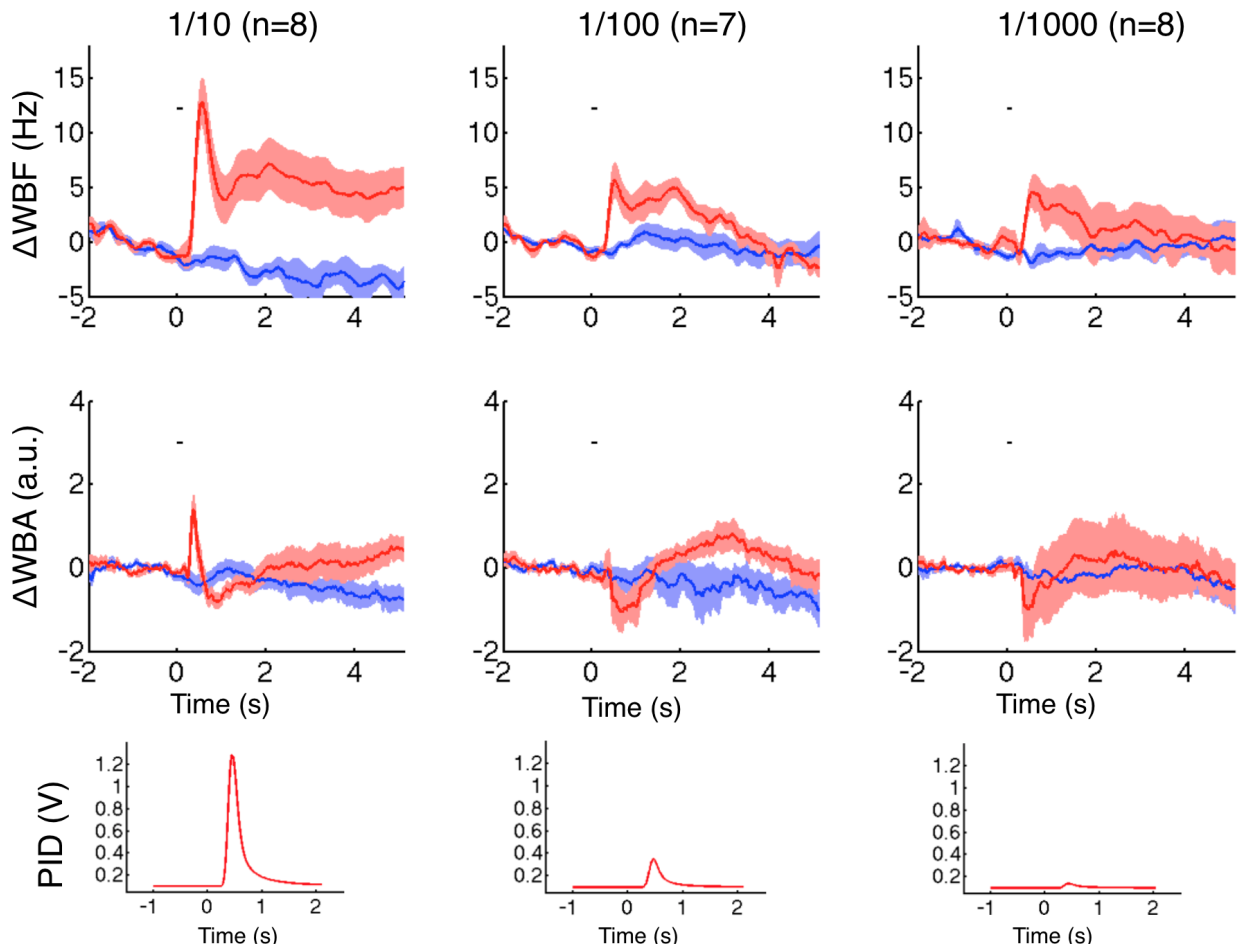


Figure 5.3: Flight responses to ethyl acetate pulses of different concentrations. (top row) Changes in WBF (top row) and changes in WBA (middle row) on presentation of ethyl acetate (red) or control (blue) pulses. Bottom row shows the pulse kinetics and amplitudes. Each column corresponds to a different concentration of ethyl acetate (diluted 1/10, 1/100 or 1/1000 in Paraffin Oil). Black lines in the first two rows indicate the duration of the pulse (100 ms). In all time traces of Δ WBF or Δ WBA, the mean WBF or WBA before the pulse onset (at $t = 0$ s) is subtracted from every trace, and the mean Δ WBF and Δ WBA is plotted with solid lines. Shading indicates the standard error of the mean.

dilution led to a ~ 10 fold change in the gas phase concentration delivered to the fly (Fig. 5.3 bottom row). Pulses with largest amplitude led to the largest changes in the WBF and WBA (Fig. 5.3 first column), while pulses with the smallest amplitude led to the smallest changes in the WBF and WBA (Fig. 5.3 last column). This suggests that (i) the behavior seen here and in Fig. 5.2 is likely olfactory in origin, and (ii) the concentration of the odor encountered modulates the amplitude and kinetics of the behavioral response.

5.2.3 Flight responses to pulses of different durations

How does the duration of the odor pulse encountered affect behavioral responses? Due to the relatively high speed at which Drosophila fly (~ 30 cm/s) [172] and the relatively narrow width of odor plumes that they would likely encounter [89, 119–121], flies may experience contact and loss with a plume almost instantaneously [16]. This suggests that flies may modulate their behavior even to very brief plumes of odorant. To test this hypothesis, I presented flies with pulses of ethyl acetate odorant with varying durations.

Flies modulated their WBF and WBA responses with the duration of the pulse delivered, with the shortest pulses eliciting the smallest and most transient increases in the WBF and WBA (Fig. 5.4, first column). As the duration of the pulse increased, responses grew larger and more long lasting (Fig. 5.4). However, since the pulses delivered using this olfactometer are not perfectly square (largely due to the fact that the valve is upstream of the odor), pulse duration is also strongly correlated with pulse amplitude in this experiment. Thus, it is not clear if the change in responses seen in Fig. 5.4 are due to changes in pulse duration, or due to changes in pulse amplitude, or some combination of the two.

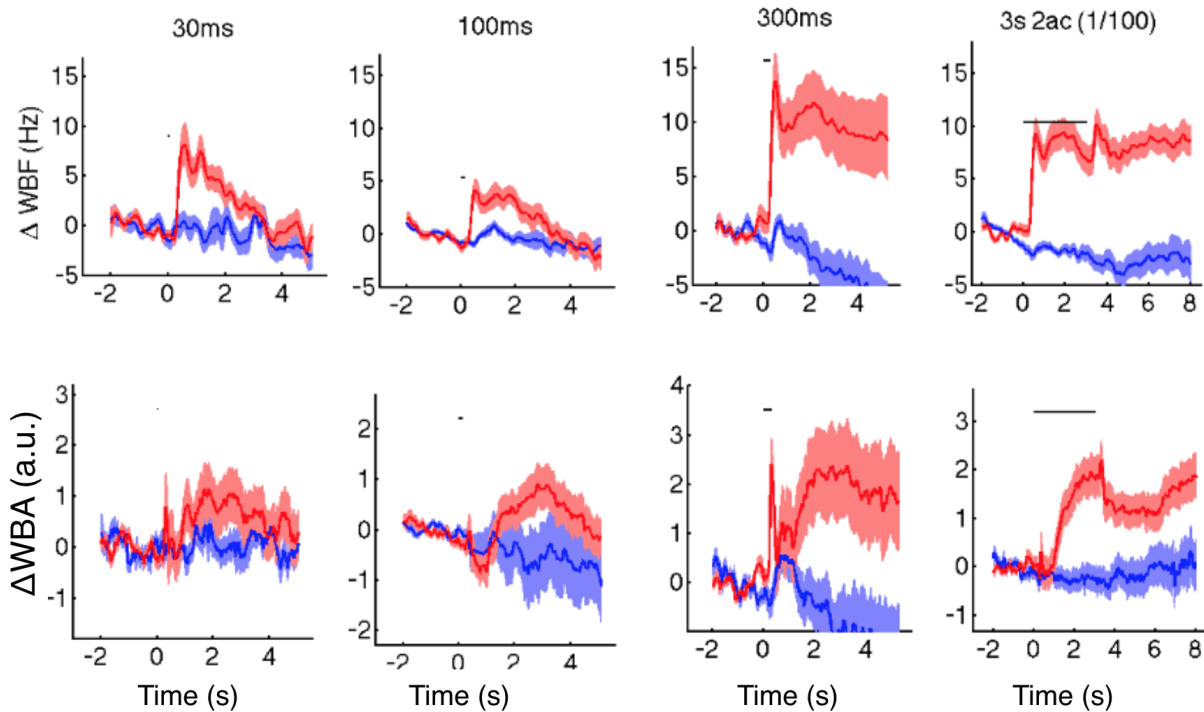


Figure 5.4: *Flight responses to ethyl acetate pulses with different durations.* (top row) Changes in WBF (top row) and changes in WBA (bottom row) on presentation of ethyl acetate (red) or control (blue) pulses. Each column corresponds to a different duration of the ethyl acetate (diluted 1/100 in Paraffin Oil) pulse. Black lines in all plots indicate the duration of the pulse (30 ms - 3 s).

5.2.4 Trial-to-trial variations in behavioral response

So far, the data presented neglects the variation in behavior from trial to trial and pools all trials to present gross averages (Fig. 5.2, 5.3, 5.4). How do fly responses vary from trial to trial? Individual trials from individual flies are very noisy, making interpretation of data challenging. I therefore averaged across different flies, and plot trends in behavior as a function of trial number.

Fig. 5.5 shows how WBF and WBA responses vary from trial to trial. This analysis reveals two features of the response that were not evident in the averaged responses:

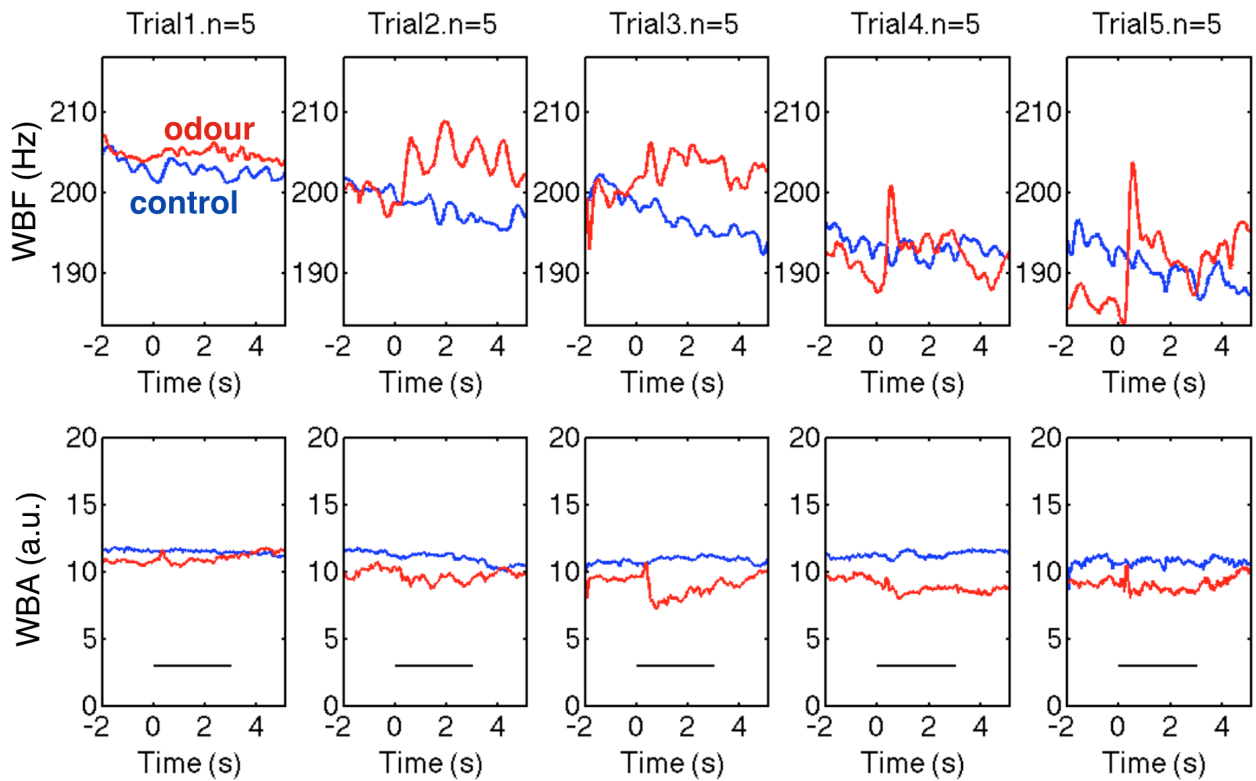


Figure 5.5: *Trial-to-trial variability in olfactory responses.* WBF for odor (red) and control (blue) presentations (top row). WBA for odor (red) and control (blue) presentations (bottom row). Each row shows responses averaged across 5 flies for a single trial. The odor used is ethyl acetate (diluted 1/10 in Paraffin Oil). Note that for the first trial, the odor evokes no response either in the WBF or the WBA. However, in the fifth trial, WBF responses are large.

- A. Pre-stimulus WBF drops steadily from trial to trial. It is relatively high in the first trial (~ 205 Hz) and drops to ~ 190 Hz by the fifth trial.
- B. Odor-evoked responses grow from trial to trial. Odor evokes no response in the WBF in the first trial, but evokes a response by the fifth trial.

One possibility for this behavior could be because laboratory reared flies (Canton S flies were used in this assay) tend to fly much closer to their maximum WBF at rest [13]. Thus, at the first trial, they are unable to increase their WBF as they are already close to the maximum. By the fifth trial, however, because their resting WBF drops, their dynamic range of response increases, manifesting as a large odor-evoked response. Why does pre-stimulus WBF drop from trial to trial? One possibility is that flies get progressively exhausted, and reduce their wing beat frequency. Consistent with this possibility was the observation that the probability of stopping increased with time in the assay.

5.2.5 *A better olfactometer*

The olfactometer used thus far (as shown in Fig. 5.1) suffers from design flaws. Amongst them are (i) non-square odorant pulses that conflated pulse amplitude and duration, see §5.2.3; (ii) dilution in paraffin oil that caused depletion of pulse amplitude over time and made changing pulse amplitude cumbersome. Therefore, I developed a new olfactometer design (Fig. 5.6).

In this design, MFCs are used to create an odorized airstream by blowing air over a scintillation vial containing pure odorant. The concentration of the odorant in the airstream is controlled by varying the

ratio¹ of the air flows through the odor vial and through the diluent vial (green box in Fig. 5.6a). This odorized airstream feeds into a dual three way valve, which switches between two states. Normally, the valve diverts the odorized airstream to waste, and directs another clean airstream to the fly. When the valve is activated, the odorized airstream is directed to the fly, and the other airstream is directed to waste. This switch is done using a single valve, that is constructed to have equal resistances along all flow paths, minimizing airspeed and pressure changes on valve operation. A second three way valve switches between two other clean airstreams, which is used to deliver control pulses with no odorant.

This design has several advantages over the earlier design. Using gas phase dilution permits delivering odorant pulses of several different amplitudes using the same device, making it much easier to acquire data as in Fig. 5.3. Fig. 5.6b shows pulses of various amplitudes that are achieved with this olfactometer, by simply varying the flow rates through the odor and clean vials. Note that these pulses are much faster, and more square, as compared to the pulses delivered by the earlier design (cf. Fig. 5.2). In addition, by varying the position of a teflon plug in the final glass funnel (see Fig. 5.6a), I can vary the volume of the mixing space between different airstreams before delivery to the fly. This has the effect of changing the kinetics of odorant pulses. In particular, odorants that have intrinsically fast kinetics, like ethyl acetate, that generate square pulses, can be made slower (Fig. 5.6b), with longer rise and decay times, resembling odorants that have intrinsically slower kinetics [113]. Finally, using pure odorants and gas phase dilutions ensures that the amplitude of the odorant pulse does not decay over time, since the concentration of the odorant in the vial does not change, as it would if it was diluted in

¹ for more detail on gas phase dilution, see §2.2.3

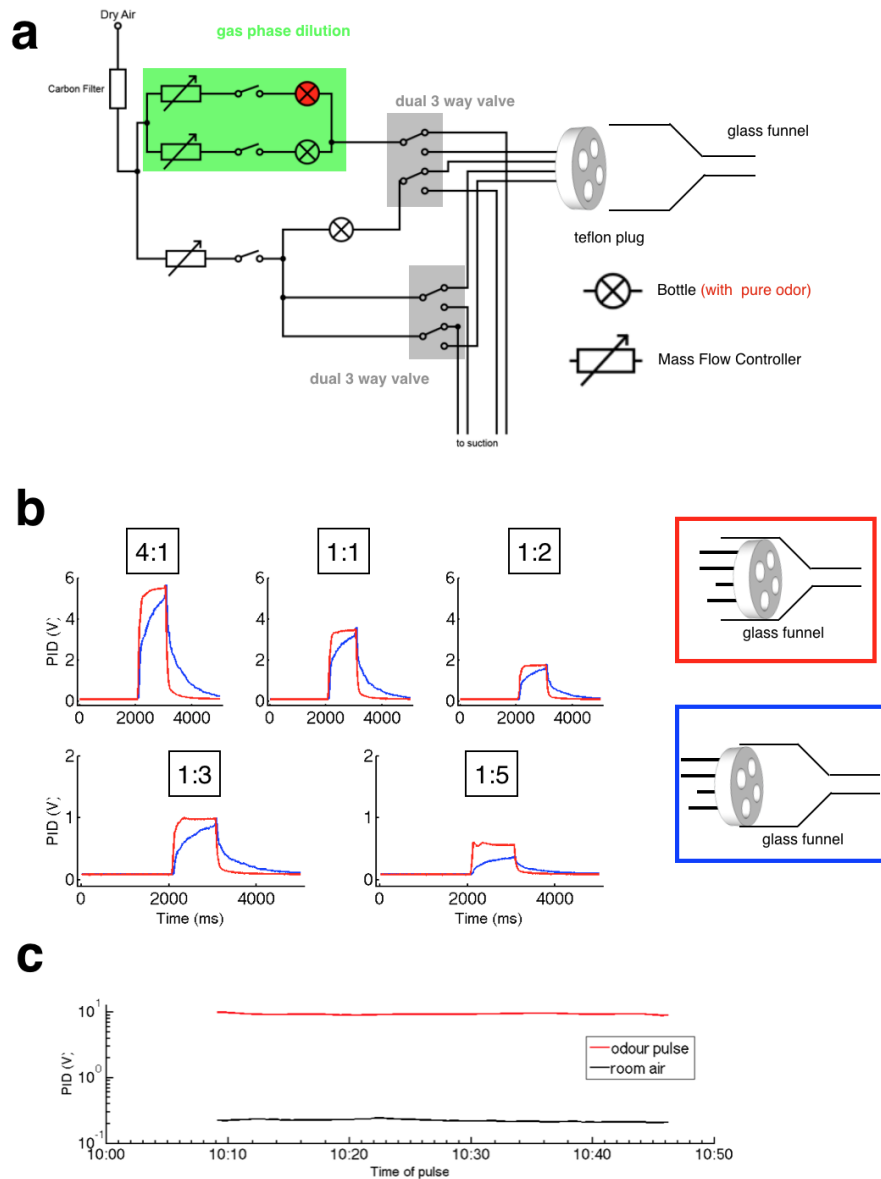


Figure 5.6: *A better olfactometer.* (a) Schematic of the redesigned olfactometer. (b) Different pulse amplitudes generated by varying the ratio of airflows through the odor and diluent vial (ratio in boxes). Different pulse kinetics can be generated by varying the position of the teflon plug in the glass funnel. (c) Constancy of pulse amplitude over time. The odorant used here is ethyl acetate.

Paraffin Oil. Fig. 5.6c shows the amplitude of a pulse of ethyl acetate remaining relatively constant over \sim 30 minutes.

5.2.6 *A tale of diminishing responses*

How do flies respond to pulses of odorant delivered with this new olfactometer? I delivered 200 ms pulses of ethyl acetate using this olfactometer to flies and measured their WBA and WBF response. Odorant pulses still elicited increases in the WBF, but the amplitude of responses was much smaller compared to those elicited by pulses delivered using the earlier design (Fig. 5.7a). While pulses of ethyl acetate elicited a complex response in the WBA, comprising of transient responses followed by a slow increase, equivalent pulses from the new olfactometer elicited a cleaner WBA response comprising mainly of a slow decrease (Fig. 5.7a). On examining the WBA responses more closely, I observed two peaks in the WBA response that occurred \sim 40ms after valve opening and closing, in both the control and odorant pulse responses. The fact that these peaks occurred so quickly after valve movement, and the fact that they existed in both responses to control pulses and odorant pulses, suggested that these peaks corresponded to a mechanical artifact associated with the motion of the valve.

To eliminate these mechanical artifacts, I redesigned the olfactometer once more, taking care to balance airstreams flowing into the two inlets of the two valves, and mechanically isolating the valves to prevent shockwaves from valve closing and opening from propagating through the entire device. These alterations to the design succeeded in greatly attenuating the transients in the WBA response following valve opening and closing (Fig. 5.8b, cf. Fig. 5.8a). However, responses to pulses of Apple Cider Vinegar delivered by design #3 were smaller

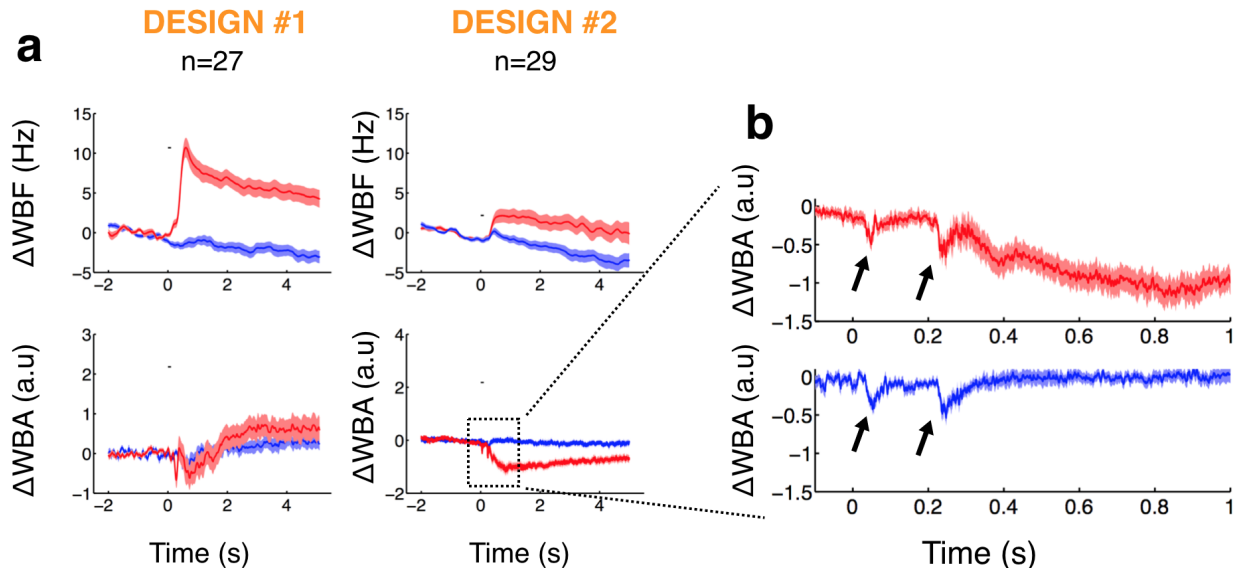


Figure 5.7: *Flight responses to ethyl acetate pulses delivered by olfactometer design #2.* (a) Comparison of WBF and WBA responses to 100 ms ethyl acetate pulses delivered by olfactometer design #1 (Fig. 5.1) and design #2 (Fig. 5.6). (b) WBA responses show transient peaks (black arrows) for both odor pulses (red) and control pulses (blue). These peaks occur \sim 40 ms after valve opening and closing.

than those elicited by pulses delivered by design #2, which in turn were smaller than those elicited by design #1 (Fig. 5.8c-e).

5.3 DISCUSSION

The flight of flies is a complex behavior, and depends on the integration of sensory cues from many modalities, including vision [58, 111, 117], mechanosensation [22] and olfaction [58, 101]. In this assay I attempted to unravel how various features of stimuli of *one* modality, olfaction, affect the response of flies. This task was made even more challenging by the fact that flies rely heavily on vision and mechanosensation during flight [111, 117, 118, 137, 156, 172]. In order to study how olfactory cues modulated flight behavior, olfactory cues had to be introduced without introducing other cues, which is a very hard problem. Since all olfactory cues need to be transported

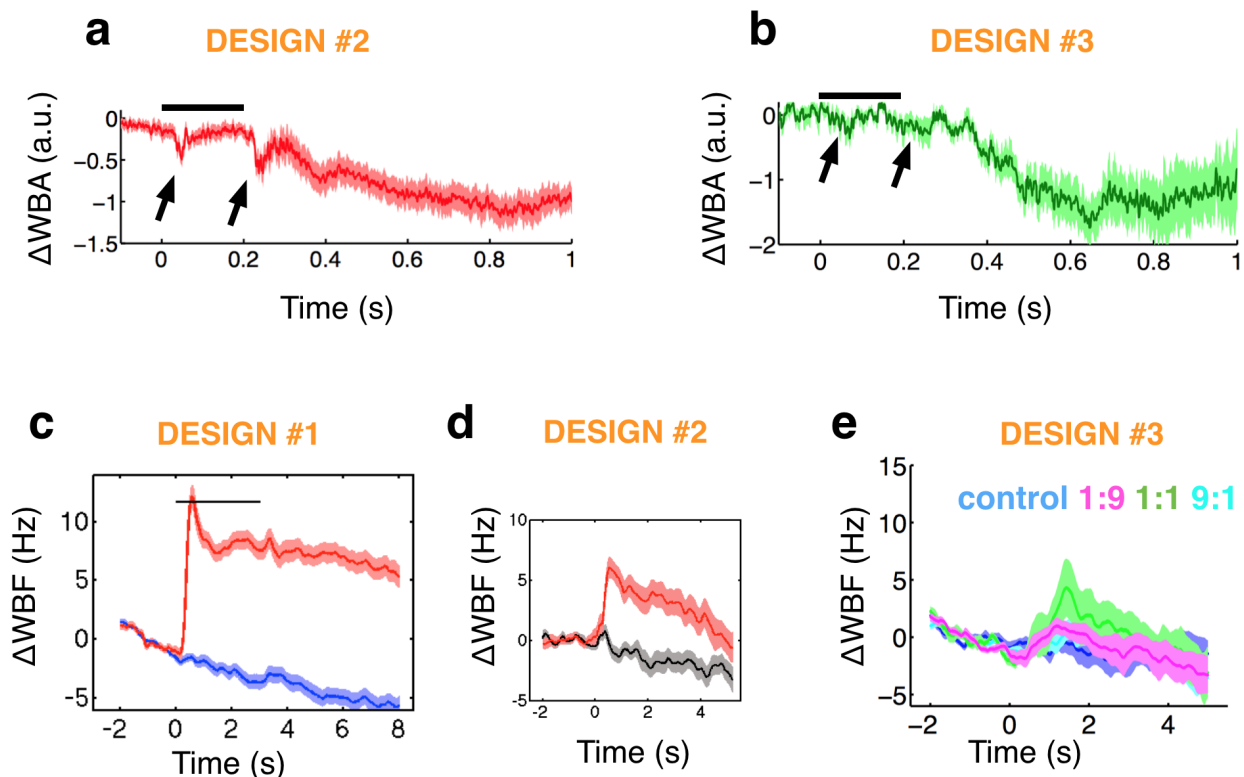


Figure 5.8: *Flight responses to ethyl acetate pulses delivered by olfactometer design*
 (a) Design #2 introduced transient peaks in the WBA response ~40 ms after valve motion, suggesting a mechanical artifact. (b) Design #3 largely eliminates this mechanical artifact. (c-e) Comparison of responses evoked by Apple Cider Vinegar by Designs #1, 2 and 3.

by moving airstreams, delivering any olfactory cue typically relies on valves that switches airstreams. Earlier studies have shown that turning valves on and off introduces large, transient fluctuations in the airspeed that occur on timescales as fast as a few milliseconds [40]. The ability of the fly to detect mechanical disturbances in airstreams exceeded that of instruments at my disposal, making it hard to know with certainty if responses observed here were not contaminated by mechanical stimuli originating from valve switching.

A further challenge in this work was that flies did not fly reliably in this assay. Compared to published studies [10, 13], I observed that flies flew at lower WBFs. Flies also tended to stop flying intermittently, making data collection arduous. The reasons for the poor flight

ability of the flies tested here is not known, but it could be due to (i) the fact that these experiments were conducted in the dark, which is an atypical flying environment for flies, and (ii) the genetic background of the flies tested in this study.

Part IV

CONCLUSION

CONCLUSION

Although this dissertation still leaves many aspects of gain control in Olfactory Receptor Neurons (ORNs) unexplored, I hope that it will serve as a framework for further studies on how ORNs encode odor signals and how they adapt their coding scheme in the face of changing stimuli. This dissertation studied gain control properties of one of three classes of ORNs [71], those expressing Olfactory Receptors (ORs), and found two important features of ORN gain control in these neurons: (i) gain control that followed the Weber-Fechner law; and (ii) complementary kinetics that preserved the timing of odor encounters despite front-end adaptation that slowed transduction responses. It is of significant interest if these two features are preserved in the two other classes of ORNs. ORNs that express IRs and GRs detect signals that are qualitatively different (like carbon dioxide), or function in ways that are mechanistically distinct from ORs [181], making it an open question if these ORNs show the same features of gain control that I described in this dissertation. Intriguingly, a recent study found that IR-expressing ORNs may not show any adaptation to prolonged pulses, or pairs of pulses, but it is not clear if they also do not follow the Weber-Fechner law [26].

We found that the slowdown in kinetics of response emerged as a natural consequence of receptor binding and activation, using a model that has been widely used to reproduce disparate phenomenon like bacterial chemotaxis [7] or activation at the neuromuscular junction [5]. Whether these systems also show a slowdown in response kinetics could be a question for further investigation, especially in

cases like bacterial chemotaxis where the overall output of the system is believed to exhibit kinetics that are invariant with the adapted state [65].

A central principle in this dissertation is the importance of measuring and precisely controlling odorant stimuli applied to ORNs, which led to a quantitative understanding of how ORNs respond to various statistical features of odorant stimuli. While pioneering studies in ORN response phenomenology that used simple odor stimuli led to a general understanding of how ORNs response to various odor stimuli [4, 19, 20], more recent studies [96, 113, 125], and this dissertation, that have relied on more sophisticated stimuli have uncovered new features of ORN response phenomenology that had not been previously quantitatively understood.

We have used the *Drosophila* olfactory system as a model system due to the large corpus of earlier studies that have established techniques to record from these neurons [19], the locations of identified neurons on the antenna [154, 155], and maps that link the morphology of sensilla to the neurons they house to the receptors they express to the odorant molecules they respond to [74, 100]. The framework we have used here could also be used in other insect species, like mosquitoes or tsetse flies, to understand how their primary olfactory neurons detect signals that help them feed on humans.

BIBLIOGRAPHY

- [1] Martin N Andersson, Fredrik Schlyter, Sharon Rose Hill, and Teun Dekker. “What reaches the antenna? How to calibrate odor flux and ligand-receptor affinities.” English. In: *Chemical Senses* 37.5 (June 2012), pp. 403–420. DOI: [10.1093/chemse/bjs009](https://doi.org/10.1093/chemse/bjs009). URL: <http://eutils.ncbi.nlm.nih.gov/entrez/eutils/elink.fcgi?dbfrom=pubmed&id=22362868&retmode=ref&cmd=prlinks> (cit. on pp. 36, 40).
- [2] Kenta Asahina, Matthieu Louis, Silvia Piccinotti, and Leslie B Vosshall. “A circuit supporting concentration-invariant odor perception in *Drosophila*.” English. In: *Journal of Biology* 8.1 (Jan. 2009), p. 1. DOI: [10.1186/jbiol108](https://doi.org/10.1186/jbiol108). URL: <http://jbiol.biomedcentral.com/articles/10.1186/jbiol108> (cit. on p. 92).
- [3] Collins Assisi, Mark Stopfer, and Maxim Bazhenov. “Using the Structure of Inhibitory Networks to Unravel Mechanisms of Spatiotemporal Patterning.” English. In: *Neuron* 69.2 (Jan. 2011), pp. 373–386. DOI: [10.1016/j.neuron.2010.12.019](https://doi.org/10.1016/j.neuron.2010.12.019). URL: <http://dx.doi.org/10.1016/j.neuron.2010.12.019> (cit. on p. 96).
- [4] Richard K Ayer and John R Carlson. “Olfactory physiology in the *Drosophila* antenna and maxillary palp: acj6 distinguishes two classes of odorant pathways.” English. In: *Journal of Neurobiology* 23.8 (Oct. 1992), pp. 965–982. DOI: [10.1002/neu.480230804](https://doi.org/10.1002/neu.480230804). URL: <http://doi.wiley.com/10.1002/neu.480230804> (cit. on p. 135).

- [5] S Thesleff B Katz. "A study of the 'desensitization' produced by acetylcholine at the motor end-plate." English. In: *The Journal of Physiology* 138.1 (Aug. 1957), pp. 63–80. URL: <https://www.ncbi.nlm.nih.gov/pmc/articles/PMC1363030/> (cit. on p. 134).
- [6] Stephen A Baccus and Markus Meister. "Fast and Slow Contrast Adaptation in Retinal Circuitry." English. In: *Neuron* 36.5 (Dec. 2002), pp. 909–919. DOI: [10.1016/S0896-6273\(02\)01050-4](https://doi.org/10.1016/S0896-6273(02)01050-4). URL: <http://linkinghub.elsevier.com/retrieve/pii/S0896627302010504> (cit. on pp. 15, 56, 67, 73, 78, 87, 99, 102, 110).
- [7] N Barkai and S Leibler. "Robustness in simple biochemical networks." In: *Nature* (1997). URL: <http://search.proquest.com/openview/0b9ed9c5a53905b017083ad9e773e876/1?pq-origsite=gscholar&cbl=40569> (cit. on pp. 92, 93, 100, 134).
- [8] M Bazhenov, Mark Stopfer, M Rabinovich, Henry Abarbanel, T J Sejnowski, and G Laurent. "Model of cellular and network mechanisms for odor-evoked temporal patterning in the locust antennal lobe." English. In: *Neuron* 30.2 (May 2001), pp. 569–581. DOI: [10.1016/s0896-6273\(01\)00286-0](https://doi.org/10.1016/s0896-6273(01)00286-0). URL: <http://linkinghub.elsevier.com/retrieve/pii/S0896627301002860> (cit. on p. 96).
- [9] D L Beaudoin and M B Manookin. "Distinct expressions of contrast gain control in parallel synaptic pathways converging on a retinal ganglion cell." English. In: *The Journal of...* 586.22 (2008), pp. 5487–5502. DOI: [10.1113/jphysiol.2008.156224](https://doi.org/10.1113/jphysiol.2008.156224). URL: <http://doi.wiley.com/10.1113/jphysiol.2008.156224> (cit. on p. 99).
- [10] John A Bender and Michael H Dickinson. "Visual stimulation of saccades in magnetically tethered *Drosophila*." In: *The Jour-*

- nal of experimental biology* 209.16 (2006), pp. 3170–3182. URL: <http://jeb.biologists.org/content/209/16/3170.short> (cit. on pp. 117, 131).
- [11] Matthew E Berck et al. “The wiring diagram of a glomerular olfactory system.” English. In: *eLife* 5 (May 2016), e14859. DOI: 10.7554/eLife.14859. URL: <http://elifesciences.org/lookup/doi/10.7554/eLife.14859> (cit. on p. 96).
- [12] V Bhandawat, S R Olsen, and N W Gouwens. “Sensory processing in the *Drosophila* antennal lobe increases reliability and separability of ensemble odor representations.” In: *Nature* 10.11 (2007), pp. 1474–1482. DOI: 10.1038/nrn1976. URL: <http://www.nature.com/doifinder/10.1038/nrn1976> (cit. on p. 62).
- [13] Vikas Bhandawat, Gaby Maimon, Michael H Dickinson, and Rachel I Wilson. “Olfactory modulation of flight in *Drosophila* is sensitive, selective and rapid.” English. In: *Journal of Experimental ...* 213.Pt 21 (Nov. 2010), pp. 3625–3635. DOI: 10.1242/jeb.040402. URL: <http://eutils.ncbi.nlm.nih.gov/entrez/eutils/elink.fcgi?dbfrom=pubmed&id=20952610&retmode=ref&cmd=prlinks> (cit. on pp. 8, 117, 118, 126, 131).
- [14] Vincent Bonin, Valerio Mante, and Matteo Carandini. “The statistical computation underlying contrast gain control.” English. In: *Journal of Neuroscience* 26.23 (June 2006), pp. 6346–6353. DOI: 10.1523/JNEUROSCI.0284-06.2006. URL: <http://www.jneurosci.org/content/26/23/6346.full> (cit. on p. 99).
- [15] Alexander Borst and Martin Heisenberg. “Osmotropotaxis in *Drosophila melanogaster*.” English. In: *Journal of Comparative Physiology A: Neuroethology, Sensory, Neural, and Behavioral Physiology* 147.4 (1982), pp. 479–484. DOI: 10.1007/BF00612013. URL:

<https://link.springer.com/article/10.1007/BF00612013> (cit. on p. 7).

- [16] Floris van Breugel and Michael H Dickinson. "Plume-Tracking Behavior of Flying Drosophila Emerges from a Set of Distinct Sensory-Motor Reflexes." English. In: *Current biology : CB* 24.3 (Jan. 2014), pp. 274–286. doi: [10.1016/j.cub.2013.12.023](https://doi.org/10.1016/j.cub.2013.12.023). URL: <http://linkinghub.elsevier.com/retrieve/pii/S0960982213015820> (cit. on pp. 36, 37, 103, 117, 123).
- [17] E G Brockerhoff and G G Grant. "Correction for Differences in Volatility Among Olfactory Stimuli and Effect on EAG Responses of Dioryctria abietivorella to Plant Volatiles." English. In: *Journal of chemical ecology* 25.6 (1999), pp. 1353–1367. doi: [10.1023/A:1020930910416](https://doi.org/10.1023/A:1020930910416). URL: <https://link.springer.com/article/10.1023/A:1020930910416> (cit. on p. 25).
- [18] M de Bruyne and T C Baker. "Odor Detection in Insects: Volatile Codes." English. In: *Journal of chemical ecology* 34.7 (June 2008), pp. 882–897. doi: [10.1007/s10886-008-9485-4](https://doi.org/10.1007/s10886-008-9485-4). URL: <http://link.springer.com/10.1007/s10886-008-9485-4> (cit. on p. 9).
- [19] M de Bruyne, K Foster, and John R Carlson. "Odor coding in the Drosophila antenna." English. In: *Neuron* 30.2 (May 2001), pp. 537–552. URL: <http://eutils.ncbi.nlm.nih.gov/entrez/eutils/elink.fcgi?dbfrom=pubmed&id=11395013&retmode=ref&cmd=prlinks> (cit. on pp. 4, 13, 14, 29, 40, 62, 65, 105, 117, 135).
- [20] Marien de Bruyne, Peter J Clyne, and John R Carlson. "Odor Coding in a Model Olfactory Organ: TheDrosophila Maxillary Palp." English. In: *The Journal of neuroscience : the official journal of the Society for Neuroscience* 19.11 (June 1999), pp. 4520–4532.

- URL: <http://www.jneurosci.org/content/19/11/4520.full> (cit. on pp. 4, 13–15, 24–26, 65, 117, 135).
- [21] Seth A Budick and Michael H Dickinson. “Free-flight responses of *Drosophila melanogaster* to attractive odors.” English. In: *The Journal of experimental biology* 209.Pt 15 (Aug. 2006), pp. 3001–3017. DOI: [10.1242/jeb.02305](https://doi.org/10.1242/jeb.02305). URL: <http://eutils.ncbi.nlm.nih.gov/entrez/eutils/elink.fcgi?dbfrom=pubmed&id=16857884&retmode=ref&cmd=prlinks> (cit. on pp. 7, 61).
- [22] Seth A Budick, Michael B Reiser, and Michael H Dickinson. “The role of visual and mechanosensory cues in structuring forward flight in *Drosophila melanogaster*.” English. In: *Journal of Experimental ...* 210.23 (2007), pp. 4092–4103. DOI: [10.1242/jeb.006502](https://doi.org/10.1242/jeb.006502). URL: <http://jeb.biologists.org/cgi/doi/10.1242/jeb.006502> (cit. on pp. 117, 130).
- [23] D A Burkhardt. “Light adaptation and photopigment bleaching in cone photoreceptors *in situ* in the retina of the turtle.” English. In: *The Journal of neuroscience : the official journal of the Society for Neuroscience* 14.3 Pt 1 (Mar. 1994), pp. 1091–1105. URL: <http://www.jneurosci.org/content/14/3/1091.abstract> (cit. on p. 98).
- [24] M E Burns, A Mendez, J Chen, and D A Baylor. “Dynamics of cyclic GMP synthesis in retinal rods.” English. In: *Neuron* 36.1 (2002), pp. 81–91. DOI: [10.1016/S0896-6273\(02\)00911-X](https://doi.org/10.1016/S0896-6273(02)00911-X). URL: <http://linkinghub.elsevier.com/retrieve/pii/S089662730200911X> (cit. on p. 102).
- [25] J Cafaro. “Multiple sites of adaptation lead to contrast encoding in the *Drosophila* olfactory system.” English. In: *Physiological Reports* 4.7 (2016), e12762. DOI: [10.14814/phy2.12762](https://doi.org/10.14814/phy2.12762). URL: <http://physreports.physiology.org/lookup/doi/10.14814/phy2.12762> (cit. on pp. 15, 62, 64, 73, 81, 98, 102).

- [26] Li-Hui Cao, Bi-Yang Jing, Dong Yang, Xiankun Zeng, Ying Shen, Yuhai Tu, and Dong-Gen Luo. “Distinct signaling of Drosophilachemoreceptors in olfactory sensory neurons.” English. In: *Proceedings of the National Academy of ...* 113.7 (Feb. 2016), pp. 201518329–15. DOI: [10.1073/pnas.1518329113](https://doi.org/10.1073/pnas.1518329113). URL: <http://www.pnas.org/lookup/doi/10.1073/pnas.1518329113> (cit. on pp. 13–16, 19, 62, 64, 73, 81, 83, 89, 99, 101–104, 134).
- [27] A Capurro, F Baroni, S B Olsson, Linda S Kuebler, Salah Karout, Bill S Hansson, and Timothy C Pearce. “Non-linear blend coding in the moth antennal lobe emerges from random glomerular networks.” In: *Frontiers in Neuroengineering* (2012). DOI: [10.3389/fneng.2012.00006](https://doi.org/10.3389/fneng.2012.00006). URL: http://books.google.com/books?hl=en&lr=&id=W0wo5NX4-xEC&oi=fnd&pg=PA97&dq=10.3389/fneng.2012.00006&ots=q0pLj1fuBP&sig=dbLiflyHC1uX0FMRAgx_4ooju8E (cit. on p. 96).
- [28] R T Cardé. *Precopulatory sexual behavior of the adult gypsy moth*. The gypsy moth: research toward integrated pest ..., 1981. URL: http://scholar.google.com/scholar?q=related:G_Q0q1RYh88J:scholar.google.com/&hl=en&num=20&as_sdt=0,5 (cit. on p. 6).
- [29] Ring T Cardé and Mark A Willis. “Navigational Strategies Used by Insects to Find Distant, Wind-Borne Sources of Odor.” English. In: *Journal of chemical ecology* 34.7 (June 2008), pp. 854–866. DOI: [10.1007/s10886-008-9484-5](https://doi.org/10.1007/s10886-008-9484-5). URL: <http://link.springer.com/10.1007/s10886-008-9484-5> (cit. on p. 61).
- [30] Antonio Celani, Emmanuel Villermaux, and Massimo Vergassola. “Odor Landscapes in Turbulent Environments.” English. In: *Physical Review X* 4.4 (Oct. 2014), pp. 041015–17. DOI: [10.1103/PhysRevX.4.041015](https://doi.org/10.1103/PhysRevX.4.041015). URL: <http://link.aps.org/doi/10.1103/PhysRevX.4.041015> (cit. on pp. 4, 5, 61, 64–66, 109, 117).

- [31] Tsai-Wen Chen et al. "Ultrasensitive fluorescent proteins for imaging neuronal activity." In: *Nature* 499.7458 (July 2013), pp. 295–300. DOI: [10.1038/nature12354](https://doi.org/10.1038/nature12354). URL: <http://www.nature.com/doifinder/10.1038/nature12354> (cit. on p. 84).
- [32] E J Chichilnisky. "A simple white noise analysis of neuronal light responses." English. In: *Network (Bristol, England)* 12.2 (May 2001), pp. 199–213. URL: <http://eutils.ncbi.nlm.nih.gov/entrez/eutils/elink.fcgi?dbfrom=pubmed&id=11405422&retmode=ref&cmd=prlinks> (cit. on pp. 43, 56, 73).
- [33] K Y Chong, A Capurro, S Karout, and T C Pearce. "Stimulus and network dynamics collide in a ratiometric model of the antennal lobe macrogglomerular complex." In: *PLoS one* (2012). URL: <http://dx.plos.org/10.1371/journal.pone.0029602> (cit. on p. 96).
- [34] Dawnis M Chow and Mark A Frye. "Context-dependent olfactory enhancement of optomotor flight control in *Drosophila*." English. In: *The Journal of experimental biology* 211.Pt 15 (Aug. 2008), pp. 2478–2485. DOI: [10.1242/jeb.018879](https://doi.org/10.1242/jeb.018879). URL: <http://eutils.ncbi.nlm.nih.gov/entrez/eutils/elink.fcgi?dbfrom=pubmed&id=18626082&retmode=ref&cmd=prlinks> (cit. on p. 8).
- [35] Dawnis M Chow, Jamie C Theobald, and Mark A Frye. "An olfactory circuit increases the fidelity of visual behavior." English. In: *Journal of Neuroscience* 31.42 (Oct. 2011), pp. 15035–15047. DOI: [10.1523/JNEUROSCI.1736-11.2011](https://doi.org/10.1523/JNEUROSCI.1736-11.2011). URL: <http://eutils.ncbi.nlm.nih.gov/entrez/eutils/elink.fcgi?dbfrom=pubmed&id=22016537&retmode=ref&cmd=prlinks> (cit. on p. 8).
- [36] Damon A Clark, Raphael Benichou, Markus Meister, and Rava Azeredo da Silveira. "Dynamical Adaptation in Photorecep-

- tors.” English. In: *PLoS Computational Biology* 9.11 (Nov. 2013), e1003289. DOI: [10.1371/journal.pcbi.1003289](https://doi.org/10.1371/journal.pcbi.1003289). URL: <http://dx.plos.org/10.1371/journal.pcbi.1003289> (cit. on pp. 16, 56, 59, 100, 101).
- [37] Peter Clyne, Alan Grant, Robert O’Connell, and John R Carlson. “Odorant response of individual sensilla on theDrosophila antenna.” English. In: *Invertebrate Neuroscience* 3.2-3 (1997), pp. 127–135. DOI: [10.1007/BF02480367](https://doi.org/10.1007/BF02480367). URL: <http://link.springer.com/article/10.1007/BF02480367> (cit. on pp. 9, 25, 26).
- [38] J E Cometto-Muñiz, W S Cain, and M H Abraham. “Quantification of chemical vapors in chemosensory research.” In: *Chemical Senses* (2003). URL: <http://chemse.oxfordjournals.org/content/28/6/467.short> (cit. on p. 36).
- [39] A L Hodgkin D A Baylor. “Changes in time scale and sensitivity in turtle photoreceptors.” English. In: *The Journal of Physiology* 242.3 (Nov. 1974), pp. 729–758. DOI: [10.1111/\(ISSN\)1469-7793](https://doi.org/10.1111/(ISSN)1469-7793). URL: [/pmc/articles/PMC1330660/?report=abstract](https://doi.org/10.1111/(ISSN)1469-7793) (cit. on pp. 101, 102).
- [40] Kevin C Daly, Faizan Kalwar, Mandy Hatfield, Erich Staudacher, and Samuel P Bradley. “Odor Detection in Manduca sexta Is Optimized when Odor Stimuli Are Pulsed at a Frequency Matching the Wing Beat during Flight.” English. In: *PloS one* 8.11 (Nov. 2013), e81863. DOI: [10.1371/journal.pone.0081863](https://doi.org/10.1371/journal.pone.0081863). URL: <http://dx.plos.org/10.1371/journal.pone.0081863> (cit. on p. 131).
- [41] C T David, J S Kennedy, and A R Ludlow. “Finding of a sex pheromone source by gypsy moths released in the field.” In: *Nature* 303.5920 (1983), pp. 804–806. DOI: [10.1038/303804a0](https://doi.org/10.1038/303804a0). URL: <http://www.nature.com/doifinder/10.1038/303804a0> (cit. on p. 7).

- [42] Peter Dayan and Larry Abbott. *Theoretical neuroscience*. English. computational and mathematical modeling of neural systems. The MIT Press, Dec. 2001. URL: http://books.google.com/books?id=5GSKQgAACAAJ&dq=intitle:Theoretical+Neuroscience&hl=&cd=2&source=gbs_api (cit. on p. 67).
- [43] E De Boer and P Kuyper. "Triggered correlation." In: *IEEE Transactions on Biomedical ...* (1968). URL: http://ieeexplore.ieee.org/xpls/abs_all.jsp?arnumber=4502561 (cit. on p. 73).
- [44] Giovanna De Palo, Anna Boccaccio, Andrew Miri, Anna Menini, and Claudio Altafini. "A Dynamical Feedback Model for Adaptation in the Olfactory Transduction Pathway." English. In: *Biophysj* 102.12 (June 2012), pp. 2677–2686. DOI: [10.1016/j.bpj.2012.04.040](https://doi.org/10.1016/j.bpj.2012.04.040). URL: <http://linkinghub.elsevier.com/retrieve/pii/S0006349512005140> (cit. on p. 101).
- [45] M Deshpande, K Venkatesh, and V Rodrigues. "The inositol 1, 4, 5-trisphosphate receptor is required for maintenance of olfactory adaptation in Drosophila antennae." In: *Journal of ...* (2000). URL: http://www.researchgate.net/profile/Monika_Deshpande/publication/12476540_The_inositol_145-trisphosphate_receptor_is_required_for_maintenance_of_olfactory_adaptation_in_Drosophila_antennae/links/0deec51f15cb47a4ac000000.pdf (cit. on p. 100).
- [46] M Diaz-Quesada and M Maravall. "Intrinsic Mechanisms for Adaptive Gain Rescaling in Barrel Cortex." English. In: *The Journal of neuroscience : the official journal of the Society for Neuroscience* 28.3 (Jan. 2008), pp. 696–710. DOI: [10.1523/JNEUROSCI.4931-07.2008](https://doi.org/10.1523/JNEUROSCI.4931-07.2008). URL: <http://www.jneurosci.org/cgi/doi/10.1523/JNEUROSCI.4931-07.2008> (cit. on pp. 87, 99).

- [47] A E Dubin and G L Harris. "Voltage-activated and odor-modulated conductances in olfactory neurons of *Drosophila melanogaster*." In: *Journal of Neurobiology* (1997). URL: https://www.researchgate.net/profile/Adrienne_Dubin/publication/246872308_Voltage-activated_and_odor-modulated_conductances_in_olfactory_neurons_ofDrosophila_melanogaster/links/55943da308ae5d8f392f6083.pdf (cit. on p. 13).
- [48] Brian J Duistermars, Dawnis M Chow, and Mark A Frye. "Flies require bilateral sensory input to track odor gradients in flight." English. In: *Current biology : CB* 19.15 (Aug. 2009), pp. 1301–1307. DOI: [10.1016/j.cub.2009.06.022](https://doi.org/10.1016/j.cub.2009.06.022). URL: <http://eutils.ncbi.nlm.nih.gov/entrez/eutils/elink.fcgi?dbfrom=pubmed&id=19576769&retmode=ref&cmd=prlinks> (cit. on pp. 7, 8, 61).
- [49] Brian J Duistermars and Mark A Frye. "Multisensory integration for odor tracking by flying *Drosophila*: behavior, circuits and speculation." In: *Communicative & integrative biology* 3.1 (2010), pp. 60–63. DOI: [10.4161/cib.3.1.10076](https://doi.org/10.4161/cib.3.1.10076). URL: <http://www.landesbioscience.com/journals/6/article/10076/> (cit. on p. 7).
- [50] F A Dunn, M J Lankheet, and F Rieke. "Light adaptation in cone vision involves switching between receptor and post-receptor sites." In: *Nature* (2007). DOI: [10.1038/nature06150](https://doi.org/10.1038/nature06150). URL: <http://www.nature.com/nature/journal/v449/n7162/abs/nature06150.html> (cit. on p. 101).
- [51] Hany KM Dweck et al. "Olfactory channels associated with the *Drosophila* maxillary palp mediate short- and long-range attraction." English. In: *eLife* 5 (May 2016), e14925. DOI: [10.7554/eLife.14925](https://doi.org/10.7554/eLife.14925). URL: <http://elifesciences.org/lookup/doi/10.7554/eLife.14925> (cit. on p. 27).

- [52] J S Edwards. "The evolution of insect flight: implications for the evolution of the nervous system." English. In: *Brain, behavior and evolution* 50.1 (July 1997), pp. 8–12. URL: <http://eutils.ncbi.nlm.nih.gov/entrez/eutils/elink.fcgi?dbfrom=pubmed&id=9209762&retmode=ref&cmd=prlinks> (cit. on p. 104).
- [53] Thierry Emonet and Philippe Cluzel. "Relationship between Cellular Response and Behavioral Variability in Bacterial Chemo-taxis." English. In: *Proceedings of the National Academy of Sciences of the United States of America* 105.9 (Mar. 2008), pp. 3304–3309. DOI: [10.1073/pnas.0725461105](https://doi.org/10.1073/pnas.0725461105)?ref=search-gateway:8b87775663b0389635b3d60a3b471bd (cit. on p. 92).
- [54] Adrienne L Fairhall, Geoffrey D Lewen, William Bialek, and Robert R de Ruyter van Steveninck. "Efficiency and ambiguity in an adaptive neural code." English. In: *Nature* 412.6849 (Aug. 2001), pp. 787–792. DOI: [10.1038/35090500](https://doi.org/10.1038/35090500). URL: <http://www.nature.com/doifinder/10.1038/35090500> (cit. on p. 78).
- [55] A S French and S Meisner. "A New Method for Wide Frequency Range Dynamic Olfactory Stimulation and Characterization." English. In: *Chemical Senses* 32.7 (June 2007), pp. 681–688. DOI: [10.1093/chemse/bjm035](https://doi.org/10.1093/chemse/bjm035). URL: <https://academic.oup.com/chemse/article-lookup/doi/10.1093/chemse/bjm035> (cit. on pp. 23, 26, 36, 37).
- [56] Andrew S French, Shannon Meisner, Chih-Ying Su, and Päivi H Torkkeli. "Carbon Dioxide and Fruit Odor Transduction in *Drosophila* Olfactory Neurons. What Controls their Dynamic Properties?" English. In: *PloS one* 9.1 (Jan. 2014), e86347. DOI: [10.1371/journal.pone.0086347](https://doi.org/10.1371/journal.pone.0086347). URL: <http://dx.plos.org/10.1371/journal.pone.0086347> (cit. on pp. 36, 37, 43).

- [57] M A Frye and M H Dickinson. "Fly flight: a model for the neural control of complex behavior." English. In: *Neuron* 32.3 (2001), pp. 385–388. DOI: [10.1016/s0896-6273\(01\)00490-1](https://doi.org/10.1016/s0896-6273(01)00490-1). URL: <http://linkinghub.elsevier.com/retrieve/pii/S0896627301004901> (cit. on pp. 7, 117).
- [58] Mark A Frye and Michael H Dickinson. "Motor output reflects the linear superposition of visual and olfactory inputs in *Drosophila*." English. In: *Journal of Experimental ...* 207.1 (2004), pp. 123–131. DOI: [10.1242/jeb.00725](https://doi.org/10.1242/jeb.00725). URL: <http://jeb.biologists.org/cgi/doi/10.1242/jeb.00725> (cit. on pp. 8, 117, 130).
- [59] Mark A Frye, Michael Tarsitano, and Michael H Dickinson. "Odor localization requires visual feedback during free flight in *Drosophila melanogaster*." English. In: *Journal of Experimental ...* 206.5 (2003), pp. 843–855. DOI: [10.1242/jeb.00175](https://doi.org/10.1242/jeb.00175). URL: <http://jeb.biologists.org/cgi/doi/10.1242/jeb.00175> (cit. on pp. 8, 117).
- [60] K S Gaudry and P Reinagel. "Contrast adaptation in a non-adapting LGN model." In: *Journal of Neurophysiology* (2007). DOI: [10.1152/jn.00618.2006](https://doi.org/10.1152/jn.00618.2006). URL: <http://jn.physiology.org/content/98/3/1287.short> (cit. on p. 87).
- [61] Quentin Gaudry, Katherine I Nagel, and Rachel I Wilson. "Smelling on the fly: sensory cues and strategies for olfactory navigation in *Drosophila*." English. In: *Current opinion in neurobiology* 22.2 (Apr. 2012), pp. 216–222. DOI: [10.1016/j.conb.2011.12.010](https://doi.org/10.1016/j.conb.2011.12.010). URL: <http://eutils.ncbi.nlm.nih.gov/entrez/eutils/elink.fcgi?dbfrom=pubmed&id=22221864&retmode=ref&cmd=prlinks> (cit. on p. 2).
- [62] Quentin Gaudry, Elizabeth J Hong, Jamey Kain, Benjamin L de Bivort, and Rachel I Wilson. "Asymmetric neurotransmitter

- release enables rapid odour lateralization in *Drosophila*.” English. In: *Nature* (Dec. 2012), pp. –. doi: [10.1038/nature11747](https://doi.org/10.1038/nature11747). URL: <http://www.nature.com/doifinder/10.1038/nature11747> (cit. on p. 7).
- [63] Merid N Getahun, Shannon B Olsson, Sofia Lavista-Llanos, Bill S Hansson, and Dieter Wicher. “Insect Odorant Response Sensitivity Is Tuned by Metabotropically Autoregulated Olfactory Receptors.” English. In: *PLoS one* 8.3 (Mar. 2013), e58889. doi: [10.1371/journal.pone.0058889](https://doi.org/10.1371/journal.pone.0058889). URL: <http://dx.plos.org/10.1371/journal.pone.0058889> (cit. on pp. 101, 104).
- [64] Lea Goentoro and Marc W Kirschner. “Evidence that Fold-Change, and Not Absolute Level, of β -Catenin Dictates Wnt Signaling.” English. In: *Molecular Cell* 36.5 (Dec. 2009), pp. 872–884. doi: [10.1016/j.molcel.2009.11.017](https://doi.org/10.1016/j.molcel.2009.11.017). URL: <http://www.cell.com/article/S1097276509008582/fulltext> (cit. on pp. 100, 104).
- [65] Lea Goentoro, Oren Shoval, Marc W Kirschner, and Uri Alon. “The Incoherent Feedforward Loop Can Provide Fold-Change Detection in Gene Regulation.” English. In: *Molecular Cell* 36.5 (Dec. 2009), pp. 894–899. doi: [10.1016/j.molcel.2009.11.018](https://doi.org/10.1016/j.molcel.2009.11.018). URL: <http://dx.doi.org/10.1016/j.molcel.2009.11.018> (cit. on pp. 104, 135).
- [66] Alex Gomez-Marin, Brian J Duistermars, Mark A Frye, and Matthieu Louis. “Mechanisms of odor-tracking: multiple sensors for enhanced perception and behavior.” English. In: *Frontiers in Cellular Neuroscience* 4 (2010), p. 6. doi: [10.3389/fncel.2010.00006](https://doi.org/10.3389/fncel.2010.00006). URL: <http://journal.frontiersin.org/article/10.3389/fncel.2010.00006/abstract> (cit. on p. 7).
- [67] Karl G Götz. “Flight control in *Drosophila* by visual perception of motion.” In: *Biological cybernetics* (1968). URL: <http://>

- www.springerlink.com/index/GU6661721Q8234T3.pdf (cit. on p. 117).
- [68] N Gupta, S S Singh, and Mark Stopfer. “Oscillatory integration windows in neurons.” In: *Nature Communications* (2016). doi: [10.1101/081471](https://doi.org/10.1101/081471). URL: <https://www.ncbi.nlm.nih.gov/pmc/articles/PMC5171764/> (cit. on p. 23).
- [69] P Gupta, D F Albeanu, and U S Bhalla. “An odor delivery system for arbitrary time-varying patterns of odors, mixtures and concentrations.” In: *bioRxiv* (2016). doi: [10.1101/077875](https://doi.org/10.1101/077875). URL: [http://biorxiv.org/content/early/2016/09/29/077875.abstract](https://doi.org/10.1101/077875) (cit. on p. 50).
- [70] Priyanka Gupta, Dinu F Albeanu, and Upinder S Bhalla. “Olfactory bulb coding of odors, mixtures and sniffs is a linear sum of odor time profiles.” In: *Nature neuroscience* 18.2 (Jan. 2015), pp. 272–281. doi: [10.1038/nn.3913](https://doi.org/10.1038/nn.3913). URL: <http://www.nature.com/doifinder/10.1038/nn.3913> (cit. on p. 23).
- [71] Elissa A Hallem and John R Carlson. “The odor coding system of *Drosophila*.” English. In: *Trends in Genetics* 20.9 (Sept. 2004), pp. 453–459. doi: [10.1016/j.tig.2004.06.015](https://doi.org/10.1016/j.tig.2004.06.015). URL: <http://linkinghub.elsevier.com/retrieve/pii/S0168952504001817> (cit. on pp. 9, 11, 117, 134).
- [72] Elissa A Hallem and John R Carlson. “The Spatial Code for Odors Is Changed by Conditioning.” English. In: *Neuron* 42.3 (May 2004), pp. 359–361. doi: [10.1016/S0896-6273\(04\)00256-9](https://doi.org/10.1016/S0896-6273(04)00256-9). URL: <http://linkinghub.elsevier.com/retrieve/pii/S0896627304002569> (cit. on p. 12).
- [73] Elissa A Hallem and John R Carlson. “Coding of Odors by a Receptor Repertoire.” English. In: *Cell* 125.1 (Apr. 2006), pp. 143–160. doi: [10.1016/j.cell.2006.01.050](https://doi.org/10.1016/j.cell.2006.01.050). URL: [http://linkinghub.elsevier.com/retrieve/pii/S0896-6273\(06\)00010-5](http://linkinghub.elsevier.com/retrieve/pii/S0896-6273(06)00010-5)

- linkinghub.elsevier.com/retrieve/pii/S0092867406003631 (cit. on pp. 23–25, 40, 62, 64, 98).
- [74] Elissa A Hallem, Michael G Ho, and John R Carlson. “The Molecular Basis of Odor Coding in the Drosophila Antenna.” English. In: *Cell* 117.7 (June 2004), pp. 965–979. DOI: [10.1016/j.cell.2004.05.012](https://doi.org/10.1016/j.cell.2004.05.012). URL: <http://linkinghub.elsevier.com/retrieve/pii/S0092867404004982> (cit. on pp. 4, 9, 12, 13, 24, 26, 29, 40, 117, 135).
- [75] B S Hansson, H Ljungberg, E Hallberg, and C Löfstedt. “Functional specialization of olfactory glomeruli in a moth.” In: *Science* (1992). URL: <http://www.academia.edu/download/39238221/09e415109878f0f8c0000000.pdf> (cit. on p. 10).
- [76] S L Helfand and John R Carlson. “Isolation and characterization of an olfactory mutant in Drosophila with a chemically specific defect.” English. In: *Proceedings of the National Academy of Sciences* 86.8 (Apr. 1989), pp. 2908–2912. URL: <http://www.pnas.org/content/86/8/2908.abstract> (cit. on pp. 23, 106).
- [77] L Hernandez-Nunez, J Belina, M Klein, G Si, L Claus, John R Carlson, and Aravinthan D T Samuel. “Reverse-correlation analysis of navigation dynamics in Drosophila larva using optogenetics.” In: *eLife* (2015). DOI: [10.7554/eLife.06225.001](https://doi.org/10.7554/eLife.06225.001). URL: <http://elifesciences.org/content/early/2015/05/05/eLife.06225.abstract> (cit. on p. 104).
- [78] J G Hildebrand and G M Shepherd. “Mechanisms of olfactory discrimination: converging evidence for common principles across phyla.” English. In: *Annual review of neuroscience* 20 (1997), pp. 595–631. DOI: [10.1146/annurev.neuro.20.1.595](https://doi.org/10.1146/annurev.neuro.20.1.595). URL: <http://eutils.ncbi.nlm.nih.gov/entrez/eutils/elink.fcgi?dbfrom=pubmed&id=9056726&retmode=ref&cmd=prlinks> (cit. on p. 10).

- [79] A H Holway and C C Pratt. "The Weber ratio for intensive discrimination." In: *Psychological review* 69.4 (1936), p. 588. doi: [10.2307/1419082](https://doi.org/10.2307/1419082). URL: <http://www.jstor.org/stable/1419082?origin=crossref> (cit. on p. 98).
- [80] S Hong, B N Lundstrom, and A L Fairhall. "Intrinsic gain modulation and adaptive neural coding." In: *PLoS Computational Biology* (2008). doi: [10.1371/journal.pcbi.1000119](https://doi.org/10.1371/journal.pcbi.1000119). URL: <http://dx.plos.org/10.1371/journal.pcbi.1000119> (cit. on p. 102).
- [81] Sungho Hong, Blaise Agüera y Arcas, and Adrienne L Fairhall. "Single Neuron Computation: From Dynamical System to Feature Detector." English. In: *Neural computation* 19.12 (Dec. 2007), pp. 3133–3172. doi: [10.1016/S0006-3495\(08\)85146-0](https://doi.org/10.1016/S0006-3495(08)85146-0). URL: <http://www.mitpressjournals.org/doi/abs/10.1162/neco.2007.19.12.3133> (cit. on pp. 87, 102).
- [82] J J Hopfield. "Olfactory computation and object perception." In: *Proceedings of the National Academy of...* 1991. doi: [10.1073/pnas.88.15.6462](https://doi.org/10.1073/pnas.88.15.6462). URL: <http://www.pnas.org/content/88/15/6462.short> (cit. on p. 96).
- [83] M Hoskovec, B Kalinová, K Konečný, B Koutek, and J Vrkoč. "Structure-activity correlations among analogs of the currant clearwing moth pheromone." English. In: *Journal of chemical ecology* 19.4 (1993), pp. 735–750. doi: [10.1007/BF00985005](https://doi.org/10.1007/BF00985005). URL: <https://link.springer.com/article/10.1007/BF00985005> (cit. on p. 27).
- [84] Y Huang, M I Simon, and J Doyle. "Robust perfect adaptation in bacterial chemotaxis through integral feedback control." English. In: *Proceedings of the...* 2000, pp. 4649–4653. doi: [10.1073/pnas.97.9.4649](https://doi.org/10.1073/pnas.97.9.4649). URL: <http://www.pnas.org/cgi/doi/10.1073/pnas.97.9.4649> (cit. on p. 100).

- [85] J M Jeanne and Rachel I Wilson. "Convergence, divergence, and reconvergence in a feedforward network improves neural speed and accuracy." English. In: *Neuron* 88.5 (2015), pp. 1014–1026. DOI: [10.1016/j.neuron.2015.10.018](https://doi.org/10.1016/j.neuron.2015.10.018). URL: <http://linkinghub.elsevier.com/retrieve/pii/S0896627315008843> (cit. on p. 99).
- [86] B N Johnson, J D Mainland, and Noam Sobel. "Rapid olfactory processing implicates subcortical control of an olfactomotor system." In: *Journal of ...* (2003). DOI: [10.1152/jn.00115.2003](https://doi.org/10.1152/jn.00115.2003). URL: <http://jn.physiology.org/content/90/2/1084.short> (cit. on p. 29).
- [87] D Johnston, SMS Wu, and R Gray. *Foundations of cellular neurophysiology*. The MIT Press, 1995. URL: <http://tocs.ulb.tu-darmstadt.de/35650478.pdf> (cit. on p. 64).
- [88] Walton D Jones, Thuy-Ai T Nguyen, Brian Kloss, Kevin J Lee, and Leslie B Vosshall. "Functional conservation of an insect odorant receptor gene across 250 million years of evolution." English. In: *Current biology : CB* 15.4 (Feb. 2005), R119–R121. DOI: [10.1016/j.cub.2005.02.007](https://doi.org/10.1016/j.cub.2005.02.007). URL: <http://linkinghub.elsevier.com/retrieve/pii/S0960982205001466> (cit. on p. 104).
- [89] Kristine A Justus, John Murlis, Chris Jones, and Ring T Cardé. "Measurement of Odor-Plume Structure in a Wind Tunnel Using a Photoionization Detector and a Tracer Gas." English. In: *Environmental Fluid Mechanics* 2.1-2 (2002), pp. 115–142. DOI: [10.1023/A:1016227601019](https://doi.org/10.1023/A:1016227601019). URL: <http://link.springer.com/10.1023/A:1016227601019> (cit. on pp. 61, 123).
- [90] K E Kaissling. "Peripheral mechanisms of pheromone reception in moths." English. In: *Chemical Senses* 21.2 (Apr. 1996), pp. 257–268. URL: <http://eutils.ncbi.nlm.nih.gov/entrez/>

- [eutils/elink.fcgi?dbfrom=pubmed&id=8670704&retmode=ref&cmd=prlinks](http://eutils.ncbi.nlm.nih.gov/entrez/eutils/elink.fcgi?dbfrom=pubmed&id=8670704&retmode=ref&cmd=prlinks) (cit. on p. 6).
- [91] K E Kaissling. "Flux detectors versus concentration detectors: two types of chemoreceptors." English. In: *Chemical Senses* 23.1 (Feb. 1998), pp. 99–111. URL: <http://eutils.ncbi.nlm.nih.gov/entrez/eutils/elink.fcgi?dbfrom=pubmed&id=9530975&retmode=ref&cmd=prlinks> (cit. on p. 49).
- [92] K E Kaissling, C Zack Strausfeld, and E R Rumbo. "Adaptation Processes in Insect Olfactory Receptors." English. In: *Annals of the New York Academy of Sciences* 510.1 (Nov. 1987), pp. 104–112. DOI: [10.1111/j.1749-6632.1987.tb43475.x](https://doi.wiley.com/10.1111/j.1749-6632.1987.tb43475.x). URL: <http://doi.wiley.com/10.1111/j.1749-6632.1987.tb43475.x> (cit. on pp. 62, 89).
- [93] K Kaissling. "Chemo-electrical transduction in insect olfactory receptors." English. In: *Annual review of neuroscience* 9.1 (1986), pp. 121–145. DOI: [10.1146/annurev.ne.09.030186.001005](https://doi.org/10.1146/annurev.ne.09.030186.001005). URL: <http://www.annualreviews.org/doi/abs/10.1146/annurev.ne.09.030186.001005> (cit. on p. 64).
- [94] Tiffany Kee, Pavel Sanda, Nitin Gupta, Mark Stopfer, and Maxim Bazhenov. "Feed-Forward versus Feedback Inhibition in a Basic Olfactory Circuit." English. In: *PLoS Computational Biology* 11.10 (Oct. 2015), e1004531. DOI: [10.1371/journal.pcbi.1004531](https://doi.org/10.1371/journal.pcbi.1004531). URL: <http://dx.plos.org/10.1371/journal.pcbi.1004531> (cit. on p. 96).
- [95] A J Kim, A A Lazar, and Y B Slutskiy. "Projection neurons in Drosophila antennal lobes signal the acceleration of odor concentrations." In: *eLife* (2015). DOI: [10.7554/eLife.06651](https://doi.org/10.7554/eLife.06651).001. URL: <http://elifesciences.org/content/early/2015/05/14/eLife.06651.abstract> (cit. on pp. 27, 36, 37, 45, 49, 62).

- [96] Anmo J Kim, Aurel A Lazar, and Yevgeniy B Slutskiy. "System identification of *Drosophila* olfactory sensory neurons." English. In: *Journal of Computational Neuroscience* 30.1 (Aug. 2010), pp. 143–161. DOI: [10.1007/s10827-010-0265-0](https://doi.org/10.1007/s10827-010-0265-0). URL: <http://www.springerlink.com/index/10.1007/s10827-010-0265-0> (cit. on pp. 14, 23, 25, 27, 36, 37, 45, 49, 71, 102, 135).
- [97] Kerry J Kim and Fred Rieke. "Temporal contrast adaptation in the input and output signals of salamander retinal ganglion cells." In: *The Journal of neuroscience : the official journal of the Society for Neuroscience* 21.1 (2001), pp. 287–299. URL: <http://www.jneurosci.org/content/21/1/287.short> (cit. on pp. 67, 99).
- [98] Nathan C Klapoetke et al. "Independent optical excitation of distinct neural populations." In: *Nature methods* 11.3 (Feb. 2014), pp. 338–346. DOI: [10.1038/nmeth.2836](https://doi.org/10.1038/nmeth.2836). URL: <http://www.nature.com/doifinder/10.1038/nmeth.2836> (cit. on p. 84).
- [99] A Koulakov, A Gelperin, and D Rinberg. "Olfactory Coding With All-or-Nothing Glomeruli." English. In: *Journal of Neurophysiology* 98.6 (Oct. 2007), pp. 3134–3142. DOI: [10.1152/jn.00560.2007](https://doi.org/10.1152/jn.00560.2007). URL: <http://jn.physiology.org/cgi/doi/10.1152/jn.00560.2007> (cit. on p. 96).
- [100] Scott A Kreher, Jae Young Kwon, and John R Carlson. "The Molecular Basis of Odor Coding in the *Drosophila* Larva." English. In: *Neuron* 46.3 (May 2005), pp. 445–456. URL: <http://linkinghub.elsevier.com/retrieve/pii/S089662730500320X> (cit. on pp. 13, 24, 135).
- [101] Parthasarathy Krishnan, Brian J Duistermars, and Mark A Frye. "Odor identity influences tracking of temporally patterned plumes in *Drosophila*." English. In: *BMC Neuroscience* 12.1 (2011), p. 62.

- DOI: [10.1186/1471-2202-12-62](https://doi.org/10.1186/1471-2202-12-62). URL: <http://www.biomedcentral.com/1471-2202/12/62> (cit. on pp. 8, 117, 130).
- [102] Mattias C Larsson, Ana I Domingos, Walton D Jones, M Eugenia Chiappe, Hubert Amrein, and Leslie B Vosshall. “Or83b Encodes a Broadly Expressed Odorant Receptor Essential for Drosophila Olfaction.” English. In: *Cell* 43.5 (Sept. 2004), pp. 703–714. DOI: [10.1016/j.neuron.2004.08.019](https://doi.org/10.1016/j.neuron.2004.08.019). URL: <http://linkinghub.elsevier.com/retrieve/pii/S0896627304005264> (cit. on pp. 10, 26).
- [103] N K Larter, J S Sun, and John R Carlson. “Organization and function of Drosophila odorant binding proteins.” In: *eLife* (2016). DOI: [10.7554/eLife.20242.001](https://doi.org/10.7554/eLife.20242.001). URL: <https://elifesciences.org/content/5/e20242v2> (cit. on pp. 23, 29, 40).
- [104] S Laughlin. “A simple coding procedure enhances a neuron’s information capacity.” In: *Zeitschrift für Naturforschung c* (1981). URL: <http://www.degruyter.com/view/j/znc.1981.36.issue-9-10/znc-1981-9-1040/znc-1981-9-1040.xml> (cit. on pp. 78, 99).
- [105] Simon B Laughlin and Roger C Hardie. “Common strategies for light adaptation in the peripheral visual systems of fly and dragonfly.” English. In: *Journal of Comparative Physiology A: Neuroethology, Sensory, Neural, and Behavioral Physiology* 128.4 (1978), pp. 319–340. DOI: [10.1007/BF00657606](https://doi.org/10.1007/BF00657606). URL: <http://link.springer.com/article/10.1007/BF00657606> (cit. on p. 98).
- [106] F O Lehmann and M H Dickinson. “The changes in power requirements and muscle efficiency during elevated force production in the fruit fly *Drosophila melanogaster*.” In: *The Journal of experimental biology* (1997). URL: <http://jeb.biologists.org/content/200/7/1133.short> (cit. on p. 117).

- [107] Nicholas A Lesica, Jianzhong Jin, Chong Weng, Chun-I Yeh, Daniel A Butts, Garrett B Stanley, and Jose-Manuel Alonso. “Adaptation to Stimulus Contrast and Correlations during Natural Visual Stimulation.” English. In: *Neuron* 55.3 (Aug. 2007), pp. 479–491. DOI: [10.1016/j.neuron.2007.07.013](https://doi.org/10.1016/j.neuron.2007.07.013). URL: <http://linkinghub.elsevier.com/retrieve/pii/S089662730700534X> (cit. on p. 99).
- [108] Matthieu Louis, Thomas Huber, Richard Benton, Thomas P Sakmar, and Leslie B Vosshall. “Bilateral olfactory sensory input enhances chemotaxis behavior.” English. In: *Nature neuroscience* 11.2 (Feb. 2008), pp. 187–199. DOI: [10.1038/nn2031](https://doi.org/10.1038/nn2031). URL: <http://eutils.ncbi.nlm.nih.gov/entrez/eutils/elink.fcgi?dbfrom=pubmed&id=18157126&retmode=ref&cmd=prlinks> (cit. on p. 27).
- [109] Brian N Lundstrom, Matthew H Higgs, William J Spain, and Adrienne L Fairhall. “Fractional differentiation by neocortical pyramidal neurons.” English. In: *Nature neuroscience* 11.11 (Oct. 2008), pp. 1335–1342. DOI: [10.1038/nn.2212](https://doi.org/10.1038/nn.2212). URL: <http://www.nature.com/doifinder/10.1038/nn.2212> (cit. on p. 102).
- [110] Sean X Luo, Richard Axel, and Larry Abbott. “Generating sparse and selective third-order responses in the olfactory system of the fly.” English. In: *Proceedings of the National Academy of...* 107.23 (June 2010), pp. 10713–10718. DOI: [10.1073/pnas.1005635107](https://doi.org/10.1073/pnas.1005635107). URL: <http://www.pnas.org/content/107/23/10713.full> (cit. on p. 62).
- [111] Gaby Maimon, Andrew D Straw, and Michael H Dickinson. “Active flight increases the gain of visual motion processing in *Drosophila*.” English. In: *Nature Neuroscience* 13.3 (Mar. 2010), pp. 393–399. DOI: [10.1038/nn.2492](https://doi.org/10.1038/nn.2492). URL: <http://eutils.ncbi.nlm.nih.gov/entrez/eutils/elink.fcgi?dbfrom=pubmed&id=20130000&retmode=ref&cmd=prlinks> (cit. on p. 102).

- [nlm.nih.gov/entrez/eutils/elink.fcgi?dbfrom=pubmed&id=20154683&retmode=ref&cmd=prlinks](http://www.ncbi.nlm.nih.gov/entrez/eutils/elink.fcgi?dbfrom=pubmed&id=20154683&retmode=ref&cmd=prlinks) (cit. on p. 130).
- [112] Akira Mamiya, Andrew D Straw, Egill Tómasson, and Michael H Dickinson. "Active and Passive Antennal Movements during Visually Guided Steering in Flying *Drosophila*." English. In: *The Journal of ...* 31.18 (2011), pp. 6900–6914. DOI: [10.1523/JNEUROSCI.0498-11.2011](https://doi.org/10.1523/JNEUROSCI.0498-11.2011). URL: <http://www.jneurosci.org/cgi/doi/10.1523/JNEUROSCI.0498-11.2011> (cit. on p. 6).
- [113] Carlotta Martelli, John R Carlson, and Thierry Emonet. "Intensity invariant dynamics and odor-specific latencies in olfactory receptor neuron response." English. In: *Journal of Neuroscience* 33.15 (Apr. 2013), pp. 6285–6297. DOI: [10.1523/JNEUROSCI.0426-12.2013](https://doi.org/10.1523/JNEUROSCI.0426-12.2013). URL: <http://eutils.ncbi.nlm.nih.gov/entrez/eutils/elink.fcgi?dbfrom=pubmed&id=23575828&retmode=ref&cmd=prlinks> (cit. on pp. xiv, 4, 13, 15, 17, 19, 21, 26, 27, 30, 35, 36, 40, 43, 45, 62, 64, 71, 73, 89, 93, 98, 102–105, 117, 127, 135).
- [114] Dennis Mathew, Carlotta Martelli, Elizabeth Kelley-Swift, Christopher Brusalis, Marc Gershow, Aravinthan D T Samuel, Thierry Emonet, and John R Carlson. "Functional diversity among sensory receptors in a *Drosophila* olfactory circuit." English. In: *Proceedings of the National Academy of ...* 110.23 (Apr. 2013), E2134–43. DOI: [10.1073/pnas.1306976110](https://doi.org/10.1073/pnas.1306976110). URL: <http://eutils.ncbi.nlm.nih.gov/entrez/eutils/elink.fcgi?dbfrom=pubmed&id=23690583&retmode=ref&cmd=prlinks> (cit. on pp. 24, 104).
- [115] C Missbach, HKM Dweck, H Vogel, and A Vilcinskas. "Evolution of insect olfactory receptors." In: *eLife* (2014). DOI: [10.7554/eLife.02115.001](https://doi.org/10.7554/eLife.02115.001). URL: <http://elifesciences.org/content/3/e02115.abstract> (cit. on p. 104).

- [116] Shelby A Montague, Dennis Mathew, and John R Carlson. “Similar odorants elicit different behavioral and physiological responses, some supersustained.” English. In: *Journal of Neuroscience* 31.21 (May 2011), pp. 7891–7899. DOI: [10.1523/JNEUROSCI.6254-10.2011](https://doi.org/10.1523/JNEUROSCI.6254-10.2011). URL: <http://eutils.ncbi.nlm.nih.gov/entrez/eutils/elink.fcgi?dbfrom=pubmed&id=21613503&retmode=ref&cmd=prlinks> (cit. on p. 23).
- [117] F T Muijres, M J Elzinga, J M Melis, and M H Dickinson. “Flies Evade Looming Targets by Executing Rapid Visually Directed Banked Turns.” English. In: *Science* 344.6180 (Apr. 2014), pp. 172–177. DOI: [10.1126/science.1248955](https://doi.org/10.1126/science.1248955). URL: <http://www.sciencemag.org/cgi/doi/10.1126/science.1248955> (cit. on p. 130).
- [118] F T Muijres, M J Elzinga, N A Iwasaki, and M H Dickinson. “Body saccades of Drosophila consist of stereotyped banked turns.” English. In: *The Journal of experimental biology* 218.6 (Mar. 2015), pp. 864–875. DOI: [10.1242/jeb.114280](https://doi.org/10.1242/jeb.114280). URL: <http://jeb.biologists.org/cgi/doi/10.1242/jeb.114280> (cit. on p. 130).
- [119] J Murlis, Joseph S Elkinton, and Ring T Cardé. “Odor plumes and how insects use them.” In: *Annual Review of Entomology* 37.1 (1992), pp. 505–532. DOI: [10.1146/annurev.en.37.010192.002445](https://doi.org/10.1146/annurev.en.37.010192.002445). URL: <http://www.annualreviews.org/doi/abs/10.1146/annurev.en.37.010192.002445> (cit. on pp. 2, 5, 7, 61, 103, 104, 123).
- [120] J Murlis and C D Jones. “Fine-scale structure of odour plumes in relation to insect orientation to distant pheromone and other attractant sources.” English. In: *Physiological entomology* 6.1 (Mar. 1981), pp. 71–86. DOI: [10.1111/j.1365-3032.1981.tb00262.x](https://doi.org/10.1111/j.1365-3032.1981.tb00262.x).

- URL: <http://doi.wiley.com/10.1111/j.1365-3032.1981.tb00262.x> (cit. on p. 123).
- [121] John Murlis, Mark A Willis, and Ring T Cardé. "Spatial and temporal structures of pheromone plumes in fields and forests." English. In: *Physiological entomology* 25.3 (Sept. 2000), pp. 211–222. DOI: [10.1046/j.1365-3032.2000.00176.x](https://doi.org/10.1046/j.1365-3032.2000.00176.x). URL: <http://onlinelibrary.wiley.com/doi/10.1046/j.1365-3032.2000.00176.x/full> (cit. on pp. 7, 61, 123).
- [122] K I Nagel and A J Doupe. "Temporal processing and adaptation in the songbird auditory forebrain." In: *Neuron* (2006). DOI: [10.1016/j.neuron.2006.08.030](https://doi.org/10.1016/j.neuron.2006.08.030). URL: <http://www.sciencedirect.com/science/article/pii/S0896627306006775> (cit. on pp. 87, 99, 101).
- [123] K I Nagel and Rachel I Wilson. "Mechanisms underlying population response dynamics in inhibitory interneurons of the Drosophila antennal lobe." English. In: *The Journal of Neuroscience* 36.15 (2016), pp. 4325–4338. DOI: [10.1523/JNEUROSCI.3887-15.2016](https://doi.org/10.1523/JNEUROSCI.3887-15.2016). URL: <http://www.jneurosci.org/cgi/doi/10.1523/JNEUROSCI.3887-15.2016> (cit. on p. 61).
- [124] Katherine I Nagel, Elizabeth J Hong, and Rachel I Wilson. "Synaptic and circuit mechanisms promoting broadband transmission of olfactory stimulus dynamics." English. In: *Nature neuroscience* (Dec. 2014). DOI: [10.1038/nn.3895](https://doi.org/10.1038/nn.3895). URL: <http://www.nature.com/doifinder/10.1038/nn.3895> (cit. on pp. 62, 103).
- [125] Katherine I Nagel and Rachel I Wilson. "Biophysical mechanisms underlying olfactory receptor neuron dynamics." In: *Nature Neuroscience* 14.2 (Jan. 2011), pp. 208–216. DOI: [10.1038/nn.2725](https://doi.org/10.1038/nn.2725). URL: <http://www.nature.com/doifinder/10.1038/nn.2725>

- nn . 2725 (cit. on pp. 4, 13–16, 19, 23, 25, 26, 36, 43, 61, 62, 64, 71, 73, 81, 83, 89, 99–103, 116, 135).
- [126] Sergei S Nikonov, Roman Kholodenko, Janis Lem, and Edward N Pugh. “Physiological features of the S- and M-cone photoreceptors of wild-type mice from single-cell recordings.” English. In: *The Journal of general physiology* 127.4 (Apr. 2006), pp. 359–374. DOI: [10.1085/jgp.200609490](https://doi.org/10.1085/jgp.200609490). URL: <http://jgp.rupress.org/content/127/4/359.full> (cit. on p. 98).
- [127] Shawn R Olsen, Vikas Bhandawat, and Rachel I Wilson. “Excitatory interactions between olfactory processing channels in the *Drosophila* antennal lobe.” English. In: *Neuron* 54.1 (Apr. 2007), pp. 89–103. DOI: [10.1016/j.neuron.2007.03.010](https://doi.org/10.1016/j.neuron.2007.03.010). URL: <http://linkinghub.elsevier.com/retrieve/pii/S0896627307002061> (cit. on p. 12).
- [128] Shawn R Olsen, Vikas Bhandawat, and Rachel I Wilson. “Divisive normalization in olfactory population codes.” English. In: *Neuron* 66.2 (Apr. 2010), pp. 287–299. DOI: [10.1016/j.neuron.2010.04.009](https://doi.org/10.1016/j.neuron.2010.04.009). URL: <http://eutils.ncbi.nlm.nih.gov/entrez/eutils/elink.fcgi?dbfrom=pubmed&id=20435004&retmode=ref&cmd=prlinks> (cit. on pp. 62, 98).
- [129] Shawn R Olsen and Rachel I Wilson. “Lateral presynaptic inhibition mediates gain control in an olfactory circuit.” In: *Nature* 452.7190 (Mar. 2008), pp. 956–960. DOI: [10.1038/nature06864](https://doi.org/10.1038/nature06864). URL: <http://www.nature.com/doifinder/10.1038/nature06864> (cit. on p. 62).
- [130] Shannon B Olsson, Charles E Linn, Andrew Michel, Hattie R Dambroski, Stewart H Berlocher, Jeffrey L Feder, and Wendell L Roelofs. “Receptor expression and sympatric speciation: unique olfactory receptor neuron responses in F₁ hybrid *Rhagoletis* populations.” English. In: *The Journal of experimen-*

- tal biology* 209.Pt 19 (Oct. 2006), pp. 3729–3741. DOI: [10.1242/jeb.02444](#). URL: <http://jeb.biologists.org/content/209/19/3729.full> (cit. on p. 105).
- [131] Shannon B Olsson, Merid N Getahun, Dieter Wicher, and Bill S Hansson. “Piezo controlled microinjection: An in vivo complement for in vitro sensory studies in insects.” English. In: *Journal of neuroscience methods* 201.2 (Oct. 2011), pp. 385–389. DOI: [10.1016/j.jneumeth.2011.08.015](#). URL: <http://dx.doi.org/10.1016/j.jneumeth.2011.08.015> (cit. on pp. 23, 36, 37).
- [132] Richard Payne and Jonathon Howard. “Response of an insect photoreceptor: a simple log-normal model.” In: *Nature* 290.5805 (Apr. 1981), pp. 415–416. DOI: [10.1038/290415a0](#). URL: <http://www.nature.com/doifinder/10.1038/290415a0> (cit. on p. 101).
- [133] J A Peacock. “Two-dimensional goodness-of-fit testing in astronomy.” In: *Monthly Notices of the Royal Astronomical ...* (1983). URL: <http://mnras.oxfordjournals.org/content/202/3/615.short> (cit. on p. 109).
- [134] Yu Tong Qiu, Joop J A van Loon, Willem Takken, Jocelijn Meijerink, and Hans M Smid. “Olfactory Coding in Antennal Neurons of the Malaria Mosquito, *Anopheles gambiae*.” English. In: *Chemical Senses* 31.9 (Nov. 2006), pp. 845–863. DOI: [10.1093/chemse/bjl027](#). URL: <http://eutils.ncbi.nlm.nih.gov/entrez/eutils/elink.fcgi?dbfrom=pubmed&id=16963500&retmode=ref&cmd=prlinks> (cit. on p. 2).
- [135] Davide Raccuglia, Li Yan McCurdy, Mahmut Demir, Srinivas Gorur-Shandilya, Michael Kunst, Thierry Emonet, and Michael N Nitabach. “Presynaptic GABA receptors mediate temporal contrast enhancement in *Drosophila* olfactory sensory neurons and modulate odor-driven behavioral kinetics.” English.

- In: *eNeuro* 3.4 (July 2016), ENEURO.0080-16.2016. doi: [10.1523/ENEURO.0080-16.2016](https://doi.org/10.1523/ENEURO.0080-16.2016). URL: <http://eneuro.sfn.org/cgi/doi/10.1523/ENEURO.0080-16.2016> (cit. on pp. 62, 103).
- [136] Michelle R Rebello, Thomas S McTavish, David C Willhite, Shaina M Short, Gordon M Shepherd, and Justus V Verhagen. "Perception of Odors Linked to Precise Timing in the Olfactory System." English. In: *PLoS Biology* 12.12 (Dec. 2014), e1002021–10. doi: [10.1371/journal.pbio.1002021](https://doi.org/10.1371/journal.pbio.1002021). URL: <http://dx.plos.org/10.1371/journal.pbio.1002021> (cit. on p. 103).
- [137] Michael B Reiser and Michael H Dickinson. "Visual motion speed determines a behavioral switch from forward flight to expansion avoidance in *Drosophila*." English. In: *Journal of Experimental ...* 216.Pt 4 (Feb. 2013), pp. 719–732. doi: [10.1242/jeb.074732](https://doi.org/10.1242/jeb.074732). URL: <http://eutils.ncbi.nlm.nih.gov/entrez/eutils/elink.fcgi?dbfrom=pubmed&id=23197097&retmode=ref&cmd=prlinks> (cit. on p. 130).
- [138] Johannes Reisert and H R Matthews. "Adaptation of the odour-induced response in frog olfactory receptor cells." English. In: *The Journal of Physiology* 519.3 (Sept. 1999), pp. 801–813. doi: [10.1111/j.1469-7793.1999.0801n.x](https://doi.org/10.1111/j.1469-7793.1999.0801n.x). URL: <http://onlinelibrary.wiley.com/doi/10.1111/j.1469-7793.1999.0801n.x/full> (cit. on p. 101).
- [139] Arbora Resulaj and Dmitry Rinberg. "Novel Behavioral Paradigm Reveals Lower Temporal Limits on Mouse Olfactory Decisions." English. In: *Journal of Neuroscience* 35.33 (Aug. 2015), pp. 11667–11673. doi: [10.1523/JNEUROSCI.4693-14.2015](https://doi.org/10.1523/JNEUROSCI.4693-14.2015). URL: <http://www.jneurosci.org/cgi/doi/10.1523/JNEUROSCI.4693-14.2015> (cit. on pp. 11, 23).

- [140] F Rieke. "Temporal contrast adaptation in salamander bipolar cells." In: *The Journal of Neuroscience* (2001). URL: <http://www.jneurosci.org/content/21/23/9445.short> (cit. on pp. 73, 78, 87, 99, 102).
- [141] R R Riesz. "Differential Intensity Sensitivity of the Ear for Pure Tones." English. In: *Physical Review* 31.5 (May 1928), pp. 867–875. DOI: [10.1103/PhysRev.31.867](https://doi.org/10.1103/PhysRev.31.867). URL: <http://link.aps.org/doi/10.1103/PhysRev.31.867> (cit. on p. 98).
- [142] Jeffrey A Riffell, Leif Abrell, and John G Hildebrand. "Physical processes and real-time chemical measurement of the insect olfactory environment." English. In: *Journal of chemical ecology* 34.7 (July 2008), pp. 837–853. DOI: [10.1007/s10886-008-9490-7](https://doi.org/10.1007/s10886-008-9490-7). URL: <http://link.springer.com/article/10.1007/s10886-008-9490-7/fulltext.html> (cit. on pp. 2, 4–6, 61).
- [143] Jeffrey A Riffell and J G Hildebrand. "Adaptive Processing in the Insect Olfactory System." In: *The Ecology of Animal Senses* (2016). DOI: [10.1007/978-3-319-25492-0_1](https://doi.org/10.1007/978-3-319-25492-0_1). URL: http://link.springer.com/chapter/10.1007/978-3-319-25492-0_1 (cit. on p. 2).
- [144] Jeffrey A Riffell, Hong Lei, Thomas A Christensen, and John G Hildebrand. "Characterization and Coding of Behaviorally Significant Odor Mixtures." English. In: *Current biology : CB* 19.4 (Feb. 2009), pp. 335–340. DOI: [10.1016/j.cub.2009.01.041](https://doi.org/10.1016/j.cub.2009.01.041). URL: <http://dx.doi.org/10.1016/j.cub.2009.01.041> (cit. on p. 8).
- [145] D L Ringach and B J Malone. "The Operating Point of the Cortex: Neurons as Large Deviation Detectors." English. In: *The Journal of neuroscience : the official journal of the Society for Neuroscience* 27.29 (July 2007), pp. 7673–7683. DOI: [10.1523/JNEUROSCI.4407-06.2007](https://doi.org/10.1523/JNEUROSCI.4407-06.2007)

- JNEUROSCI. 1048 - 07. 2007. URL: <http://www.jneurosci.org/cgi/doi/10.1523/JNEUROSCI.1048-07.2007> (cit. on p. 99).
- [146] Angela Rouyar, Virginie Party, Janez Prešern, Andrej Blejec, and Michel Renou. "A General Odorant Background Affects the Coding of Pheromone Stimulus Intermittency in Specialist Olfactory Receptor Neurones." English. In: *PloS one* 6.10 (Oct. 2011), e26443–13. DOI: [10.1371/journal.pone.0026443](https://doi.org/10.1371/journal.pone.0026443). URL: <http://dx.plos.org/10.1371/journal.pone.0026443> (cit. on p. 36).
- [147] Pavel Sanda, Tiffany Kee, Nitin Gupta, Mark Stopfer, and Maxim Bazhenov. "Classification of odorants across layers in locust olfactory pathway." English. In: *Journal of Neurophysiology* 115.5 (May 2016), pp. 2303–2316. DOI: [10.1152/jn.00921.2015](https://doi.org/10.1152/jn.00921.2015). URL: <http://jn.physiology.org/lookup/doi/10.1152/jn.00921.2015> (cit. on p. 96).
- [148] R Satoh, M Oizumi, H Kazama, and M Okada. "Mechanisms of maximum information preservation in the Drosophila antennal lobe." In: *PloS one* (2010). URL: <http://dx.plos.org/10.1371/journal.pone.0010644.g013> (cit. on p. 96).
- [149] J Schuckel, P H Torkkeli, and A S French. "Two Interacting Olfactory Transduction Mechanisms Have Linked Polarities and Dynamics in *Drosophila melanogaster* Antennal Basiconic Sensilla Neurons." English. In: *Journal of Neurophysiology* 102.1 (June 2009), pp. 214–223. DOI: [10.1152/jn.00162.2009](https://doi.org/10.1152/jn.00162.2009). URL: <http://jn.physiology.org/cgi/doi/10.1152/jn.00162.2009> (cit. on p. 23).
- [150] Julia Schuckel and Andrew S French. "A digital sequence method of dynamic olfactory characterization." English. In: *Journal of neuroscience methods* 171.1 (June 2008), pp. 98–103. DOI: [10.1016/j.jneumeth.2008.02.013](https://doi.org/10.1016/j.jneumeth.2008.02.013). URL: <http://linkinghub>.

elsevier.com/retrieve/pii/S0165027008001234 (cit. on pp. 23, 26, 43).

- [151] Julia Schuckel, Shannon Meisner, Päivi H Torkkeli, and Andrew S French. "Dynamic properties of Drosophila olfactory electroantennograms." English. In: *Journal of Comparative Physiology A: Neuroethology, Sensory, Neural, and Behavioral Physiology* 194.5 (Mar. 2008), pp. 483–489. DOI: [10.1007/s00359-008-0322-6](https://doi.org/10.1007/s00359-008-0322-6). URL: <http://link.springer.com/10.1007/s00359-008-0322-6> (cit. on pp. 23, 43).
- [152] A Schulze, A Gomez-Marin, V G Rajendran, G Lott, Matthieu Louis, Vivek Jayaraman, and S druckman. "Dynamical feature extraction at the sensory periphery guides chemotaxis." In: *eLife* (2015). DOI: [10.7554/eLife.06694.001](https://doi.org/10.7554/eLife.06694.001). URL: <https://elifesciences.org/content/4/e06694v1> (cit. on pp. 16, 27, 49, 100, 101, 104).
- [153] H S Seung. "Amplification, attenuation, and integration." In: *The handbook of brain theory and neural networks* (2003). URL: <http://gliamac.mit.edu/people/seung/papers/hbtnn.pdf> (cit. on pp. 16, 101).
- [154] S R Shanbhag, B Müller, and R A Steinbrecht. "Atlas of olfactory organs of Drosophila melanogaster: 1. Types, external organization, innervation and distribution of olfactory sensilla." In: *International Journal of Insect Morphology and Embryology* 28.4 (1999), pp. 377–397. URL: <http://www.sciencedirect.com/science/article/pii/S0020732299000392> (cit. on pp. 9, 135).
- [155] S R Shanbhag, B Müller, and R A Steinbrecht. "Atlas of olfactory organs of Drosophila melanogaster." English. In: *Arthropod Structure & Development* 29.3 (July 2000), pp. 211–229. DOI: [10.1016/S1467-8039\(00\)00028-1](https://doi.org/10.1016/S1467-8039(00)00028-1). URL: <http://linkinghub>.

- elsevier.com/retrieve/pii/S1467803900000281 (cit. on pp. 9, 135).
- [156] Alana Sherman and Michael H Dickinson. "A comparison of visual and haltere-mediated equilibrium reflexes in the fruit fly *Drosophila melanogaster*." In: *The Journal of experimental biology* 206.2 (2003), pp. 295–302. URL: <http://jeb.biologists.org/content/206/2/295.short> (cit. on pp. 117, 130).
- [157] Thomas S Shimizu, Yuhai Tu, and Howard C Berg. "A modular gradient-sensing network for chemotaxis in *Escherichia coli* revealed by responses to time-varying stimuli." In: *Molecular Systems Biology* 6 (June 2010), pp. 1–14. DOI: [10.1038/msb.2010.37](https://doi.org/10.1038/msb.2010.37). URL: <http://dx.doi.org/10.1038/msb.2010.37> (cit. on pp. 92, 93).
- [158] Roman Shusterman, Matthew C Smear, Alexei A Koulakov, and Dmitry Rinberg. "Precise olfactory responses tile the sniff cycle." In: *Nature neuroscience* 14.8 (July 2011), pp. 1039–1044. DOI: [10.1038/nn.2877](https://doi.org/10.1038/nn.2877). URL: <http://www.nature.com/doifinder/10.1038/nn.2877> (cit. on pp. 11, 23, 103).
- [159] M M Skanata, N M Bernat, M Kaplow, and Marc Gershon. "Computations underlying *Drosophila* photo-taxis, odor-taxis, and multi-sensory integration." In: *eLife* (2015). DOI: [10.7554/eLife.06229.001](https://doi.org/10.7554/eLife.06229.001). URL: <http://elifesciences.org/content/early/2015/05/06/eLife.06229.abstract> (cit. on p. 104).
- [160] Monica Skoge, Sahin Naqvi, Yigal Meir, and Ned S Wingreen. "Chemical Sensing by Nonequilibrium Cooperative Receptors." English. In: *Physical Review Letters* 110.24 (June 2013), pp. 248102–5. DOI: [10.1103/PhysRevLett.110.248102](https://doi.org/10.1103/PhysRevLett.110.248102). URL: <http://link.aps.org/doi/10.1103/PhysRevLett.110.248102> (cit. on p. 113).

- [161] Matthew Smear, Roman Shusterman, Rodney O'Connor, Thomas Bozza, and Dmitry Rinberg. "Perception of sniff phase in mouse olfaction." In: *Nature* 479.7373 (Nov. 2011), pp. 397–400. DOI: [10.1038/nature10521](https://doi.org/10.1038/nature10521). URL: <http://dx.doi.org/10.1038/nature10521> (cit. on pp. 11, 103).
- [162] Matthew Smear, Admir Resulaj, Jingji Zhang, Thomas Bozza, and Dmitry Rinberg. "Multiple perceptible signals from a single olfactory glomerulus." In: *Nature Neuroscience* 16.11 (Sept. 2013), pp. 1687–1691. DOI: [10.1038/nn.3519](https://doi.org/10.1038/nn.3519). URL: <http://www.nature.com/doifinder/10.1038/nn.3519> (cit. on p. 103).
- [163] E Song, Benjamin L de Bivort, C Dan, and S Kunes. "Determinants of the Drosophila odorant receptor pattern." English. In: *Developmental cell* 22.2 (2012), pp. 363–376. DOI: [10.1016/j.devcel.2011.12.015](https://doi.org/10.1016/j.devcel.2011.12.015). URL: <http://linkinghub.elsevier.com/retrieve/pii/S1534580711005818> (cit. on p. 105).
- [164] Charles F Stevens. "A statistical property of fly odor responses is conserved across odors." English. In: *Proceedings of the National Academy of ...* 113.24 (June 2016), pp. 6737–6742. DOI: [10.1073/pnas.1606339113](https://doi.org/10.1073/pnas.1606339113). URL: <http://www.pnas.org/lookup/doi/10.1073/pnas.1606339113> (cit. on p. 96).
- [165] S S Stevens. "On the psychophysical law." English. In: *Psychological review* 64.3 (May 1957), pp. 153–181. DOI: [10.1037/h0046162](https://doi.org/10.1037/h0046162). URL: <http://psycnet.apa.org/journals/rev/64/3/153.html> (cit. on pp. 73, 75).
- [166] K F Störtkuhl, B T Hovemann, and John R Carlson. "Olfactory adaptation depends on the Trp Ca₂₊ channel in Drosophila." English. In: *Journal of Neuroscience* 19.12 (June 1999), pp. 4839–4846. URL: <http://www.jneurosci.org/content/19/12/4839.full> (cit. on p. 100).

- [167] Chih-Ying Su, Karen Menuz, and John R Carlson. "Olfactory perception: receptors, cells, and circuits." English. In: *Cell* 139.1 (Oct. 2009), pp. 45–59. DOI: [10.1016/j.cell.2009.09.015](https://doi.org/10.1016/j.cell.2009.09.015). URL: <http://eutils.ncbi.nlm.nih.gov/entrez/eutils/elink.fcgi?dbfrom=pubmed&id=19804753&retmode=ref&cmd=prlinks> (cit. on p. 10).
- [168] Chih-Ying Su, Carlotta Martelli, Thierry Emonet, and John R Carlson. "Temporal coding of odor mixtures in an olfactory receptor neuron." English. In: *Proceedings of the National Academy of ...* 108.12 (Mar. 2011), pp. 5075–5080. DOI: [10.1073/pnas.1100369108](https://doi.org/10.1073/pnas.1100369108). URL: <http://eutils.ncbi.nlm.nih.gov/entrez/eutils/elink.fcgi?dbfrom=pubmed&id=21383179&retmode=ref&cmd=prlinks> (cit. on p. 40).
- [169] Chih-Ying Su, Karen Menuz, Johannes Reisert, and John R Carlson. "Non-synaptic inhibition between grouped neurons in an olfactory circuit." English. In: *Nature* 492.7427 (Nov. 2012), pp. 66–71. DOI: [10.1038/nature11712](https://doi.org/10.1038/nature11712). URL: <http://www.nature.com/doifinder/10.1038/nature11712> (cit. on p. 64).
- [170] Paul Szymszka, Richard C Gerkin, C Giovanni Galizia, and Brian H Smith. "High-speed odor transduction and pulse tracking by insect olfactory receptor neurons." English. In: *Proceedings of the National Academy of ...* (Nov. 2014), p. 201412051. DOI: [10.1073/pnas.1412051111](https://doi.org/10.1073/pnas.1412051111). URL: <http://www.pnas.org/cgi/doi/10.1073/pnas.1412051111> (cit. on pp. 13, 23, 27, 62).
- [171] W Takken and B G Knols. "Odor-mediated behavior of Afrotrropical malaria mosquitoes." English. In: *Annual Review of Entomology* 44 (1999), pp. 131–157. DOI: [10.1146/annurev.ento.44.1.131](https://doi.org/10.1146/annurev.ento.44.1.131). URL: <http://eutils.ncbi.nlm.nih.gov/entrez/eutils/elink.fcgi?dbfrom=pubmed&id=9990718&retmode=ref&cmd=prlinks> (cit. on pp. 2, 6).

- [172] Lance F Tammero and Michael H Dickinson. "The influence of visual landscape on the free flight behavior of the fruit fly *Drosophila melanogaster*." English. In: *The Journal of experimental biology* 205.Pt 3 (Feb. 2002), pp. 327–343. URL: <http://eutils.ncbi.nlm.nih.gov/entrez/eutils/elink.fcgi?dbfrom=pubmed&id=11854370&retmode=ref&cmd=prlinks> (cit. on pp. 7, 103, 123, 130).
- [173] Gašper Tkačik, Anandamohan Ghosh, Elad Schneidman, and Ronen Segev. "Adaptation to Changes in Higher-Order Stimulus Statistics in the Salamander Retina." English. In: *PloS one* 9.1 (Jan. 2014), e85841. DOI: [10.1371/journal.pone.0085841](https://doi.org/10.1371/journal.pone.0085841). URL: <http://dx.plos.org/10.1371/journal.pone.0085841> (cit. on p. 99).
- [174] Massimo Vergassola, Emmanuel Villermaux, and Boris I Shraiman. "'Infotaxis' as a strategy for searching without gradients." In: *Nature* 445.7126 (Jan. 2007), pp. 406–409. DOI: [10.1038/nature05464](https://doi.org/10.1038/nature05464). URL: <http://www.nature.com/doifinder/10.1038/nature05464> (cit. on p. 61).
- [175] Niels O Verhulst, Phoebe A Mbadi, Gabriella Bukovinszkiné Kiss, Wolfgang R Mukabana, Joop J A van Loon, Willem Takken, and Renate C Smallegange. "Improvement of a synthetic lure for *Anopheles gambiae* using compounds produced by human skin microbiota." English. In: *Malaria Journal* 10.1 (Feb. 2011), p. 28. DOI: [10.1186/1475-2875-10-28](https://doi.org/10.1186/1475-2875-10-28). URL: <http://www.malariajournal.com/content/10/1/28> (cit. on p. 2).
- [176] Neil J Vickers, Thomas A Christensen, Thomas C Baker, and John G Hildebrand. "Odour-plume dynamics influence the brain's olfactory code : Abstract : Nature." In: *Nature* 410.6827 (Mar. 2001), pp. 466–470. DOI: [10.1038/35068559](https://doi.org/10.1038/35068559). URL: <http://www.nature.com/doifinder/10.1038/35068559>

- //www.nature.com/doifinder/10.1038/35068559 (cit. on p. 8).
- [177] L B Vosshall. "Olfaction in drosophila." English. In: *Current opinion in neurobiology* 10.4 (2000), pp. 498–503. DOI: 10.1016/S0959-4388(00)00111-2. URL: <http://linkinghub.elsevier.com/retrieve/pii/S0959438800001112> (cit. on pp. 11, 12).
- [178] C Wall and J N Perry. "Range of action of moth sex-attractant sources." English. In: *Entomologia experimentalis et applicata* 44.1 (June 1987), pp. 5–14. DOI: 10.1111/j.1570-7458.1987.tb02232.x. URL: <http://doi.wiley.com/10.1111/j.1570-7458.1987.tb02232.x> (cit. on p. 2).
- [179] Barry Wark, Adrienne Fairhall, and Fred Rieke. "Timescales of Inference in Visual Adaptation." English. In: *Neuron* 61.5 (Mar. 2009), pp. 750–761. DOI: 10.1016/j.neuron.2009.01.019. URL: <http://linkinghub.elsevier.com/retrieve/pii/S0896627309000865> (cit. on p. 87).
- [180] Dieter Wicher, Ronny Schäfer, René Bauernfeind, Marcus C Stensmyr, Regine Heller, Stefan H Heinemann, and Bill S Hansson. "dOr83b—Receptor or Ion Channel?" English. In: *Annals of the New York Academy of Sciences* 1170.1 (July 2009), pp. 164–167. DOI: 10.1111/j.1749-6632.2009.04101.x. URL: <http://onlinelibrary.wiley.com/doi/10.1111/j.1749-6632.2009.04101.x/full> (cit. on p. 10).
- [181] Rachel I Wilson. "Early Olfactory Processing in Drosophila: Mechanisms and Principles." English. In: *Annual review of neuroscience* 36 (July 2013), pp. 217–241. DOI: 10.1146/annurev-neuro-062111-150533. URL: <http://eutils.ncbi.nlm.nih.gov/entrez/eutils/elink.fcgi?dbfrom=pubmed&id=23841839&retmode=ref&cmd=prlinks> (cit. on pp. 8, 9, 14, 134).

- [182] Rachel I Wilson and Zachary F Mainen. "Early events in olfactory processing." In: *Annual review of neuroscience* 29 (2006), pp. 163–201. URL: <http://www.annualreviews.org/doi/abs/10.1146/annurev.neuro.29.051605.112950> (cit. on pp. 12, 13).
- [183] C Andrea Yao, Rickard Ignell, and John R Carlson. "Chemosensory coding by neurons in the coeloconic sensilla of the Drosophila antenna." In: *The Journal of neuroscience : the official journal of the Society for Neuroscience* 25.37 (2005), pp. 8359–8367. URL: <http://www.jneurosci.org/content/25/37/8359.short> (cit. on p. 29).
- [184] Y Yu, B Potetz, and T S Lee. "The role of spiking nonlinearity in contrast gain control and information transmission." In: *Vision research* (2005). DOI: [10.1016/j.visres.2004.09.024](https://doi.org/10.1016/j.visres.2004.09.024). URL: <http://www.sciencedirect.com/science/article/pii/S0042698904004882> (cit. on p. 87).
- [185] Yuguo Yu and Tai Sing Lee. "Dynamical mechanisms underlying contrast gain control in single neurons." English. In: *Physical Review E* 68.1 (July 2003), p. 011901. DOI: [10.1103/PhysRevE.68.011901](https://doi.org/10.1103/PhysRevE.68.011901). URL: <http://link.aps.org/doi/10.1103/PhysRevE.68.011901> (cit. on pp. 87, 102).
- [186] K A Zaghloul, K Boahen, and J B Demb. "Contrast adaptation in subthreshold and spiking responses of mammalian Y-type retinal ganglion cells." In: *The Journal of Neuroscience* (2005). DOI: [10.1523/JNEUROSCI.2782-04.2005](https://doi.org/10.1523/JNEUROSCI.2782-04.2005). URL: <https://www.jneurosci.org/content/25/4/860.full> (cit. on pp. 87, 99).
- [187] Yi Zhou and Rachel I Wilson. "Transduction in Drosophila olfactory receptor neurons is invariant to air speed." English. In: *Journal of Neurophysiology* 108.7 (Oct. 2012), pp. 2051–2059. DOI: [10.1152/jn.01146.2011](https://doi.org/10.1152/jn.01146.2011). URL: http://eutils.ncbi.nlm.nih.gov/entrez/query.fcgi?cmd=Retrieve&db=PubMed&list_uids=23081000&dopt=Abstract.

nih.gov/entrez/eutils/elink.fcgi?dbfrom=pubmed&id=22815404&retmode=ref&cmd=prlinks (cit. on p. 22).

COLOPHON

This document is a dissertation written by Srinivas Gorur-Shandilya.

It was generated using LyX 2.2.2 and the source is available here:

<https://github.com/sg-s/phd-thesis/>

This document was typeset using the `classicthesis` package developed by André Miede. `classicthesis` is available for both L^AT_EX and LyX here:

<https://bitbucket.org/amiede/classicthesis/.>

Software

- A. `kontroller`, a MATLAB package to acquire data and automate experiments on National Instruments hardware. Available at <https://github.com/sg-s/kontroller>
- B. `spikesort`, a MATLAB package to sort spikes from extracellular recordings of *Drosophila* ORNs. Available at <https://github.com/sg-s/spikesort>
- C. `fly-voyeur`, a MATLAB package to quantify courtship behavior in *Drosophila*. Available at <https://github.com/sg-s/fly-voyeur>

Final Version as of July 27, 2017 (classicthesis version 4.2).